

OBSERVATOIRE DE PARIS

**MEMOIRE D'HABILITATION A DIRIGER DES
RECHERCHES**

Présenté par Valéry LAINEY

**Natural moons dynamics
and astrometry**

Soutenue le 29 mai 2017

Jury:

Anne LEMAITRE (Rapporteur)

François MIGNARD (Rapporteur)

William FOLKNER (Rapporteur)

Doris BREUER (Examinatrice)

Athéna COUSTENIS (Examinatrice)

Carl MURRAY (Examineur)

Francis NIMMO (Examineur)

Bruno SICARDY (Président)

Index

Curriculum Vitae	5
Dossier de synthèse	11
Note d'accompagnement	31
<i>Coordination d'équipes et de réseaux internationaux</i>	31
<i>Encadrement de thèses</i>	34
<i>Tâches de service</i>	36
<i>Enseignement</i>	38
Résumé	41
Annexe	43
Lainey et al. 2007 : First numerical ephemerides of the Martian moons	
Lainey et al. 2009 : Strong tidal dissipation in Io and Jupiter from astrometric observations	
Lainey et al. 2012 : Strong Tidal Dissipation in Saturn and Constraints on Enceladus' Thermal State from Astrometry	
Lainey et al. 2017 : New constraints on Saturn's interior from Cassini astrometric data	
Lainey 2008 : A new dynamical model for the Uranian satellites	

Curriculum Vitae

Name: Valéry Lainey

Address: IMCCE/Observatoire de Paris,
77 Avenue Denfert-Rochereau, 75014 Paris, France
Email: lainey@imcce.fr; Tel.: (+33) (0)1 40 51 22 69



Birth: 19/08/1974

Qualifications:

Ph.D. Observatoire de Paris, December 2002

Title of thesis: “*Théorie dynamique des satellites galiléens*”

Master degree “Astronomie fondamentale, mécanique céleste et géodésie” Observatoire de Paris 1998.

Academic Career:

Sep. 2006 - Present	Astronomer at the Paris Observatory
Apr. 2004 - Aug. 2006	Post-doc position at the Royal Observatory of Belgium
Jun. 2003 - Mar. 2004	Post-doc position at the Paris Observatory
Mar. - May 2003	Invited fellow at the Indian Institute of Astrophysics
Dec. 2002 - Feb. 2003	Post-doc position at the Paris Observatory
Sep. 1999 - Nov. 2002	PhD thesis at the Paris Observatory

Scientific Responsibilities:

Apr. 2015 - Present	ESTEC provider of the Galilean moon ephemerides for the JUICE mission
Jan. 2015 - Present	Leader of the IMCCE scientific team Pegase (about 25 pers.)
Apr. 2013 - Present	Coordinator of the ENCELADE 2.0 ISSI-international team
Jun. 2011 - Present	Deputy coordinator of the ESPaCE FP7-network
Mar. 2010 - 2013	Expert of the ISSI-Phobos network
2009- Present	Member of the GRGS (Groupe de Recherche en Géodésie Spatiale)
2009 - 2010	Member of ESA- EJSM/JGO WG4
Sep. 2007 - Mar. 2013	Coordinator of the ENCELADE international working group
Sep. 2006 - Present	Provider of natural satellite ephemerides for the Gaia mission
Sep. 2006 - Present	In charge of the Annuaire du Bureau des longitudes
Apr.2004 - Jun. 2006	Member of the MAGE (MArs Geophysical European) network

Institutional Responsibilities:

Jan. 2011 - Dec. 2014	Elected member at the Scientific Council of the Paris Observatory
Feb.2011 - Feb.2014	Deputy director of the IMCCE
Jan. 2007 - Oct. 2011	Elected member at the Scientific Council of the IMCCE

Space Missions Involvement:

M5-ESA Open Call (2016): core member on the JEM proposal
ESA-JUICE (2013, present): Co-I on GALA, Co-I on PRIDE, Associate Scientist on JANUS, member of JUICE-WG-1
ESA-PLATO (2013, present): Associate Scientist
NASA-InSight (2013, present): Associate Scientist on SEIS
NASA-CASSINI (2012, present): ISS collaborator
ESA-Gaia (2006, present): Member of the CU4 on the Gaia mission since 2006
M3-ESA Open Call (2009): Co-PI on the project mission GETEMME submitted in 2009
ESA-Mars Express (2004, 2006): Member of the Radio-Science Team

PhD students (Paris Observatory): (4 defended, 2 to be defended)

V.Robert (J.E.Arlot, [V.Lainey](#)) defended in 2011, L.Beauvalet ([V.Lainey](#), J.E.Arlot) defended in 2011, R.Tajeddine ([V.Lainey](#), S.Charnoz) defended in 2013, F.Remus (J.P.Zahn, [V.Lainey](#) and S.Mathis) defended in 2013, Y.Duchemin (J.E.Arlot, [V.Lainey](#)) to be defended in 2017, W.Polycarpe ([V.Lainey](#), A.Vienne) to be defended in 2018.

Master students (Paris Observatory):

R.Tajeddine, S.Bertone, S.Chloé, L.Beauvalet, K.Chemla, Y.Duchemin

Jury:

Expert for the thesis of M. Le Feuvre (defended at IPGP in 2008) and J. Besserer (defended at Nantes University in 2012)

Membership of Professional Organisations:

Member of the IAU (since 2015)

International Affiliate Membership of the American Astronomical Society (since 2009)

Member of the AAS Division of Planetary Sciences (since 2009)

Member of the SF2A (2007)

Review Panel:

Member of the SIMI5 ANR 2013 and ANR 2012, referee for CMDA, MNRAS, Icarus, PSS, A&A, AJ journals.

Teaching at OBSPM:

Master course on astrometry, observation training at OHP, training course on orbitography, supervision of engineer training courses

Outreach:

Interview in Nature and Sky & Telescope journals, E=M6 (high audience TV programme), UPMC communication, Fête de la Science, Festival d'Astronomie de Haute Maurienne (2013), teaching to medium-school pupils, podcast, 8 min. movie "Saturn, an ecosystem".

Award:

MESR Award for Scientific Excellence ("PEDR", 2014-2017)

Certificate in Excellence of Reviewing, *Icarus* 2013

MESR Award for Scientific Excellence ("PES", 2010-2013)

CoAuthor on the Prix La Recherche 2012 (Charnoz et al. *Icarus* 2011)

One of my PhD students, F.Remus, has obtained the L'Oréal prize 2012 for her PhD work

Funding ID:

Team leader of the ISSI International team selected in 2014

CNES Open Call 2014/2015 – 5100 Euros

P.I. RS/CNRS funding (2011/R1 ref. IE110421) – 8000 Euros

Dep. Coord. FP7/2008-2017 (under grant agreement n. 263466) – 1,930,256 Euros

Coord. ENCELADÉ UPMC-EMERGENCE (contract number EME0911) – 110,000 Euros

Publications

Refereed publications (57 publications, estimated *h*-index from ADS of 19.5, ADS citations number: 1120)

10 of the most cited papers are given below

1. Lainey, V., Arlot, J.-E., Karatekin, Ö., van Hoolst, T. (2009) Strong tidal dissipation in Io and Jupiter from astrometric observations. *Nature* 459, 957-959.
2. Efroimsky, M., Lainey, V. (2007) Physics of bodily tides in terrestrial planets and the appropriate scales of dynamical evolution. *Journal of Geophysical Research (Planets)* 112, 12003.
3. Lainey, V., Dehant, V., Pätzold, M. (2007) First numerical ephemerides of the Martian moons. *Astronomy and Astrophysics* 465, 1075-1084.
4. Lainey, V., Karatekin, O., Desmars, J., Charnoz, S., Arlot, J.E., Emelyanov, N., Le Poncin-Lafitte, C., Mathis, S., Remus, F., Tobie, G., Zahn, J.P., Strong tidal dissipation in Saturn and constraints on Enceladus' thermal state from astrometry. *Ap. J.*, Volume 752, Issue 1 (2012).
5. Lainey, V., Duriez, L., Vienne, A. (2004) New accurate ephemerides for the Galilean satellites of Jupiter. I. Numerical integration of elaborated equations of motion. *Astronomy and Astrophysics* 420, 1171-1183.

6. Lainey, V., Arlot, J.E., Vienne, A. (2004) New accurate ephemerides for the Galilean satellites of Jupiter. II. Fitting the observations. *Astronomy and Astrophysics* 427, 371-376.
7. Vasundhara, R., Arlot, J.-E., Lainey, V., Thuillot, W. (2003) Astrometry from mutual events of Jovian satellites in 1997. *Astronomy and Astrophysics* 410, 337-341.
8. Lainey, V., Duriez, L., Vienne, A. (2006) Synthetic representation of the Galilean satellites' orbital motions from L1 ephemerides. *Astronomy and Astrophysics* 456, 783-788.
9. Arlot, J.-E., Lainey, V., Thuillot, W. (2006) Predictions of the mutual events of the Uranian satellites occurring in 2006-2009. *Astronomy and Astrophysics* 456, 1173-1179.
10. Lainey, V. (2008) A new dynamical model for the Uranian satellites. *Planetary and Space Science* 56, 1766-1772.

Refereed publications with the PhD students that I co-supervised as the first author:

1. Beauvalet, L., Robert, V., Lainey, V., Arlot, J.-E., Colas, F., *A&A* (2013)
2. Beauvalet, L., Lainey, V., Arlot, J.-E., Bancelin, D., Binzel, R. P., Marchis, F., *P&SS* (2012)
3. Beauvalet, L., Lainey, V., Arlot, J.-E., Binzel, R. P., *A&A* (2012)
4. Remus, F., Mathis, S., Zahn, J.-P., Lainey, V., *A&A* (2012)
5. Robert, V., Lainey, V., Pascu, D., Arlot, J.-E., De Cuyper, J.-P., Dehant, V., Thuillot, W., *A&A* (2014)
6. Robert, V., de Cuyper, J.-P., Arlot, J.-E., de Decker, G., Guibert, J., Lainey, V., Pascu, D., Winter, L., Zacharias, N., *MNRAS* (2011)
7. Tajeddine, R., Rambaux, N., Lainey, V., Charnoz, S., Richard, A., Rivoldini, A., Noyelles, B., *Science* (2014)
8. Tajeddine, R., Cooper, N. J., Lainey, V., Charnoz, S., Murray, C. D., *A&A* (2013)

Publications related to the M3 ESA open call:

Oberst, J., Lainey, V., Le Poncin-Lafitte, C., Dehant, V., Rosenblatt, P., Ulamec, S., Biele, J., Hoffmann, H., Willner, K., Schreiber, U., Rambaux, N., Laurent, P., Zakharov, A., Foulon, B., Gurvits, L., Murchie, S., Reed, C., Turyshev, S.G., Noyelles, B., Gil, J., Graziano, M., Kahle, R., Klein, V., Pasewaldt, A., Schlicht, A., Spurmann, J., Uchaev, D., Wählisch, M., Wickhusen, K., *GETEMME - A Mission to Explore the Martian Satellites and the Fundamentals of Solar System Physics*, *Experimental Astronomy*, 34, Issue 2, 243-271 (2012).

Invited presentations to internationally established conferences:

1. V. Lainey, *Tidal dissipation in planets and satellites from astrometry*, XVIII CBDO Brazil, city of Aguas de Lindoia 2016.
2. V. Lainey, *Observational constraints on the tidal ratio k_2/Q in the solar system*, Saclay, Octobre 2014.

3. V.Lainey, Small Bodies Dynamics (SBD), *New insight into tidal dissipation of the Saturn system with astrometric data from ISS-Cassini*, Brazil, August 2014.
4. V.Lainey, *Tidal dissipation in Giant planet systems from astrometry*, COSPAR, Mysore 2012.
5. V.Lainey, *Martian satellite ephemerides and long term evolution models*, ISSI workshop – Phobos, Bern, 30 march 2010.
6. V. Lainey, *Tidal dissipation and orbital evolution of large satellites*, ISSI workshop – icy satellites 20 November 2008.
7. V. Lainey, J.E. Arlot, O. Karatekin, T. Van Hoolst, *Observed tidal dissipation in the Jovian system from satellite motions*, Asia Oceania Geosciences Society, Busan South Korea, 16-20 June 2008.
8. V. Lainey, *Natural satellite dynamics: what Gaia will bring*, Gaia Workshop Beaulieu-sur-mer 28 October 2008.
9. V.Lainey, A.Vienne, *Ephemerides of planetary satellites*, ESOC, 21-22 Juin 2007.

International advanced schools:

Systèmes Autogravitants Granulaires (SAG), 17-21 october, Nice, 2011 (teaching : 1 hour).

Sino-French spring school on astrometry, Observational campaigns of Solar System bodies, Beijing, April 7-12, 2008 (teaching: 10 hours).

Given talks (seminar):

Jinan University/Guangzhou (2016), Univ.Bologna/Forli (2016), QMUL/London (2015,2011), IPGP/Paris (2014), BDL/Paris (2012), USNO/USA (2011, 2008, 2005, 2004), OBSPM/Paris (2010, 2005, 2002), DLR/Berlin (2006), Lille 1/Lille (2005), LPGNantes/Nantes (2005), IIA/Bangalore (2003), SAI/Moscow (2002), ROB/Bruxelles (2002)

Organisation of international conferences:

Member of the Scientific Program Committee of the “Astrometry/photometry of Solar System objects after Gaia” Workshop, Paris 2015.

Co-convener at EPSC 2013 session: *Phobos, Deimos, and Other Small bodies of the Solar System*

Member of the Scientific Program Committee of the NAROO Workshop, Paris 2012.

Member of the Scientific Program Committee of the Europlanet JRA1-NA1 Workshop, Moscow 2011.

Dossier de synthèse

Introduction

From the ocean underneath Europa, to the intense volcanic activity of Io or the deep atmosphere of Titan, natural satellites present a large variety of worlds still mostly unexplored. While simple temperature considerations previously constrained the presence of liquid water to just beyond Mars' orbit, tidal effects mean that liquid water can exist much further from the Sun. Hence, habitability could exist in a wider variety of places, whether in our Solar system or extra-solar ones. In this context I revisited some part of our current knowledge in planetology from the perspective of astrometry. Indeed, monitoring and analysing the orbital motion of moons can provide an alternative and straightforward insight into the orbital and interior evolution of satellite systems. As I demonstrated for Io's activity (Lainey et al., *Nature* 2009), it may be the *only* way to assess some fundamental processes arising deep within these worlds. Once the key physical parameters are quantified, there are clear applications to the possible orbital states of exoplanets and their putative moons.

Astrometry of natural satellites

Astrometry is the discipline that aims to provide positions of celestial objects in space with the highest accuracy. Ground based observations are made by measuring angles on the celestial sphere. For moving solar system objects, the images are calibrated using stars present in the field after comparison with an astrometric star catalogue. While natural satellites have been observed with telescopes since the XVIIth century, accurate astrometric observations (few hundred milli-arcsec, or mas) which are still useful today, have only been available since the end of the XIXth century thanks to the use of photographic plates. Modern observations now benefit from CCD devices and accurate star catalogues which permit an accuracy below 100 mas.

While classical imaging astrometry can be performed at anytime, astrometrists may also use eclipses or occultations to derive geometric positions of natural satellites in space with great accuracy. Eclipses by Jupiter have been observed since the XVIIth century but, since 1973, observations of mutual intersatellite eclipses or occultations of one moon by another have proved to be extremely accurate, in fact more than regular imaging astrometry. These mutual events are now regularly observed thanks to the international campaign (Arlot et al., 1997) led by IMCCE (Institut de Mécanique Céleste et de Calcul des Ephémérides) and provide an accuracy of few tens of mas (Lainey et al., 2004). Even though they are comparatively rare (occurring only every 6, 15 and 42 years for the Jovian, Saturnian and Uranian system, respectively), mutual event observations can significantly improve the accuracy of the whole astrometric data set.

With the advent of spacecraft, astrometric observations from space of the natural satellites of giant planets have become available. The accuracy of these observations is generally about a few to a few tens of kilometres (a few mas, geocentric). In particular, observations of previous space missions used the star catalogues available at the time. In that context, I have initiated with William Thuillot a FP7 network, called ESPaCE and funded since 2011, to perform a new astrometric reduction of these old data using the more recent and more accurate star catalogues (Thuillot, Lainey et al. 2011).

Two space missions are currently completely pushing the limits of astrometry. The first one is Cassini, which after approaching the Jovian system at the end of 2000 has been orbiting Saturn since 2004. To benefit from the success of this mission, I have initiated in 2010 collaboration with Carl Murray's team based at Queen Mary University of London (QMUL) which is performing high accuracy astrometric reduction of images of Saturn's moons on a regular basis (Murray et al. 2005; Cooper et al. 2008). In addition, I have supervised the thesis of R.Tajeddine on astrometric reduction and dynamics of Mimas and Enceladus moons (Tajeddine et al. 2013). The Cassini mission will continue to monitor the Saturnian system until 2017. The second is the European Gaia mission. Launched in 2013 and active until 2019, it will provide the most accurate astrometric catalogue ever obtained and will allow the calibrations of all astrometric imaging observations (even those which were not able to be calibrated because of a lack of useful star catalogues). Benefiting from such a catalogue will allow an increase by a factor of two in the global astrometric accuracy of natural satellites of the giant planets. Furthermore, several tens of astrometric observations of most moons over the 5 years mission will be available with an accuracy of about 1 mas. This is why I have participated in CU4 of Gaia as the person in charge of natural satellites ephemerides.

The solar system bodies and especially natural planetary satellites are fast moving objects. Their dynamics may be known only through complex modeling based on regularly-made astrometric observations. The older the observations, the better the dynamical modeling will be, so that old data, not currently accurate enough for present studies may recover a new life through a revised analysis with modern tools. Benefiting from a modern scanning machine accurate to a few nanometers, V.Robert, another of my PhD students has showed recently that selected old photographic plates can compete with modern observations (Robert et al. 2011, 2015, 2016). In that respect, an accuracy of few tens of mas on intersatellite positions is possible after an appropriate treatment. Hence, combining modern observations with new reductions of old photographic plates opens the door to the monitoring of large main moons of the giant planets with unprecedented accuracy and over a wide extended time span (more than a century).

In the coming decades, astrometry will be tightly linked to space missions. This is why I have joined three instrument/experiment of the ESA JUICE mission (as Co-I on the GALA altimeter, Co-I on the PRIDE experiment and Associated Scientist on the JANUS camera). Similarly, I am an ISS collaborator on CASSINI, also. More, I am a core member on two M5-ESA proposal for space missions, called DePhine (PI J.Oberst) and JEM (PI M.Blanc), respectively.

Planetology

Tidal deformation and dissipation of stars, planets, and satellites is a fundamental mechanism for driving their orbital and thermal evolution. For instance, in the Earth-Moon system, the Moon is observed to be moving away from the Earth at a rate of few centimeters per year, because of the tides it raises essentially in the ocean. Another striking observation is the intense volcanism on Io, generally associated with the large tides raised by Jupiter due to Io's eccentric orbit. While constraining global tidal dissipation in telluric or icy bodies is difficult even with spacecraft instruments and while it often makes use of important assumptions (like possible thermal equilibrium), determining tidal dissipation in a giant planet may seem almost impossible. Fortunately, using the current distance of the main moons of icy giant planets and assuming they formed 4.5 Byr ago, Goldreich and Soter (1966) have already derived the first lower bound value of tidal dissipation in these gaseous planets. Almost half a century later their line of reasoning is still widely used, strongly constraining the dynamics of the whole

systems.

It is in this context that Voyager, Galileo and Cassini mission measurements have been considered. While our knowledge of these systems greatly increased in recent decades thanks to these missions, embarrassing questions arose. This is particularly true of the Saturn system, despite the huge amount of data available today. For example: Why is there no resurfacing on Mimas? What is the origin of Mimas' and Titan's eccentric orbits? What has caused the heating that has resulted in the active geyser activity discovered in 2005 at the South pole of Enceladus? These phenomena are still poorly understood. Another example is the origin of the Cassini division in Saturn's rings; it was discovered by Jean-Dominique Cassini about 400 years ago, and yet it is still largely unexplained.

Saturn is not the only system that challenges our imagination. The origin of the tilt of Uranus' rotation axis is still an open question. While a collision scenario was first proposed by Safronov (1966), this explanation was believed to be in contradiction with the presence of the main moons orbiting in Uranus' equatorial plane. In 2010, Boué & Laskar (2010) proposed the existence of a large, distant satellite to act secularly on the Uranian pole. Nevertheless, this last model seemed showing low numerical probability of success. Even more recently, Morbidelli et al. (2012) presented a collisional scenario of Uranus, compatible with the presence of the main moons. All these models, however, consider generally a rather limited tidal expansion of the moons, due implicitly to our old assumptions on Solar system formation (Goldreich & Soter, 1966).

It seems that we have arrived at a time where the mere increase of data concerning these systems may not significantly help us to solve these paradoxes. In particular, it may be time to look seriously for a different strategy, benefiting from all our current knowledge of the giant planet systems, but based on a different approach.

Using astrometry for planetology?

While fundamental for our understanding of the Solar system and the long-term evolution of the exo-planetary systems, tidal parameters are difficult to determine from observations. Indeed, they provide a small dynamical signal, both on natural and artificial celestial objects, in comparison to other perturbations arising in the system (see next section). However, tides do provide large effects on the long term evolution of the natural bodies. This is why estimations of the tidal parameters have often been done from the assumed past evolution of planets and moons.

In that respect, estimation of the average tidal ratio k_2/Q for the giant planets was done already back in the 60s by Goldreich & Soter (1966). We recall that k_2 is the first of the second order Love number (Love 1911), while Q is a quality factor relative to the amount of mechanical energy dissipated by friction inside an object (Goldreich & Soter, 1966). Both are unit-less quantities. Considering the average secular drift over 4.5 Byr on the semi-major axes of the innermost main moon of the Jupiter, Saturn and Uranus systems, the authors obtained an averaged estimation of k_2/Q . While having been the reference for several decades, these values were estimated assuming a specific formation and evolution scenario. In particular, alternative formation models now exist for these moons, that may suggest younger age for some of the main moons (Charnoz et al. (2011), Crida & Charnoz (2012), Cuk (2014)). Moreover, resonances crossings and possibility of strong dissipative episodes of the moons makes the question even more complex.

Another way for constraining the tidal ratio k_2/Q may be, at least for very active bodies, to simply consider the amount of heat radiated from their surface, and after having considered the presence of radiogenic heating. IR-emission values may be used for Io (Matson et al. 1981) and Enceladus (Spencer et al. 2006) to this task. However, this line of reasoning assumes a thermal equilibrium state to infer the amount of heat produce in the whole interior, which is not granted. Indeed, such equilibrium would require a very efficient heat transport mechanism inside Io. Such fast transport would be easier with low viscosity, but low viscosity may prevent large tidal dissipation. Moreover, the Laplace resonance itself (and so the eccentricities of the moons) might have changed over these last hundred millions of years.

The use of astrometry for planetology may not seem obvious. For example, spacecraft radio data have long since superseded astrometric data in the determination of gravity fields of planetary systems. While the former are much more precise and numerous, astrometric data have a unique advantage in covering a much extended time span. Even though this asset has been undervalued for a long time, I have tried reviving astrometry in order to allow the long-term dynamical effects to be studied accurately, alongside the short-term ones for a broad variety of systems. To reach such goal, I have developed over many years a numerical code NOE (Numerical Orbit and Ephemerides). Composed of more than 12,000 lines (excluding comments) my code computes the evolution of the state vectors of any N-body problem, as well as the partial derivatives of these vectors as function of initial conditions and physical parameters of interest. Comparing predicted positions with observed ones, I can then compute corrections to apply on the initial parameters of my model, including (but non exhaustively) masses, extended gravity field coefficients, precession/nutations of the primary, temporal variation of gravity fields, and tidal effects (Lainey et al. 2004b; Lainey et al. 2007; Lainey 2008). The reader may refer to the methodology section of this document for details.

Following this philosophy I have succeeded in quantifying global dissipation in the Io/Jupiter system (Lainey et al., Nature 2009). In particular, I have shown that the associated orbital energy loss, quantified from astrometry, matches the heat loss at Io's surface giving constraints on interior models and the heat transport mechanism. At the same time, I could also quantify global dissipation in a giant planet directly from observations, and give a new reference value for exoplanets similar to Jupiter. Just after five years, my paper had already gathered 59 citations (excluding auto-citations) from both Solar and extra-Solar system communities.

Encouraged by this result, I have raised a working group called ENCELADE (funded by EMERGENCE-UPMC) to extend my work to the Saturnian system. Such group revealed being an active "think tank" due to the various physical fields involved (ring dynamics, icy moons interior, stellar interior models applied to giant planets...). After some work, our results appeared even more striking than one would have expected. Using astrometric observations from 1886 until 2009, we succeeded in quantifying not only the tidal ratio k_2/Q in Saturn, but we even calculated it at four different tidal frequencies (Lainey et al., 2012). We found an intense tidal dissipation about ten times higher than the usual value estimated from theoretical arguments. As a consequence, the eccentricity equilibrium for Enceladus can now account for the huge heat emitted from Enceladus' South pole! Moreover, the measured k_2/Q was found to be poorly sensitive to the tidal frequency on the short frequency interval considered (Figure 1). This suggested that Saturn's dissipation may not be controlled by turbulent friction in the fluid envelope as commonly believed. The large tidal expansion of the

moon's orbit due to Saturn's strong dissipation also suggested that all the moons should have formed at close distance from Saturn. This led to a new model of satellite formation at the ring's outer edge (Charnoz et al. 2011).

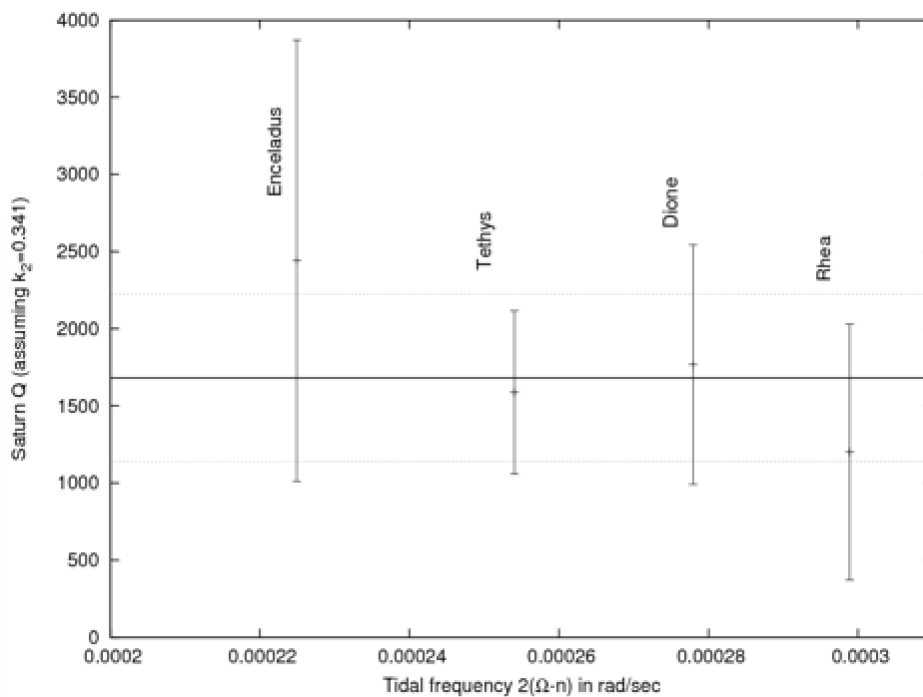
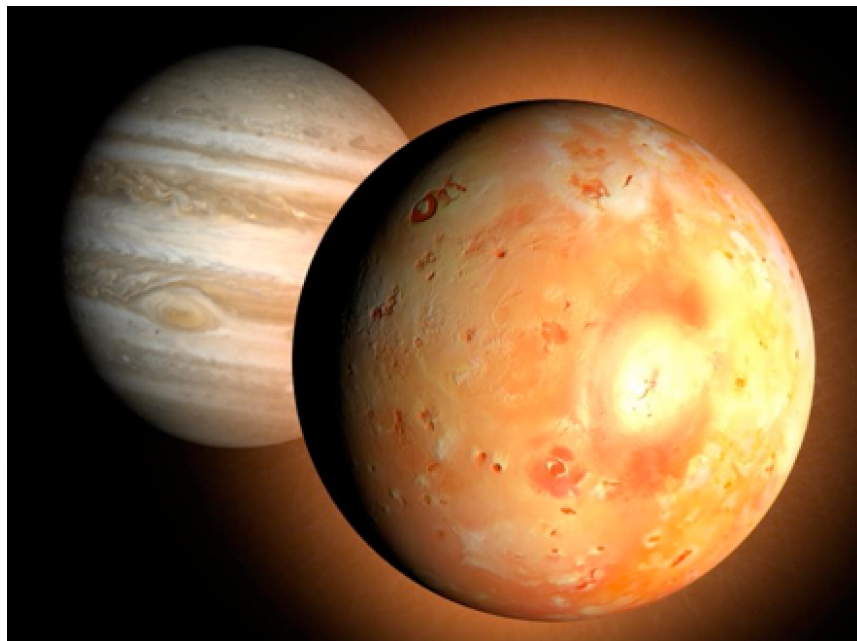


Figure 1 : On the top: strong tidal dissipation in Io suggesting thermal equilibrium has been recently demonstrated using astrometry (Lainey et al., Nature 2009); on the bottom: tidal dissipation in Saturn vs. tidal frequency (Lainey et al., ApJ 2012).

Between 2012 and 2015, I worked hard with the ENCELADE team to take into account the huge number of astrometric ISS-Cassini data. Thanks to my collaboration with Carl Murray and Nick Cooper from the Queen Mary University of London, as well as the PhD work of Radwan Tajeddine, I could beneficiate from about 800 astrometric data per satellite. Thanks

to this large data set I could solve for much more parameters, including the gravity field of the moons and their primary. Moreover, the error bars on the tidal ratio k_2/Q at different tidal frequencies were significantly reduced (Figure 2). This allowed us to point out an intense dissipation at the tidal frequency of Rhea. We explained such specific behaviour by two different sources of tidal dissipation : dissipation inside the core and dissipation inside the turbulent atmosphere. In 2016, Fuller et al. (2016) explained this by just the tidal dissipation in a stably stratified layer, probably present in the deep interior of Saturn above its core (Fuller 2014).

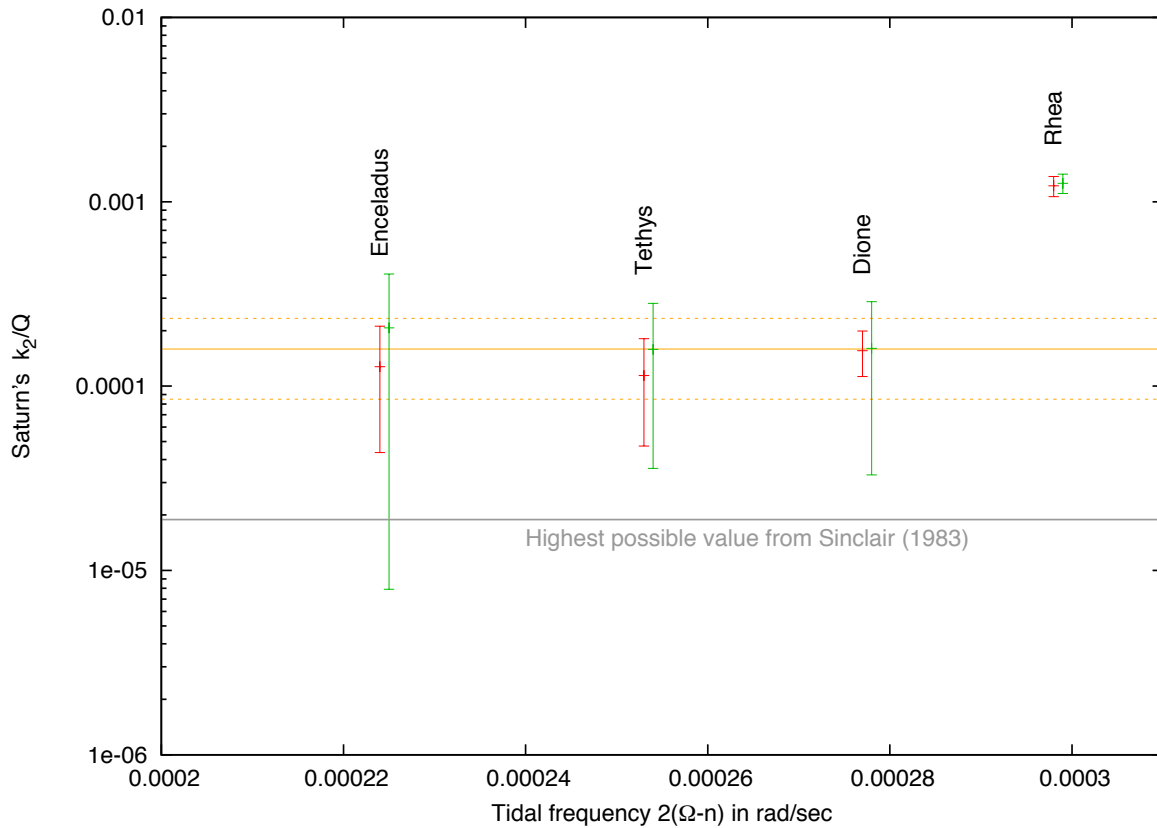


Figure 2: Variation of the Saturnian tidal ratio k_2/Q as a function of tidal frequency $2(\Omega-n)$ from Lainey et al. (2017). Ω and n denote Saturn's rotation rate and the moon's mean motion, respectively. Four frequencies are presented associated with Enceladus', Tethys', Dione's and Rhea's tides. IMCCE and JPL solutions are in red and green, respectively. They are shown slightly shifted from each other along the X-axis for better visibility. Orange lines refer to the global estimation $k_2/Q = (15.9 \pm 7.4) \times 10^{-5}$.

The large number and accuracy of the ISS-Cassini dataset concerned also the small coorbital moons of Thetys and Dione, called Telesto, Calypso, Helen and Polydeuces. In particular, I could use the orbital motion of these moons to determine, for the first time from observations, the Love number k_2 of Saturn. This determination allowed us to discriminate significantly the interior modeling of Saturn. In particular, the Love number appeared to be extremely complementary to the usual J_2 , J_4 and J_6 determined from radio-science data (Lainey et al. 2017).

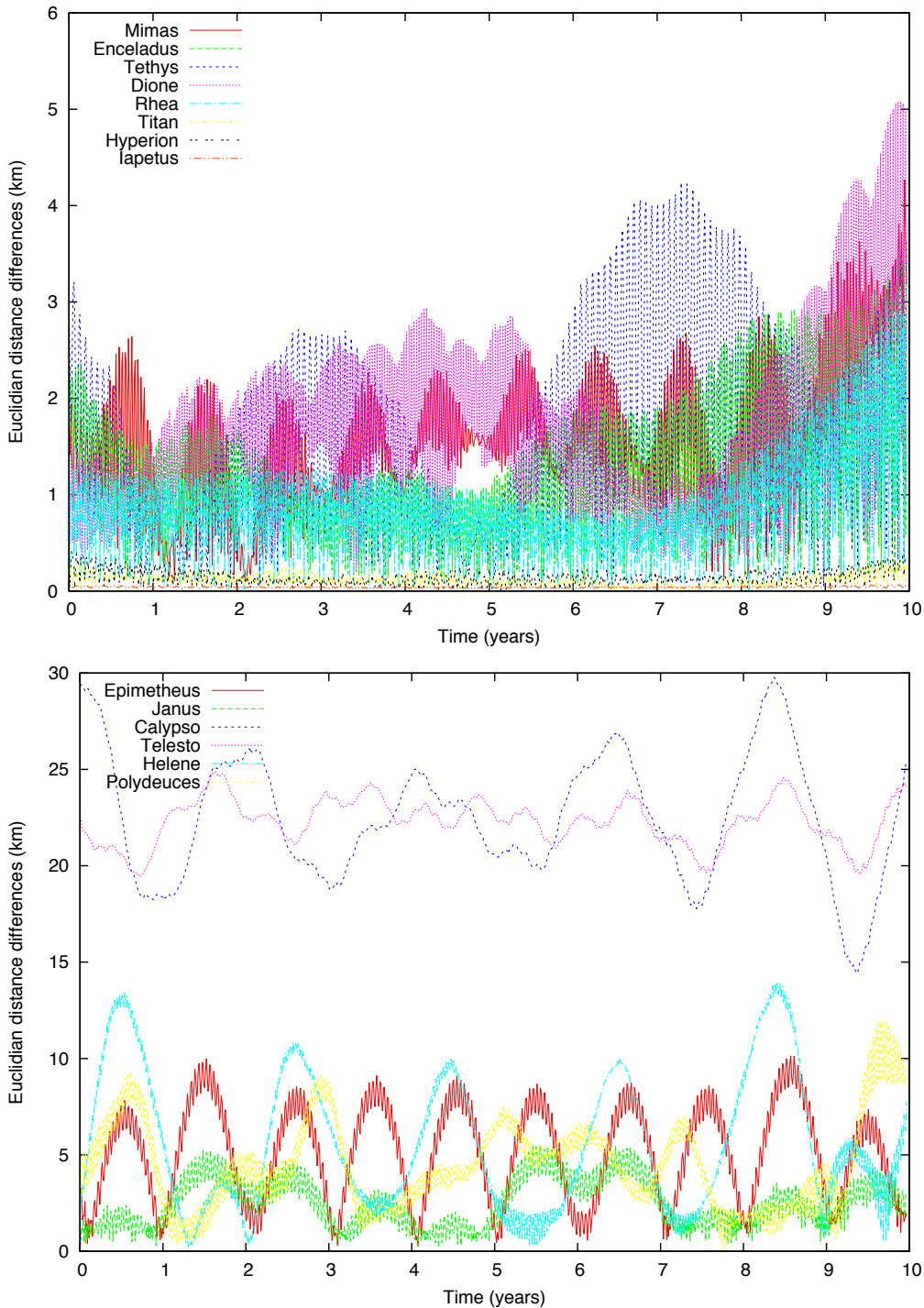


Figure 3: Postfit residuals associated with cross-tidal effects from Lainey et al. (2017). Kilometric signals appear associated with the Saturn's tidal bulge at Janus/Epimetheus', Mimas', Enceladus', Tethys' and Dione's tidal frequencies.

It appears that the quest for a better understanding of the Jupiter and Saturn systems by means of astrometry has just started. As an example, the error bar on Io's tidal ratio needs to be reduced from its current 25%. Moreover, global tidal dissipation inside Enceladus and Mimas, tidal dissipation in Saturn at other frequencies, exchange of angular momentum between Mimas and the B ring have all still to be quantified from astrometry. As with the Galilean system, this will require simultaneously considering the inner and main moon systems.

In the future, we shall quantify, more accurately than ever, the tidal dissipation in giant planets and their satellites with potential consequences for habitability. This will be of high importance for the selected ESA-PLATO mission.

Tidal parameters quantified today

I give in Table 1 the most up-to-date values of the principal tidal parameters that have been determined from astrometric measurements. When available, error bars computation are given, most of the time as function of the formal standard deviation. When a purely Gaussian noise is assumed, there are about 66% of chances that the real physical value lies in the $1\text{-}\sigma$ formal uncertainty. However, observations may not follow a Gaussian error profile. More importantly, constrains are often introduced in the least squares inversion. This is generally done when working with artificial objects, since on one hand, some perturbations cannot be perfectly modeled (wheel-off loadings, orientation of solar panel, drag), and on the other hand the observables quantities (Doppler, ranging) do not allow to recover easily the full motion of the spacecraft in 3-D space. As a result, an uncertainty of $10\text{-}\sigma$ shall not be considered as necessarily more robust than a $2\text{-}\sigma$ error bar. More likely, such larger choice of error bar is a consequence of strong correlations and associated constrains inserted in the fitting process. In practice, it may be wiser to consider the error bars as the likely range in which the real physical value is lying. Sometimes, studies provide a double-check of their results by performing two independent fits (using different codes and weight) like in Iess et al. (2012). Alternatively, both independent solutions may be merged in one single solution (including error bars). Such solutions are indicated by *MS* (merged solutions) in Table 1.

Since Mercury and Venus do not have moons, the measurement of their geophysical parameters must rely on spacecraft data. Considering the semi-diurnal tides raised by the Sun, Mazarico et al. (2014) and Konopliv et al. (1996) succeeded in estimating the k_2 of Mercury and Venus, respectively. While Messenger's second extended mission data might provide a better determination in the future, no estimation of Venus' k_2 has been published since 1996, and the analysis of the Pioneer Venus Orbiter and Magellan space probes. In particular, Venus Express orbit is too far and eccentric to provide a good S/N ratio on Venus' k_2 .

On the contrary, Mars, Jupiter and Saturn's system have moons, close enough to provide reliable signal over a century of accurate astrometric observations. In particular, it is astonishing that the secular acceleration of Phobos around Mars was first pointed out in 1945 by Sharpless (1945) with a 50% error in his determination, only. While the acceleration of Phobos provides the tidal ratio k_2/Q , it is the Mars' spacecraft that allow to quantify the Mars k_2 associated to Solar tides. Assuming the same Mars' k_2 at Solar and Phobos tidal frequency, Jacobson & Lainey (2014) published the most up-to-date Q value.

Body	k_{lm}	Q	k_2/Q	Reference
Mercury	$k_2 = 0.451 \pm 0.014 (10\sigma)$			Mazarico et al. (2014)
Venus	$k_2 = 0.295 \pm 0.066 (2\sigma)$			Konopliv et al. (1996)
Earth	$k_{20} = 0.29525$ $k_{21} = 0.29470$ $k_{22} = 0.29801$ $k_{30} = 0.093$ $k_{31} = 0.093$ $k_{32} = 0.093$ $k_{33} = 0.094$	280 (230, 360) (1σ)		Lunar semi-diurnal terrestrial tide (Ray et al. 2001) using $k_2 = 0.302$ (Wahr 1981) Nominal values of solid Earth tide (elastic Earth) from IERS 2010
Moon		37.5 ± 4		at month frequency (Williams et al. 2014) using $k_2 = 0.024059$ (Konopliv et al. 2013) Konopliv et al. (2013)
	$k_{20} = 0.02408 \pm 0.00045$ $k_{21} = 0.02414 \pm 0.00025$ $k_{22} = 0.02394 \pm 0.00028$ $k_2 = 0.02405 \pm 0.000176$ $k_3 = 0.0089 \pm 0.0021$			
	$k_{20} = 0.024165 \pm 0.00228$ $k_{21} = 0.023915 \pm 0.00033$ $k_{22} = 0.024852 \pm 0.00042$ $k_2 = 0.02427 \pm 0.00026$ $k_{30} = 0.00734 \pm 0.00375$			Lemoine et al. (2013)
Mars	$k_2 = 0.173 \pm 0.009 (5\sigma)$ $k_2 = 0.164 \pm 0.009 (5\sigma)$	99.5 ± 4.9		Konopliv et al. (2011), Jacobson & Lainey (2014) after correction for atmospheric tide
Jupiter			$(1.102 \pm 0.203) \times 10^{-5} (1\sigma)$	Lainey et al. (2009)
Io			$0.015 \pm 0.003 (1\sigma)$	Lainey et al. (2009)
Saturn	$k_2 = 0.390 \pm 0.024 (MS)$		$(1.59 \pm 0.74) \times 10^{-4} (MS)$ $(123.94 \pm 17.27) \times 10^{-5} (MS)$	Lainey et al. (2015) at Rhea's tidal frequency
Titan	$k_2 = 0.589 \pm 0.150 (2\sigma)$ $k_2 = 0.637 \pm 0.224 (2\sigma)$			Iess et al. (2012)

Table 1 : Current estimate of the principal tidal parameters of the objects of the Solar system, as determined from astrometric measurements.

While the first estimation of the Jovian k_2 is a goal of the Juno mission, Lainey et al. (2009) succeeded in fitting the tidal ratio k_2/Q of both Jupiter and Io, using astrometric measurements of the Galilean moons. In a similar way, Lainey et al. (2017) used a large set of astrometric data, including numerous ISS-Cassini data to quantify Saturn's k_2/Q and its dependence on tidal frequency. More, they used astrometric observations of the Lagrangian moons of Tethys and Dione to provide the first determination of the Saturn's k_2 . Still with Cassini spacecraft, but this time from the radiometric measurement of six flybys of Titan, Iess et al. (2012) could provide the first determination of Titan's k_2 , suggesting a potential global ocean under the moon's shell.

The Earth-Moon system is evidently the most studied, but also the most complex. In particular, the presence of oceans, atmosphere and convection in the mantle of the Earth makes the data treatment quite difficult. For the Moon, the latest Love numbers estimations were obtained from the GRAIL mission, with two independent published studies (Konopliv et al. 2013, Lemoine et al. 2013). Benefiting from GRAIL mission results, Williams et al. (2014) reanalyzed lunar laser ranging data and provided the latest estimation of the Lunar tidal quality factor Q at month frequency.

The difficult proper treatment of Earth data and modeling made the determination of terrestrial tides extremely difficult. Its first determination arose in 1996 only (Ray et al. 1996), and was improved in 2001 (Ray et al. 2001). To conclude this section, I provide in Table 1 the nominal values of Love numbers for a solid (elastic) Earth tide from IERS 2010. The interested reader may find more informations on Earth's tides in IERS (2010) and references therein.

Methodology

The methods used to constrain tidal parameters from astrometric data of the natural objects of the Solar system on one hand, and of the spacecraft on the other hand, are actually extremely similar. They require three steps: i) the development of an orbital model of the objects studied; ii) the gathering of observation sets of the objects; iii) the fitting of the dynamical model to the observations.

The modeling of the system stands on a N-body code that takes into account all the perturbations that may influence the orbit, at the level of accuracy of the astrometric observations. In the case of space geodesy, only one body is integrated over time, making $N=1$. Still, several other celestial objects have to be considered as perturbers of the spacecraft/artificial satellite dynamics. For the perturbations, the minimum is to consider all objects as point mass, but it is most of the time necessary to take into account the harmonic expansion of the gravity fields. In that case, the direction of the north pole and prime meridian into space of each body needs to be considered, generally by mean of forced frequencies (Archinal et al. 2011), and ultimately fitted. Depending on the system studied, the list of perturbations that have to be introduced can be pretty long. Let us just mention here, the extended gravity fields of the objects, the object's precession and nutations, the forced

librations on rotation, the tidal effects, the relativistic effects. In the case of space geodesy, we may add to the perturbations' list, the drag into the atmosphere (if any) of the primary, the solar and planetary radiation pressure, the wheel-off loadings, etc. Once a proper modeling is set, and using Newton's second law, one will have to integrate the ordinary differential equation (ODE) of second order

$$\frac{d^2 \mathbf{r}_i}{dt^2} = \frac{\mathbf{F}_i(\dots, \mathbf{r}_j, \dots, \mathbf{v}_j, \dots, \mathbf{p})}{m_i} \quad (1)$$

where m_i is the mass of the considered object, \mathbf{r}_j , \mathbf{v}_j denote the state vectors of any body influencing the system and \mathbf{p} vector denotes a set of any physical parameters relevant in the dynamics (masses, spherical harmonic coefficients C_{np} , S_{np} , tidal parameters, etc.). The integration of this system consists in $3N$ differential equations and is, in most cases, not problematic. In the case of natural satellites, initial conditions associated with eq. (1) are generally borrowed from a former ephemeris. If none is available, a simplified dynamical model may be used in a first step, with possible constrains on initial inclination and eccentricity. In the case of spacecraft, extrapolation of a former orbit (sometimes associated with an earlier phase of the mission) may be used.

Observations useful for constraining the orbits can have very different forms: astrometric images, laser ranging, photometric, radiometric and VLBI measurements. The gathering of these astrometric observations is a lengthy and thankless task. Fortunately astrometric databases exist like the Planetary Data System (<https://pds.nasa.gov>) for space probes data and the Natural Satellite Data Base (Arlot & Emelyanov, 2009) for the natural moons. Still, a huge amount of observations have been performed worldwide, and taking care of all various format, observation corrections, and even sometimes typos becomes extremely fastidious.

The last step requires to compare observed and computed positions of the celestial objects. In practice, one does not observe directly 3-D cartesian coordinates, and the numerical output of the integration of eq. (1) has to be rewritten, for each observation time, introducing observed variables like angles on the celestial sphere, ranging, Doppler, etc. These observation quantities can be dependent on the state vectors of the observed body, but also on a set of parameters \mathbf{p}' related to the observation treatment. Denoting g such observation kind, and in the vicinity of the exact solution, we may express the differences between the observed and computed quantities, as a Taylor expansion, limiting ourselves to the first order

$$g(\mathbf{r}_i^o, \mathbf{v}_i^o, \mathbf{p}'^o) - g(\mathbf{r}_i^c, \mathbf{v}_i^c, \mathbf{p}'^c) \simeq \sum_{l=1}^{6N+p+p'} \left(\frac{\partial g}{\partial \mathbf{r}_i^c} \cdot \frac{\partial \mathbf{r}_i^c}{\partial c_l} + \frac{\partial g}{\partial \mathbf{v}_i^c} \cdot \frac{\partial \mathbf{v}_i^c}{\partial c_l} + \frac{\partial g}{\partial \mathbf{p}'^c} \cdot \frac{\partial \mathbf{p}'^c}{\partial c_l} \right) \Delta c_l \quad (2)$$

where o and c refer to observed and computed quantities, respectively, and c_l denotes any unknown scalar to be fitted. Clearly, there will be as many linear equations as observation data. The linear system may then be solved by more or less sophisticated least squares method. In particular, the weight of each data, the choice of the physical parameters to be fitted and the way these parameters may be fitted (all in once, or using successive steps) will depend on the ephemeris developer and expertise.

In the former equation, the partial derivative of state vectors as function of initial parameters

have to be known. There exists few different methods to obtain these quantities. But the most widely used method consists in integrating the so-called variational equations (Peters 1981; Moyer 2003). Starting from eq. (1) and assuming c_l to be independent of time, one obtains after applying partial derivation

$$\frac{d^2}{dt^2} \left(\frac{\partial \mathbf{r}_i}{\partial c_l} \right) = \frac{1}{m_i} \sum_{j=1}^N \left[\frac{\partial \mathbf{F}_i}{\partial \mathbf{r}_j} \cdot \frac{\partial \mathbf{r}_j}{\partial c_l} + \frac{\partial \mathbf{F}_i}{\partial \mathbf{v}_j} \cdot \frac{d}{dt} \left(\frac{\partial \mathbf{r}_j}{\partial c_l} \right) \right] + \overline{\frac{\partial \mathbf{F}_i}{\partial c_l}} \quad (3)$$

where the last term denotes the derivation of the force with respect to c_l , when it comes explicitly in the expression of \mathbf{F} . The numerical integration of eq. (3) is much more complex than the standard equations of motions and often implies the simultaneous integration of thousands of ODE. In practice, system of eq. (3) needs to be integrated simultaneously with system of eq. (1). This method is the one used regularly by space geodesy codes like DPODP (Moyer 1971) and GEODYN II (Pavlis et al. 2013). It is also extremely used for natural moons (Peters 1981), asteroids, comets and even for exoplanet systems. Moreover, this method can be used indifferently for regular satellite orbits, flyby analysis and even rotation analysis (replacing the equations of motion by the Euler-Liouville equations).

Last but not least, let us emphasize that the validity of eq. (2) implicitly assumes that the modeling is perfect and the data contains no errors. In that respect, the least squares method handles the observation errors properly if the data are not biased, only. And it is optimal if the random errors have a Gaussian profile. But a perfect modeling and no observations biases (a requirement for a Gaussian error distribution) are two conditions that are never completely reached. Combined with correlations between fitted parameters, the former method will provide different solutions, depending on the modeling, the biases treatment, the weight of the data and the selection of the released parameters.

My projects

In the coming years, the Cassini and Juno space missions devoted to the study of the giant planets of our Solar system will end. I have already spent a lot of efforts using ISS-Cassini astrometric data. The final objective is a full characterization of the tidal effects in the Saturn system. This concerns the tidal dissipation within Saturn and its origin, but also the amount of global heat produced inside Enceladus and possibly other moons like Mimas (Tajeddine et al. 2014). Hence, I will go on studying the Saturn system, using now all data available, including radio-science data of all missions that visited the Saturn system.

The grand final of the Cassini mission will also be the opportunity to use a more than ever accurate gravity field of Saturn. This will allow having a much better physical modelling of the gravity interactions in the Saturn system, while decreasing the number of unknown parameters in the fit.

Last, the end of the Juno mission will be the opportunity to do a similar work for Jupiter, allowing for a cross understanding the two giant planets of the Solar system. Moreover, this will help preparing the coming results of the EMFM (ex. Clipper) and the JUICE space missions, also.

I give below several items describing the work to be done.

General methodology and procedures to be followed

Ephemerides rely on a three steps approach: i) observations; ii) dynamical modeling; iii) fitting of the model to the observations. In my project, all three steps shall be revisited.

Astrometry

From space

Thanks to Caviar software developed jointly at QMUL and IMCCE (Cooper et al. 2016), the astrometric reduction of ISS-Cassini data can be done rather easily. While measurements can have a precision at few to ten kilometers level, we identified two ways of future improvements. The first improvement to be done will be adding Gaia intermediate catalogue for astrometric calibration of the field. Indeed, while many stars regularly appear on images, there exist many cases where just a few of them are identified with a modern astrometric star catalogue (UCAC4). Since Gaia catalogue will provide absolute coordinates for all stars of magnitude lower than 20.7, the introduction of such catalogue in Caviar will significantly increase the number of stars to be used in the astrometric reduction. A second improvement to be done is to re-reduce all images with a more accurate shape model currently available, thanks to recent Cassini data (P. Thomas, private communication). This is particularly relevant for Saturn's inner moons (see Figure 4) that are more sensitive to tidal perturbations. These improved astrometric data can be used to better constrain Saturn's Love number k_2 at higher frequencies and possibly temporal changes in the Saturn's gravity field as well.

Looking for new moons?

Despite the huge number of observations of the Saturn system, it is still possible that unknown small moons may exist. A systematic search for undiscovered objects will be conducted in parallel to the re-reduction of ISS images. Indeed, thanks to a Gaia intermediate catalogue, all stars on the images will be identified. This will make the task easier, even though the significant noise on the images will require a specific treatment method. In that respect, the use of successive image series will be useful to discriminate between noise and a potential new object. Once potential targets have been identified, a simple Keplerian fit will be performed in the first step to identify possible combinations of matching positions associated with different set of images. This step will be followed by a full N-body integration to set properly the orbital characteristics of the new moon.

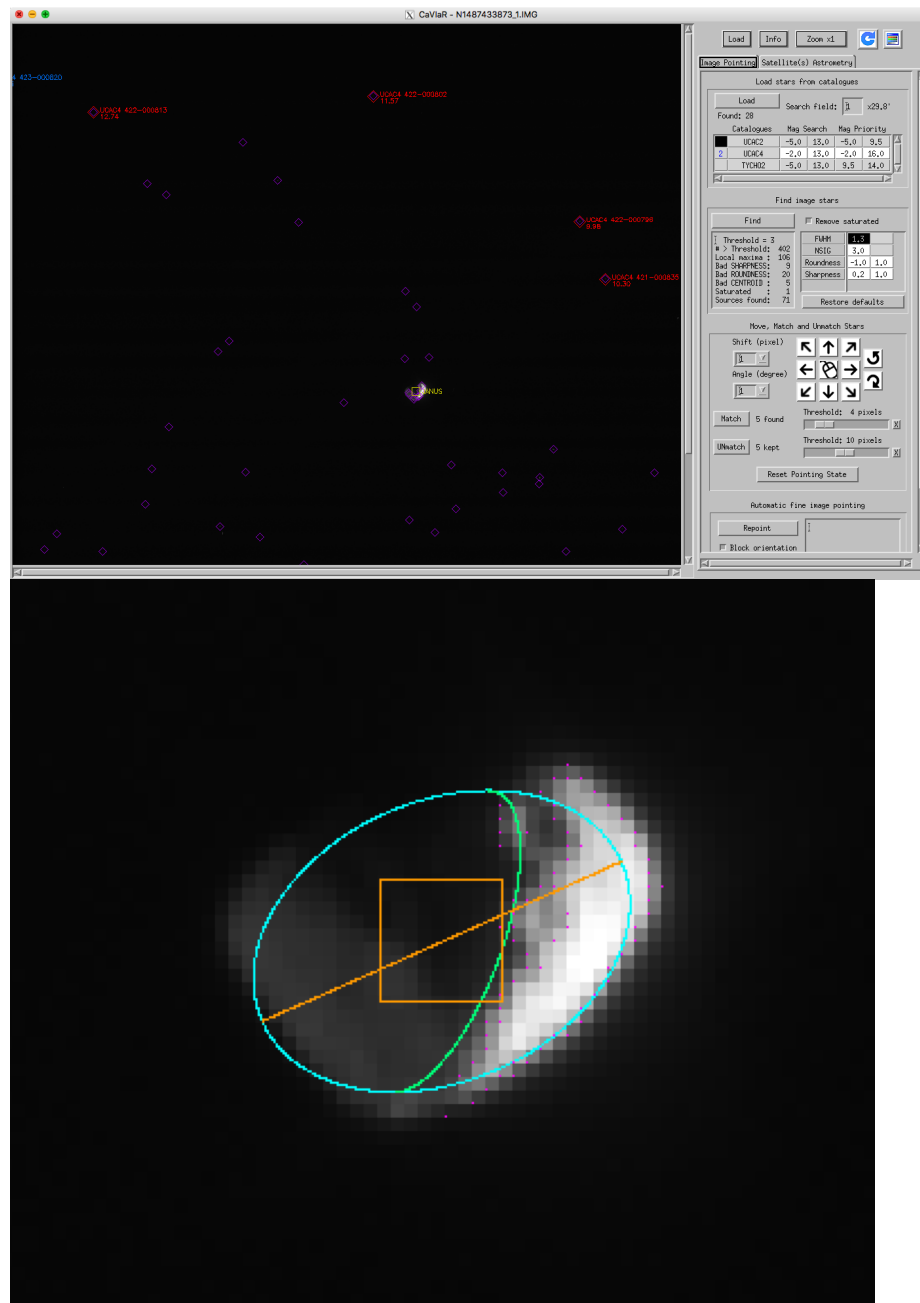


Figure 4: On the top is the Caviar user interface. On the bottom is a zoom on Janus moon and its current assumed shape model in the software. A more complex shape model is required to fully benefit from the high accuracy of ISS data.

From the ground

While Cassini has provided a huge amount of astrometric and radiometric observations for the Saturnian system, the Juno mission will provide limited data. The only observation from the Juno mission applicable for studying tides will be the Deep Space Network-based radiometric observations for the Jupiter gravity science investigation and no science-quality astrometric observations of the moons are planned to be conducted. However, a new campaign of ground-based astrometric observations of the Galilean moons is being conducted in France since

2014. It benefits from a new technique that uses staking images to obtain stars in the background field, without saturation of the CCD images of the moons (a common issue with the extremely bright Galilean moons). These data will be reduced with the Gaia intermediate catalogue in the end of 2016 to provide an accuracy of about 30 mas. Since stars will be present in the field, Jupiter's position on the celestial sphere can be deduced. This will complement the radioscience data allowing for an accurate quantification of Jupiter's 3-dimensional position relative to the Earth.

Dynamics

Tidal dissipation within giant planets is expected to arise in their core (Dermott 1979; Remus et al. 2012; 2015), possibly stratified He layer (Morales et al. 2009; Fuller 2014), and convective atmosphere (Ogilvie and Lin 2004). Depending on which part of the planet's tides are considered, the response of the body will show extremely different behavior in frequency. A variety of different modeling will be introduced for all cases. In the case of tides in the core, a Maxwell model will be introduced (Remus et al. 2012). In particular, shear modulus G and its viscosity η will appear as two new unknowns in the model. For modeling tidal dissipation within the He layer, we will rely on the recent work of Fuller et al. (2016) and introduce the two quantities t_p and t_a . These parameters describe the spin-up of the planet and the time scale on which the angular frequency of an oscillation mode changes, respectively. In the case of tides in the atmosphere, both tidal locking mechanism and erratic variation on the tidal Q will be considered (Fuller et al. 2016; Ogilvie and Lin 2004). For this last case, we will introduce extra da/dt terms, one for each of tide raising moon, in the dynamics. Indeed, if the tidal ratio k_2/Q follows an erratic distribution in frequency, a statistical approach will be necessary. All models will be introduced in a compatible way, since their physics are not exclusive and may be presently at work simultaneously within Jupiter and Saturn today.

The tidal Love number k_2 is so far assumed (for simplicity) to be constant while it is expected to be frequency sensitive. In this study, we will consider a variable k_2 except for the satellite pairs that share the same tidal response. For example, Tethys and Telesto/Calypso pair are Lagrangian co-orbital moons so that their tidal frequencies will be the same. In this case, k_2 will be assumed to be constant. These selective models will provide a higher precision on the measurements by introducing a coherent treatment of the cross-tidal effects. Lastly, we will implement the capability to estimate the higher order Love number k_3 and assess its recovery.

Global inversion

This part shall rely on a global inversion of all astrometry and radioscience data. A proper weighting for each data type is crucial to guarantee the best accuracy for the recovered dynamical parameters. An exploration of various dynamical models will be performed in parallel to different weightings to determine the best modeling options and parameters to be solved for during the final fitting procedure. All inner and main moons will be considered here, for both Jupiter and Saturn system. A comparison between JPL and IMCCE approaches will be extremely fruitful in helping obtaining the best modeling and relative weightings of all data.

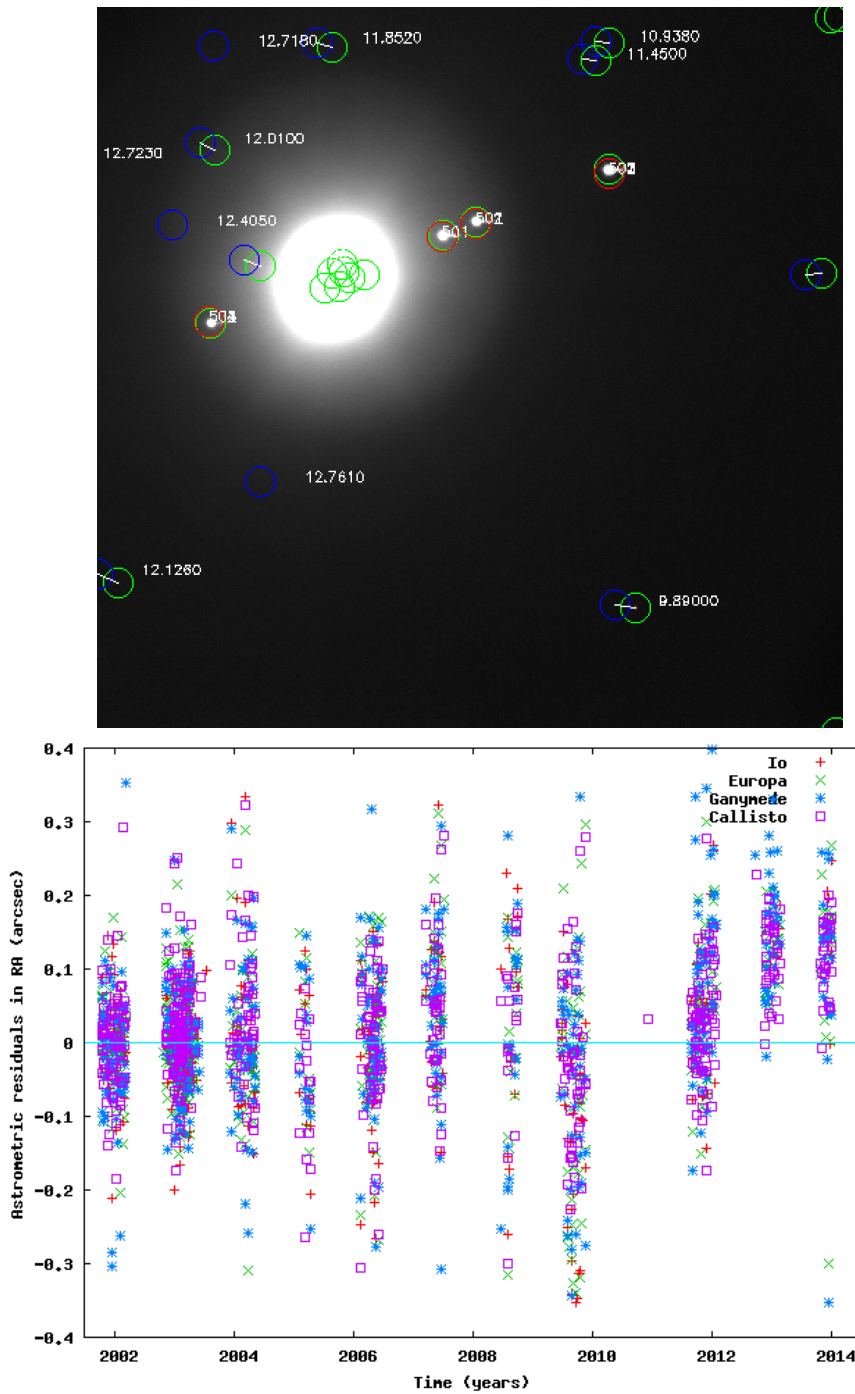


Figure 5: On the top, a CCD observation of Jupiter and the four Galilean moons obtained from the T120 at Haute-Provence Observatory in 2015. The stacking method allows getting stars while not saturating the bright moons. On the bottom are astrometric residuals of the four Galilean moons obtained from the FASTT survey (Stone et al. 2003). The offset after 2012 could be associated with an error on Jupiter ephemeris.

Expected results and their significance and application

This work shall provide the most extensive values on tidal parameters for Jupiter and Saturn allowing for discriminating among the various tidal and interior models that exist today. Physical parameters like k_2/Q , G , η , t_p , and t_a that are associated with specific tidal models will be solved directly by processing the radioscience and astrometry data. Simultaneous determination of the tidal ratio k_2/Q for Enceladus and possibly Europa/Ganymede will help probing the existence and sustainment of liquid ocean underneath their icy crust. This will have direct consequences for exobiology, in particular considering the development of life in the outer Solar System, where tides are the main source of heat.

Moreover, long-term evolution of exoplanets will have to be reconsidered using our results and key parameter values. For example, the excess of close resonant pairs, just outside the 2:1 and 3:2 mean motion resonances, could potentially be explained by resonance locking mechanism allowing for strong tides. Moreover, recent evidence of a quadratic acceleration on the mid-transit times of WASP12-b (Maciejewski et al. 2016) may have a different interpretation if high tidal dissipation within giant gaseous planets becomes a new paradigm. In general, a clear quantification of dissipative processes by tides within Jupiter and Saturn will serve as a fundamental basis for both observational and theoretical studies in planetary formation, dynamics and support to life's development in the Galaxy.

References

- Archinal, B.A., et al.: Report of the IAU Working Group on Cartographic Coordinates and Rotational Elements: 2009 *Celestial Mechanics and Dynamical Astronomy* 109, 101-135 (2011)
- Arlot, J.-E. and Emelyanov, N.V.: The NSDB natural satellites astrometric database *Astronomy and Astrophysics* 503, 631-638 (2009)
- Arlot, J.-E., Ruatti, C., Thuillot, W. et al., A catalogue of the observations of the mutual phenomena of the Galilean satellites made in 1991 during the PHEMU91 campaign, *A&A Supplement series*, 125, 399-405 (1997).
- Boué, G., Laskar, J. A collisionless scenario for Uranus' tilting. *Ap. J. Letters* 712, L44-L47 (2010).
- Charnoz, S. et al. Accretion of Saturn's mid-sized moons during the viscous spreading of young massive rings: Solving the paradox of silicate-poor rings versus silicate-rich moons. *Icarus* 216, 535 (2011).
- Cooper, N.J., Murray, C.D., Evans, M.W., Beurle, K., Jacobson, R.A. Astrometry and dynamics of Anthe (S2007 S 4), a new satellite of Saturn. *Icarus* 195, 765-777 (2008).
- Cooper, N., Evans, M.W., Meunier, L.E., Zhang Q.F., Baillie, K., Lainey, V., Murray, C.D., Thuillot, W., Vienne, A., Caviar: a software package for the astrometric reduction of spacecraft images, 6th ICATT Conference, Darmstadt (2016)

- Crida, A., Charnoz, S., Formation of Regular Satellites from Ancient Massive Rings in the Solar System, *Science*, Volume 338, Issue 6111, pp. 1196- (2012).
- Ćuk, M.; Dones, L.; Nesvorný, D., Dynamical Evidence for a Late Formation of Saturn's Moons, *The Astrophysical Journal*, Volume 820, Issue 2, article id. 97, 16 pp. (2016).
- Dermott, S. F. Tidal dissipation in the solid core of major planets *Icarus* 37, 310 (1979)
- Fuller, Jim; Luan, Jing; Quataert, Eliot, Resonance locking as the source of rapid tidal migration in the Jupiter and Saturn moon systems. *Monthly Notices of the Royal Astronomical Society*, Volume 458, Issue 4, p.3867-3879 (2016).
- Goldreich, P., Soter, S. Q in the solar system. *Icarus* 5, 375-389 (1966).
- Fuller, J. Saturn ring seismology: Evidence for stable stratification in the deep interior of Saturn. *Icarus* 242, 283-296 (2014)
- Iess, L., et al.: The Tides of Titan *Science* 337, 457-459 (2012)
- Jacobson, R. A. and Lainey, V.: Martian satellite orbits and ephemerides *Planetary and Space Science* 102, 35-44 (2014)
- Konopliv, A. S., et al.: The JPL lunar gravity field to spherical harmonic degree 660 from the GRAIL Primary Mission *Journal of Geophysical Research (Planets)* 118, 1415-1434 (2013)
- Konopliv, A. S., et al.: Mars high resolution gravity fields from MRO, Mars seasonal gravity, and other dynamical parameters *Icarus* 211, 401-428 (2011)
- Konopliv, A. S. and Yoder, C. F.: Venusian k2 tidal Love number from Magellan and PVO tracking data *Geophysical Research Letter* 23, 1857-1860 (1996)
- Lainey, V., Arlot, J.E., Vienne, A., New accurate ephemerides for the Galilean satellites of Jupiter. II. Fitting the observations, *A&A* 427, p.371-376 (2004).
- Lainey, V., Duriez, L., Vienne, A., New accurate ephemerides for the Galilean satellites of Jupiter. I. Numerical integration of elaborated equations of motion, *A&A* 420, p.1171-1183 (2004b).
- Lainey, V., Dehant, V., Pätzold, M., First numerical ephemerides of the Martian moons, *A&A* 465, Issue 3, 1075-1084 (2007).
- Lainey, V., A new dynamical model for the Uranian satellites, *PSS* 56, Issue 14, 1766-1772 (2008).
- Lainey, V., Arlot, J.E., Karatekin, Ö., Van Hoolst, T. Strong tidal dissipation in Io and Jupiter from astrometric observations, *Nature*, Volume 459, Issue 7249, pp. 957-959 (2009)
- Lainey, V., Karatekin, O., Desmars, J., Charnoz, S., Arlot, J.E., Emelyanov, N., Le Poncin-Lafitte, C., Mathis, S., Remus, F., Tobie, G., Zahn, J.P., Strong tidal dissipation in Saturn and constraints on Enceladus' thermal state from astrometry. *Ap. J.*, Volume 752, Issue 1 (2012).

Lainey, V., Jacobson, R. A., Tajeddine, R., Cooper, N. J., Murray, C., Robert, V., Tobie, G., Guillot, T., Mathis, S., Remus, F. and 8 coauthors, New constraints on Saturn's interior from Cassini astrometric data, *Icarus*, Volume 281, p. 286-296. (2017).

Lemoine, F. G., et al.: High-degree gravity models from GRAIL primary mission data *Journal of Geophysical Research (Planets)* 118, 1676-1698 (2013)

Love, A. E. H.: *Some Problems of Geodynamics* (Cambridge University Press) (1911)

Maciejewski, G. et al. Departure from the constant-period ephemeris for the transiting exoplanet WASP-12b, *Astronomy & Astrophysics*, Volume 588, id.L6, 6 pp. (2016)

Matson, D. L., et al.: Heat flow from Io *Journal of Geophysical Research* 86, 1664-1672 (1981)

Mazarico, E., et al.: The gravity field, orientation, and ephemeris of Mercury from MESSENGER observations after three years in orbit *Journal of Geophysical Research (Planets)*, 119, 2417 (2014)

Morbidelli, A.; Tsiganis, K.; Batygin, K.; Crida, A.; Gomes, R., Explaining why the uranian satellites have equatorial prograde orbits despite the large planetary obliquity. *Icarus*, Volume 219, Issue 2, p. 737-740 (2012).

Moyer, T.D.: *Formulation for observed and computed values of Deep Space Network observables* 576pp., Wiley, Hoboken, N.J. (2003)

Moyer, T.D.: *Mathematical formulation of the double-precision orbit determination program (DPDOP)* Technical report 32-1527, National Aeronautics and Space Administration (1971)

Murray, C.D., Cooper, N.J., Evans, M.W., Beurle, K. S/2004 S5: A new co-orbital companion for Dione. *Icarus* 179, 222-234 (2005).

Ogilvie, G. I., Lin, D. N. C. Tidal Dissipation in Rotating Giant Planets. *The Astrophysical Journal* 610, 477-509 (2004).

Pavlis, D.E., et al.: *GEODYN II system description, vol. 1-5, contractor report*, SGT Inc., Greenbelt, Md. (2013)

Peters, C. F.: Numerical integration of the satellites of the outer planets *Astronomy and Astrophysics* 104, 37-41 (1981)

Ray, R. D., et al.: Constraints on energy dissipation in the Earth's body tide from satellite tracking and altimetry *Geophysical Journal International* 144, 471-480 (2001)

Ray, R.D., et al.: Detection of tidal dissipation in the solid Earth by satellite tracking and altimetry *Nature* 381, 595-597 (1996)

- Remus, F., Mathis, S., Zahn, J.-P., Lainey, V. The surface signature of the tidal dissipation of the core in a two-layer planet. *Astronomy & Astrophysics* 573, 23 (2015).
- Remus, F., Mathis, S., Zahn, J.-P., Lainey, V. Anelastic tidal dissipation in multi-layer planets. *Astronomy & Astrophysics* 541, 165 (2012).
- Robert, V. et al., A new astrometric measurement and reduction of USNO photographic observations of the main Saturnian satellites: 1974-1998. *A&A*, Volume 596, id.A37, 10 pp (2016).
- Robert, V. et al. A new astrometric reduction of photographic plates using the DAMIAN digitizer: improving the dynamics of the Jovian system, *Monthly Notices of the Royal Astronomical Society* 415, 701 (2011).
- Robert, V., Pascu, D., Lainey, V., Arlot, J.E., A new astrometric measurement and reduction of USNO photographic observations of Phobos and Deimos: 1967-1997, *A&A* Volume 582, id.A36, 8 pp. (2015).
- Safronov, V.S., Sizes of the largest bodies falling onto the planets during their formation, *Sov. Astron.*, vol. 9, p. 987-991 (1966).
- Sharpless, B.P.: Secular accelerations in the longitudes of the satellites of Mars *Astronomical Journal* 51, 185-186 (1945)
- Spencer, J.R., et al., Cassini encounters Enceladus: Background and the discovery of a south polar Hot Spot *Science* 311, 1401-1405 (2006)
- Stone, Ronald C. et al. Upgrades to the Flagstaff Astrometric Scanning Transit Telescope: A Fully Automated Telescope for Astrometry, *The Astronomical Journal*, Volume 126, Issue 4, pp. 2060-2080 (2003).
- Tajeddine, R., Cooper, N., Lainey, V., Charnoz, S., Murray, C. Astrometric reduction of Cassini ISS images of the Saturnian satellites Mimas and Enceladus, *A&A*, 551 (2013).
- Tajeddine, R., Rambaux, N., Lainey, V., Charnoz, S., Richard, A., Rivoldini, A., Noyelles, B., *Science*, Volume 346, Issue 6207, pp. 322-324 (2014).
- Thuillot, W, Lainey, V., Dehant, V., Gurvits, L., Oberst, J., Vermeersen, L.L.A., Marty, J.C., Hussmann, H., European Partnership for Computing Ephemerides, FP7-SPACE-2010-1, area 9.2.1-SPA.2010.2.1-03, grant agreement n. 263466 (2011).
- Wahr, J.M.: Body tides on an elliptical, rotating, elastic and oceanless earth *Geophys. J. R. astr. Soc.* 64, 677-703 (1981)
- Williams, J. G., et al.: Lunar interior properties from the GRAIL mission *Journal of Geophysical Research (Planets)* 119, 1546-1578 (2014)

Note d'accompagnement

Coordination of scientific teams and international networks :

Coordination of scientific work is an important part in the career of a researcher today. During the 15 years following my PhD defense, I took the lead of various working groups, including international teams and networks. I give below a list of the major scientific teams in which I was involved and coordinated.

ENCELADE Team :

2007 until - : coordinator of the ENCELADE international team (UPMC, Paris Scientific council and ISSI fundings)

<http://www.issibern.ch/teams/saturnastrometry/>

I initiated in 2007 a working groupe called ENCELADE. The main objectiv of our team was to quantify the orbital deceleration of the Saturnian moon, Enceladus, due to the tides it suffers from its primary. This happened to be the beginning of a whole quest, requiring larger expertise from stellar physics to the dynamics of rings and interior modeling of icy moons. My team now gathers a bit less than 20 researchers, including 4 post-docs (3 of them where formerly PhD students within ENCELADE) and over 8 laboratories. We meet twice per year, inviting external researchers some times. We study the systems of the four outer planets of the Solar system, with special emphasize on astrometry, orbital/rotational dynamics and tidal effects.

In 2009, our team obtained an EMERGENCE funding from UPMC. This allowed us to obtain a PhD student (R.Tajeddine) and enough funding for meeting regularly in Europe.

In 2014, our working group was selected to be an International ISSI (International Space Science Institute) team and renamed ENCELADE 2.0. We are now in process of extending our collaboration with ISSI for two more years. This shall allow us to go on working properly until the end of Cassini and Juno missions.



The ENCELADE team at UPMC the 22nd January 2014 (from left to right: R.Tajeddine, V.Lainey, K.Baillié, J.E.Arlot, C.Le Poncin-Lafitte, V.Robert, J.P.Zahn, Ö.Karatekin, B.Noyelles, S.Mathis, N.Rambaux, S.Charnoz, S.Renner, N.Cooper, M.Elmoutamid, C.Murray, F.Remus).

ESPaCE Network :

June 2011 until - : Deputy coordinator of the European FP7 network ESPaCE (**FP7-SPACE funding**)

<http://www.imcce.fr/espace/start>

In 2010, I submitted with William Thuillot a proposal to the European FP7-Space open call. The basic idea was coming from my experience as a post-doc at the Royal Observatory of Belgium. There, I realized the close similitude between the technics involved in space geodesy and in the development of ephemerides of Solar system objects. In particular, the idea of merging radio-science data and astrometric data appeared promising if not necessary. As a matter of fact, such method was already applied since decades in the United States with their own space data. It was time for Europe to do the same.

Fortunately, our proposal was selected. The ESPaCE (European Space Partnership in Computing Ephemerides) European network provided new ephemerides of the Mars, Jupiter, Saturn and Uranus moons, while making important progress toward global inversion. European space missions like Mars Express and JUICE are still benefiting from our network. Today, ESPaCE is still alive and partly funded, looking for the next European open call.



The ESPaCE network the 30th of May 2012 at Dwingeloo. W.Thuillot (coordinator) and myself (deputy coordinator) are at the center on the right.

Pégase Team :

Jan 2015 until - : Coordinator of the scientific team Pégase (IMCCE)

In 2014, I decided to take the lead of a new scientific team at IMCCE. In particular, I wanted to have more synergy inside my laboratory, open to many aspects of celestial mechanics and astrometry (including exo-planets), and allowing young students to share efficiently the knowledge of the other researchers in their team. In January 2015, the Pégase team was officially born and gathered more than 20 persons (researchers, PhD students and post-docs).

Our topic includes basically astrometry and celestial mechanics as two important disciplines. The objects we are studying go from artificial satellites and space debris to natural moons, asteroids, comets and exo-planets.



The Pégase team on the 11th of June 2015 at the Lille Observatory. From left to right and top to bottom : S.Eggl, D.Hestroffer, B.Noyelles, M.Fouchard, J.E.Arlot, S.Renner, P.David, K.Baillié, J.Desmars, W.Polycarpe, myself, W.Thuillot, M. Kudryashova, E.Saquet, F.Deleflie, A.Vienne, X.Xi, S.li, N.Thouvenin, J.Daquin. Mrs Balenguin and her daughter, as well as N.Emelianov (invited resaecher) are on the picture.

Thesis advisor :

I co-advised 6 PhD students between 2010 and 2017 :

1-V.Robert (J.E.Arlot, V.Lainey) : PhD thesis defended in 2011

J.E.Arlot was officialy the principal advisor. In practice, we supervised his work 50% each. V.Robert is a permanent researcher at the IPSA (Institut Polytechnique des Sciences Avancées) and is one of my closest collaborator. He is a member of Pégase team since its creation.

-Robert, V., Lainey, V., Pascu, D., Arlot, J.-E., De Cuyper, J.-P., Dehant, V., Thuillot, W., A&A (2014)

-Beauvalet, L., **Robert, V., Lainey, V.,** Arlot, J.E., Colas, F., Astronomy & Astrophysics, Volume 553, id.A14, 22 pp.(2013)

-Arlot, J.E., Desmars, J., **Lainey, V., Robert, V.**, Planetary and Space Science, Volume 73, Issue 1, p. 66-69 (2012).

-**Robert, V.**, de Cuyper, J.-P., Arlot, J.-E., de Decker, G., Guibert, J., **Lainey, V.**, Pascu, D., Winter, L., Zacharias, N., MNRAS (2011)

2-L.Beauvalet (V.Lainey, J.E.Arlot) : PhD thesis defended in 2011

Even though Jean-Eudes Arlot was the official advisor, I supervised 80% of Laurène's work. After her PhD thesis, L.Beauvalet had a post-doc position at the Shanghai observatory for two years. She then moved to the Rio observatory. She has now moved to the private industry.

-**Beauvalet, L.**, Robert, V., **Lainey, V.**, Arlot, J.E., Colas, F., Astronomy & Astrophysics, Volume 553, id.A14, 22 pp.(2013)

-**Beauvalet, L., Lainey, V.**, Arlot, J.-E., Bancelin, D., Binzel, R. P., Marchis, F., Planetary and Space Science, Volume 73, Issue 1, p. 62-65 (2012).

-**Beauvalet, L., Lainey, V.**, Arlot, J.E., Binzel, R., Astronomy & Astrophysics, Volume 540, id.A65, 9 pp. (2012)

3-R.Tajeddine (V.Lainey, S.Charnoz) : PhD thesis defended in 2013

Radwan Tajeddine benefited from my EMERGENCE / UPMC funding that I obtained in 2009. I supervised 90% of his thesis, with the help of Sébastien Charnoz. After his defense, R.Tajeddine moved to Cornell University. He is still post-doc there, working on Saturnian rings and satellites with the Cassini-ISS data. In 2014, we had the pleasure to see one of his paper accepted in the Science journal (Tajeddine et al. 2014).

-**Tajeddine, R., Lainey, V.**, Cooper, N., Murray, C., Astronomy & Astrophysics, Volume 575, id.A73, 6 pp. (2015).

-Cooper, N. J., Murray, C. D., **Lainey, V., Tajeddine, R.**, Evans, M. W., Williams, G. A., Astronomy & Astrophysics, Volume 572, id.A43, 8 pp. (2014).

-**Tajeddine, R.**, Rambaux, N., **Lainey, V.**, Charnoz, S., Richard, A., Rivoldini, A., Noyelles, B., Science, Volume 346, Issue 6207, pp. 322-324 (2014).

-**Tajeddine, R.**, Cooper, N. J., **Lainey, V.**, Charnoz, S., Murray, C. D., Astronomy & Astrophysics, Volume 551, id.A129, 11 pp. (2013).

4-F.Remus (J.P.Zahn, V.Lainey et S.Mathis) : PhD thesis defended in 2013

Jean-Paul Zahn and Stéphane Mathis supervised most of Françoise's work. In practice, my involvement was at the level of 15% for my expertise in orbital dynamics and determination of tidal effects from astrometry. F.Remus obtained in 2012 the L'Oréal prize « Pour les femmes et la science » for her PhD work. After her defense she obtained an ATER (1-year University

contract) and did simultaneously her research at IMCCE. Then, she moved to a post-doc position at CEA/LUTH.

-**Remus, F.**, Mathis, S., Zahn, J.-P., **Lainey, V.**, *Astronomy & Astrophysics*, Volume 573, id.A23, 5 pp. (2015).

-**Lainey, Valéry**, Karatekin, Özgür, Desmars, Josselin, Charnoz, Sébastien, Arlot, Jean-Eudes, Emelyanov, Nicolai, Le Poncin-Lafitte, Christophe, Mathis, Stéphane, **Remus, Françoise**, Tobie, Gabriel, Zahn, Jean-Paul, *The Astrophysical Journal*, Volume 752, Issue 1, article id. 14, 19 pp. (2012).

-**Remus, F.**, Mathis, S., Zahn, J.-P., **Lainey, V.**, *Astronomy & Astrophysics*, Volume 541, id.A165, 17 pp. (2012).

5-Y.Duchemin (J.E.Arlot, V.Lainey) : PhD thesis to be defended in 2017

Jean-Eudes Arlot and myself are co-supervising Yann Duchemin's work. He is an engineer working and teaching at ESIGELEC engineer school. His PhD topic deals with autonomous navigation in space.

6-W.Polycarpe (A.Vienne, V.Lainey) : PhD thesis to be defended in 2018

I am supervising with Alain Vienne the work of William Polycarpe. His topic deals with the study of the long term past evolution of the Saturnian system. In particular, we are considering the possibilities associated with strong tides within Saturn and the Nice model. This thesis work is part of the ENCELADE 2.0 activities.

I supervised many master and engineer training courses including those of (non exhaustive list) : L.Beauvalet, S.Bertone, F.Boudinot, Y.Duchemin, S.Lounis, R.Tajeddine, C.Yao...

Last, I recently worked with Kévin Baillié (post-doc) on the dynamical interaction between Saturn's rings and moons.

Ephemerides development :

Since my PhD in 2002, I developed new ephemerides of many natural satellites of the Solar system.

Mars moons :

Mars moons ephemerides have been reconsidered in 2004 with the arrival of Mars Express. Several flybys between Mars Express and Phobos devoted to radio-science arose and some of them were considered essential for understanding the interior of Phobos and its formation history. The last one arose on the 29th of December 2013. The success of the experiment required an accuracy in the Phobos ephemeris of 100 meters. During my work I exhibited (in

parallel with R.Jacobson at JPL) a misfit of about one kilometer between SRC-Mars Express data and Mars Reconnaissance Orbiter. Such possible error prevented us to guarantee 100 m accuracy (not precision). Later on, it appeared that 10 m accuracy would be required to reach the scientific objective of Mars Radio Science team (Mars Express). If 100 meters is still feasible, assuming no biases affects the astrometric data, 10 m accuracy will require different observation mean like a Phobos lander.

Galilean moons :

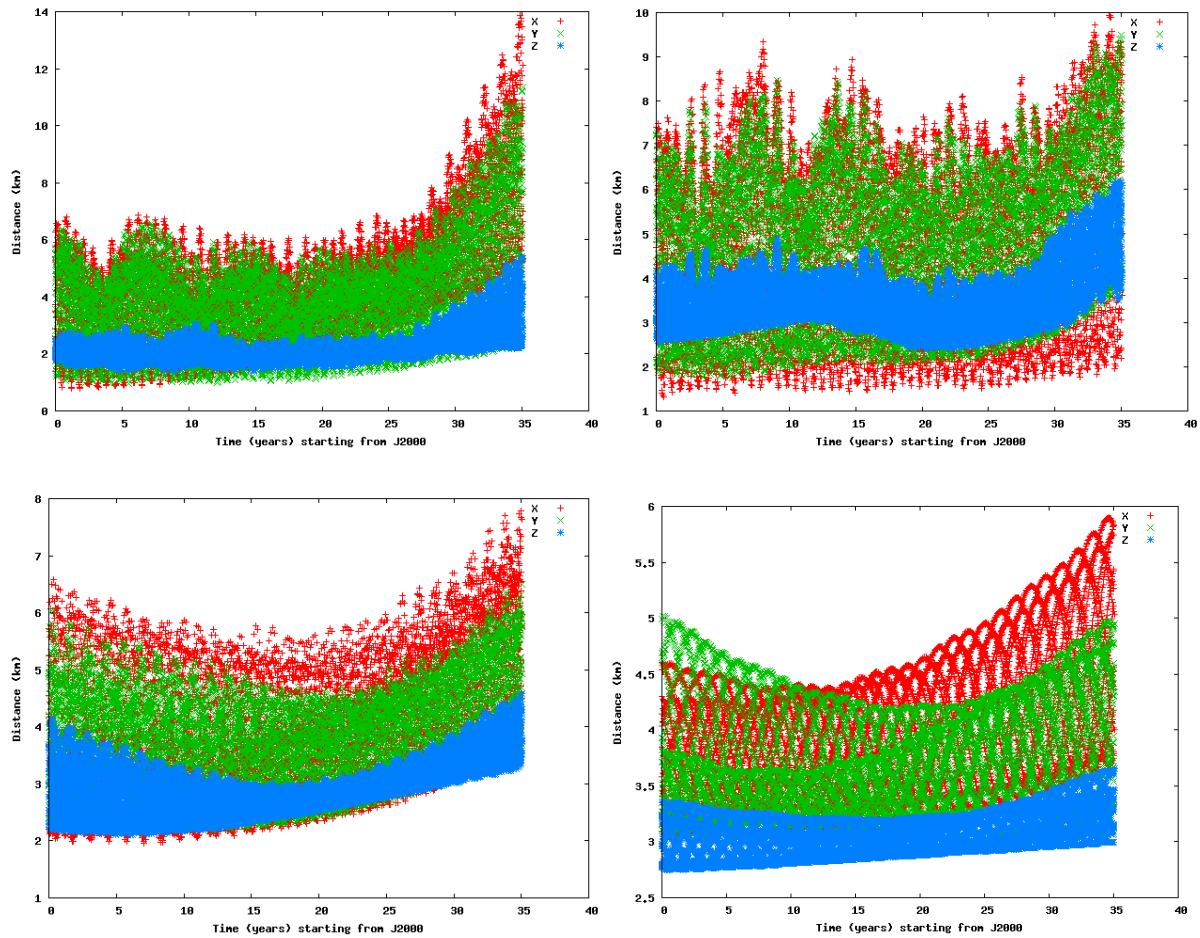
The ephemerides of the Galilean moons are useful for both, forecasting the mutual events between the moons arising every six years, and responding to space agencies for mission development like JUICE. Since my thesis, already devoted to the Galilean system, I regularly updated the ephemerides of the main Jovian moons. More recently, I am collaborating with the European Space Operational Center (ESOC) to provide the uncertainty on the Galilean moon position at the time of the arrival of JUICE.

Saturnian moons :

The huge success of the Cassini mission allowed us to obtain about 1000 astrometric image per Saturnian satellite and with an accuracy of typically 10 km. Up-to-date ephemerides of the Saturn system required to consider these data. Moreover, ESPaCE network allowed to rereduce the USNO photographic plates of the Saturn system. New ephemerides developed in 2015 consider the new sets, in addition with former data. A global inversion of all Saturn data, including radio-science and the totality of the ISS astrometric data is planned after the end of the Cassini mission. I will be part of it by moving to JPL for three years, starting on July 2017.

Uranian moons :

In 2008, the first observations of the mutual events of the Uranian moons occurred. Such observations arise every 42 years (half of the Uranian revolution period). To predict properly such events, I provided new ephemerides of these moons just before the campaign. It appeared that the Uranus position in space was itself not properly known. In particular, the improvement of the Uranian moon ephemerides is necessary for improving the ephemeris of Uranus itself.



From left to right and top to bottom : uncertainty on the orbital position of Io, Europa, Ganymede and Callisto after considering a realistic set of observations up to 2029.

Specific teaching :

I am teaching since 2007 in the master of the Paris Observatory. One of my lesson deals with the numerical simulation of a spaceprobe perturbed by the Sun and planets. The students are supposed develop their own code, almost from scratch, and be able to fit the initial state vector of the probe to real ephemeris provided by the SPICE. The idea is to allow students understanding the possibility of masking a dynamical effect (at least in a part) into the fit.

I also teach astrometry as a semester course and go every year for a full week at the OHP (Haute-Provence Observatory).

More marginally, I participate to international school and lessons (Beijing 2008, Nice 2011, Guangzhou 2016).



Alain Vienne and myself giving lectures at the Jinan University (Guangzhou, December 2016).

Abstract

From the ocean underneath Europa, to the intense volcanic activity of Io or the deep atmosphere of Titan, natural satellites present a large variety of worlds still mostly unexplored. While simple temperature considerations previously constrained the presence of liquid water to just beyond Mars' orbit, tidal effects mean that liquid water can exist much further from the Sun. Hence, habitability could exist in a wider variety of places, whether in our Solar system or extra-solar ones. In this context I revisited part of our current knowledge in planetology from the perspective of astrometry. Monitoring and analysing the orbital motion of moons can provide an alternative and straightforward insight into the orbital and interior evolution of satellite systems. As already demonstrated for Io's activity (Lainey et al., *Nature* 2009), it may be the *only* way to assess some fundamental processes arising deep within these worlds. Once the key physical parameters are quantified, there are clear applications to the possible orbital states of exoplanets and their putative moons.

The global methodology is similar to space geodesy. Variational equations are solved simultaneously with the equations of motion. Since 2004, I am developing a specific N-body code, called NOE (Numerical Orbit and Ephemerides), aimed at simulating the orbit of solar system objects with more emphasis on natural satellites. Using a large number of observation kinds, obtained with several different techniques and including spaceprobe data, I can solve for many parameters ruling the physics of the system. Besides the initial state vectors of each moon, the parameters of interest can be the gravity fields (including the mass and C_{np} , S_{np} coefficients), the precession and nutations of the primary (including the orientation of the pole in space), the principal forced libration amplitude of the secondaries, the tidal parameters k_2 and Q , the relativistic PPN terms γ and β ...

In addition to the scientific results of sometimes high importance coming from the comparison between predicted orbital motions and the observed ones, I can provide as a subproduct high accurate ephemerides. The accuracy of these latter are directly related to the degree of accuracy in the modeling, and so in the accuracy of our vision of the system. For many satellite systems, the largest unknown is on the physics itself, directly associated with our vision of the system, ultimately derived from our believe on the formation and longterm evolution of the moons. All this is a neverending story for three reasons : i) space agencies and the professional community are always looking for more ephemerides precision ; ii) ephemerides are drifting with time and, as a consequence, need to be refitted regularly ; iii) mankind is curious about the nature, the creation and the evolution of its own world.

Appendix

First numerical ephemerides of the Martian moons

V. Lainey^{1,2}, V. Dehant¹, and M. Pätzold³

¹ Royal Observatory of Belgium, 3 avenue Circulaire, 1180 Bruxelles, Belgium
e-mail: Lainey@oma.be

² Institut de Mécanique Céleste et de Calcul des Ephémérides-Observatoire de Paris, UMR 8028 du CNRS,
77 avenue Denfert-Rochereau, 75014 Paris, France

³ Institut für Geophysik und Meteorologie, Universität zu Köln, Albertus-Magnus-Platz, 50923 Cologne, Germany

Received 20 April 2006 / Accepted 22 December 2006

ABSTRACT

We present new ephemerides of Phobos and Deimos that are fit to observations from 1877 to 2005 and include recent spacecraft observations by Mars Global Surveyor and Mars Express. In contrast to earlier models, this is the first completely numerical one. In particular, the tidal effects have been modeled by the tidal bulge raised by each moon on the planet, instead of fitting secular accelerations in the satellite longitudes. This partly avoids absorbing the Deimos observational errors in its related tidal acceleration. Moreover, applying this model to other systems will be easier. Our estimate of the Martian dissipation is $Q = 79.91 \pm 0.69$ (1σ -formal error) when assuming $k_2 = 0.152$ for the Martian Love number and $Gm_{\text{Ph}} = 0.68 \times 10^6 \text{ m}^3/\text{s}^2$ for the Phobos mass. We also report the possibility of fitting the Phobos oblateness gravity field. We suspect a non-uniform density for Phobos or a bias in either the observations or the Martian gravity field. A FORTRAN subroutine that computes the Martian moons' ephemerides is available on request.

Key words. planets and satellites: general – ephemerides – celestial mechanics – astrometry

1. Introduction

The orbital motions of the Martian moons are among those most studied in the Solar System. Since their discovery in 1877, a variety of dynamical models, first fit to Earth-based observations and then to spacecraft observations, have been developed. Ephemerides have been developed by Sinclair (1972), Shor (1975), and Sinclair (1978) during the Viking era, confirming the secular tidal acceleration previously found by Sharpless (1945). Later, in the early 1990's, more orbital studies were developed mainly in support of the Phobos 2 spacecraft mission. Of particular interest were the ephemerides derived by Jacobson et al. (1989) and by Morley (1990) that were used by JPL and ESOC, respectively. These ephemerides are available in the SPICE library at the address <ftp://naif.jpl.nasa.gov/pub/naif/MEX/kernels/spk>.

No new adjustments to the observations were done before 2005. As a result, the Martian moon ephemerides have drifted, as pointed out by Neumann et al. (2004), who used the passive mode of the MOLA instrument onboard Mars Global Surveyor (MGS) to detect the Phobos shadow on the Martian surface. After data reduction, they found that the observed position of Phobos was ahead of its predicted position by a difference of 6 s of time (12 km). This was later confirmed by Bell et al. (2005), using observations from the Mars Exploration rovers (MER). With some 6 transit events (including two events by Deimos), they also found a significant drift of 38 km on the Deimos position.

Bills et al. (2005) used some 16 observations covering the years 1998–2004 to correct the shift between the observed and computed positions of Phobos. They used the model of Jacobson et al. (1989) and fit only three terms from the longitude

expression to the MGS observations. They succeeded in reducing the former drift on the Phobos orbital motion. However, as only Phobos was observed by MOLA (the shadow of Deimos on the Martian surface being too faint), no attempt could be made to improve the motion of Deimos. Moreover, the physical parameters from 1989 are still being used. Of particular importance are the Martian gravity field and the precession, which have been significantly improved in recent years (Lemoine et al. 2001; Yuan et al. 2001; Seidelmann et al. 2002; Konopliv et al. 2006).

The Super Resolution Camera (SRC), part of the High-Resolution Stereo Camera (HRSC) onboard Mars Express (MEX), started an observation campaign of the Martian moons (see Oberst et al. 2006) in 2004–2005. The analysis of the ephemerides residuals between the predictions from ESOC and JPL with a set of 36 satellite observations again confirmed the drift of the ephemerides (mainly across track for the ESOC model and along track for the JPL model). Phobos and Deimos were found 12 km and 50 km, respectively, ahead of their predicted positions by the JPL model. The ESOC model predicted better with 8 km and 18 km discrepancies on the Phobos and Deimos positions, respectively.

One of the most interesting purposes for studying the orbital evolution of the Martian moons is to investigate the Martian tidal dissipation factor. Tidal dissipation induces a phase lag between the bulge direction raised by one satellite and the Mars-satellite direction. As a consequence, momentum between the planetary rotation and the satellite orbital motion is exchanged. When the satellite revolves faster than the planet rotates, a secular acceleration on the satellite longitude is generated. This effect is observed on the orbital motion of Phobos. More difficult is detecting the tidal deceleration of Deimos (this satellite revolves more

Table 1. Catalogue of all observations used in this paper.

Reference	Frame	Type	Period	Place	P/M	D/M	P/D	P	D
Morley (1989)	1+2+3	0+1+2	1877–1982	23 sites	2212	2600	100		
Christie et al. (1878)	1	0	1877–1877	Greenwich, Oxford	3	12			
Young (1880)	1	0	1879–1879	Princeton	4	10			
Shor (1989)	1+3+4	1	1978–1988	7 sites	268	221	195		
Kiselev et al. (1989)	1	1	1986–1986	Ordubad	117	56			
Kiseleva & Chanturiia (1988)	1	1	1986–1986	Ordubad	6				
Bobylev et al. (1991)	1	1	1988–1988	Pulkovo, Ordubad	164	54	147		
Colas (1992)	1	1	1988–1988	Pic-du-Midi			813		
Izhakevich et al. (1990)	4	1	1988–1988	Majdanak	65	47	88		
Jones et al. (1989)	1	0	1988–1988	La Palma	88	12	66		
Kalinichenko et al. (1990)	1	1	1988–1988	Abastuman	19	1	17		
Nikonov et al. (1991)	1	1	1988–1988	Boyeros	23				
Tel'nyuk-Adamchuk et al. (1990)	4	1	1988–1988	Kiev	99	74	32		
Kudryavtsev et al. (1992)	4	3	1988–1988	Majdanak				660	639
Duxbury & Callahan (1988)	3	3	1976–1980	Viking 1-2				166	109
Duxbury & Callahan (1989)	3	3	1971–1972	Mariner 9				49	31
Kolyuka et al. (1991)	3	3	1989–1989	Phobos 2				37	8
Pascu (1995)*	1	1	1967–1988	Flagstaff, Washington	217	223			
Ledovskaya (2001)*	4	3	1963–1988	Kiev, Kitab, Maid.				133	283
Rohde (2003)*	1	0	2003–2003	Flagstaff			196		
Bills et al. (2005)	4	3	1977–2004	MGS, Viking lander 1				17	
Oberst et al. (2006)	4	3	2004–2005	Mars Express				26	10

slowly than Mars rotates). Both accelerations, however, were fit in the former models, providing a good agreement with the Phobos acceleration. The deceleration of Deimos is still uncertain and probably more a matter of observational errors.

The density of Phobos is less constrained than the Martian tidal dissipation and usually assumed to be uniform. So far, the different flybys at Phobos by the Viking 1 and Phobos 2 spacecrafts only quantified the satellite mass. The Phobos gravity field (essentially the coefficients C_{20} and C_{22}), however, induces secular terms on the mean anomaly, node, and pericenter of the Phobos motion, which are different from the quadratic behavior induced by the tidal effects. Several authors tried to use their ephemerides solution to verify the constant density assumption (see Chapront-Touze 1990; Emelyanov et al. 1993). The uncertainties on the Martian gravity field (often fit during the Martian moon ephemerides construction) were probably too large to answer this question definitively.

This paper is divided as follows. Section 2 describes all available observations of the Martian moons. Section 3 presents the numerical method introduced to model the satellite motions. Section 4 presents the fit of the model to the JPL model. In Sect. 5 the fit of our model directly to the observations is presented. Section 6 summarizes the procedure to provide the Martian moons ephemerides representation to the user. Section 7 compares the ephemerides with the JPL/ESOC ephemerides. The last section discusses the influence of few non introduced perturbations in the present model, along with the question of the density of Phobos.

2. The observations

The observations of the Martian moons are numerous and have different levels of accuracy. An important available database¹

was developed jointly at the Sternberg institute and the Institut de Mécanique Céleste et de Calcul des Ephémérides by Emelianov and Arlot. This database includes the widely used catalogue compiled by Morley (1989), which considers most of the ground-based observations from 1877 to 1982. Several other Earth-based observations (sometimes unpublished) are also included. Of great interest are the observations in 1988 by Kudryavtsev et al. (1992) at the time of the Phobos 2 mission.

Between 1988 and 1998, the Martian moons seem to have been disregarded by the observers. In 2003 Rohde, Ries, and Pascu (priv. com.) made 196 CCD observations over 4 nights of the Martian moons at Flagstaff. These are intersatellite observations (the observed position of Phobos with respect to the position of Deimos) and are among the most accurate observations made from the Earth.

The model presented here benefited from the large set of spacecraft observations done with Mariner 9, Viking 1-2, Phobos 2, but also from MGS (Bills et al. 2005) and Mars Express observations (Oberst et al. 2006). The last set includes 26 observations of Phobos with an accuracy of 0.5–5 km and 10 observations of Deimos with an accuracy of 1 km.

Table 1 summarizes the whole set of observations considered in this work. A star (*) denotes unpublished observations. The letters P, D, and M denote respectively Phobos, Deimos, and Mars. P/M and D/M refers to observations relative to Mars, P/D refers to intersatellite observations and P, D are absolute observations. For the second and third columns respectively, the conventions are as follow: 1 = true equator of the date, 2 = B1900 equator, 3 = B1950 equator, 4 = J2000 equator; 0 = separation and position angle coordinates (s, p), 1 = tangential coordinates (X, Y), 2 = differential coordinates ($\Delta\alpha, \Delta\delta$), 3 = absolute coordinates (α, δ). A part of the data set has not been used after a preliminary study of the residuals revealed that there is a discrepancy between the different observational sets (see Sect. 5 for details).

In view of the number and full coverage of the most accurate observations of the Martian moons, we decided to perform three different fits. In particular, the possibility of using new spacecraft

¹ This database is available on the internet at the following addresses:
<http://lnfm1.sai.msu.ru/neb/nss/index.htm>
<http://www.imcce.fr/fr/ephemerides/generateur/saimirror/obsindhf.htm>

observations (MGS-MEX) makes it feasible to fit the Martian moons' ephemerides (and so the Martian dissipation) on shorter time scales than is usually done. The first fit introduced spacecraft observations from 1971 to 2005 only (Sect. 5.2). A second fit used the most accurate Earth-based astronomical observations starting with Pasqu's observations in 1967 and all spacecraft observations until 2005. This fit is presented in Sect. 5.3. The last fit combined the spacecraft observations and a number of observations available from 1877 to 1950. This fit is described in Sect. 5.4.

A limitation to the Viking observations (and to a lesser extent also the Mariner 9 observations) is the uncertainty in the spacecraft positions at the time of the observations. Those have been estimated to be 8 km and 4 km for Viking 1-2 and Mariner 9 spacecraft, respectively (Duxbury & Callahan 1988, 1989). To reduce these uncertainties, the authors have suggested estimating two more parameters related to the spacecrafts' position errors, during the fit process. Following Chapront-Touze (1990), these have not been introduced to avoid a high number of parameters. We introduced updated spacecraft positions using SPICE kernel when available. These new positions were computed by Konopliv in 1995 (SPICE file header). We found differences between the SPICE positions and the positions published in Duxbury & Callahan (1988), and Duxbury & Callahan (1989) of less than 500 m for the Mariner 9 data and a few tens of kilometers for the Viking spacecraft.

3. The numerical model

The software used for numerical integration is called Numerical Orbit and Ephemerides (NOE) and is based on the work developed in Lainey et al. (2004). It was developed at the Royal Observatory of Belgium mainly for computing the ephemerides of natural satellites. It is an N-body code that incorporates highly sensitive modeling and can generate partial derivatives, which are needed to fit the initial positions, velocities, and other parameters (masses, C_{20} , C_{40} , ...) to the observation data.

The model presented in this work introduces (i) the Martian gravity field MGM1041C up to degree² 10 (Tyler et al. 2003); (ii) the perturbations of the Sun, Jupiter, Saturn, the Earth, and the Moon using DE406 ephemerides (Standish 1998); (iii) the mass of each Martian moon³ (Phobos mass borrowed from Tyler et al. 2003 and Deimos mass from Yuan et al. 2001); and (iv) the IAU2000 Martian precession/rotation (Seidelmann et al. 2002).

In principle, the secular acceleration (deceleration) of the Martian moons is directly related to the Martian Love number k_2 , the Martian dissipation factor Q , and the mass of each moon. While the usual method fits two uncorrelated quadratic terms in the satellite longitudes, the tidal effects are modeled here in a more rigorous way by introducing a tidal potential. This method allows a better fit of the Phobos and Deimos secular accelerations by linking them to the same physical parameters. In particular, unrealistic acceleration of the motion of Deimos is automatically rejected, as Deimos revolves more slowly than Mars rotates. The tidal effects were introduced using Mignard's formulation (Mignard 1980), which models the tidal bulge by a time

shift Δt between the gravitational excitation by the satellite and the viscoelastic response of the planet. Actually Δt can be related to the Martian dissipation factor Q by the simple relation

$$\Delta t = \frac{T \arcsin(1/Q)}{2\pi} \quad (1)$$

where T is the tidal excitation period depending on the Martian rotation period T_p . The satellite orbital motion period T_s is related to it by

$$T = \frac{T_p T_s}{2|T_p - T_s|}. \quad (2)$$

We introduced two different time shifts to take the tidal bulges of Phobos and Deimos into account. Mignard (1980) neglected the first part of his potential U_0 , because he was mainly interested in the long-term evolution. This missing part has been added in the final tidal force \mathbf{F}^T acting on a moon, which is induced by the tidal bulge raised by this moon on the planet. \mathbf{F}^T takes the form

$$\mathbf{F}^T = -\frac{3k_2 G m^2 (E_r)^5}{r^8} \left(\mathbf{r} + \Delta t \left[\frac{2\mathbf{r}(\mathbf{r} \cdot \mathbf{v})}{r^2} + (\mathbf{r} \times \boldsymbol{\Omega} + \mathbf{v}) \right] \right) \quad (3)$$

where m , E_r , \mathbf{r} , \mathbf{v} , $\boldsymbol{\Omega}$ are the moon mass, the Martian equatorial radius, the position and velocity vectors of the moon, and the Martian angular velocity vector, respectively. In the following, the Martian Love number has been fixed to $k_2 = 0.152$ (Konopliv et al. 2006). Bills et al. (2005) mention, however, the necessity of introducing the higher harmonic terms involving k_3 and k_4 in the dynamics. As these terms are still mostly unknown, it was preferred to keep only the k_2 term. Hence, the fit of the dissipation factor Q more likely provides an effective value of Q by partly absorbing the loss of the higher harmonics. The related acceleration in the model will, however, be correct.

The dynamical system is numerically integrated in a planetocentric frame with inertial axes (conveniently the Earth mean equator J2000). Hence, denoting \mathbf{r}_j the position vector of a body P_j (a satellite, the Sun, or a perturbing planet), the equation of motion of the satellites has the usual form of

$$\ddot{\mathbf{r}}_i = -\frac{G(m_0 + m_i)\mathbf{r}_i}{r_i^3} + \sum_{j=1, j \neq i}^N Gm_j \left(\frac{\mathbf{r}_j - \mathbf{r}_i}{r_{ij}^3} - \frac{\mathbf{r}_j}{r_j^3} \right) + G(m_0 + m_i)\nabla_i U_{j0} + \sum_{j=1, j \neq i}^N Gm_j \nabla_j U_{j0} \quad (4)$$

where U_{j0} denotes the oblateness gravity field of the planet. The associated force is computed using a rotation matrix of angles⁴ ($\alpha_0 + \frac{\pi}{2}$, $\frac{\pi}{2} - \delta_0$, W) and its associated inverse.

Denoting c_l as an unspecified parameter of the model that shall be fit (e.g. $\mathbf{r}(t_0)$, $\dot{\mathbf{r}}(t_0)$, Q ...), a useful relation is

$$\frac{\partial}{\partial c_l} \left(\frac{d^2 \mathbf{r}_i}{dt^2} \right) = \frac{1}{m_i} \left[\sum_j \left(\frac{\partial \mathbf{F}_i}{\partial \mathbf{r}_j} \frac{\partial \mathbf{r}_j}{\partial c_l} + \frac{\partial \mathbf{F}_i}{\partial \dot{\mathbf{r}}_j} \frac{\partial \dot{\mathbf{r}}_j}{\partial c_l} \right) + \frac{\partial \mathbf{F}_i}{\partial c_l} \right]. \quad (5)$$

Hence, partial derivatives of the solutions with respect to initial positions and velocities of the satellites and dynamical parameters are computed from numerical integration of Eq. (4) and simultaneously with Eq. (5). For an explicit formulation of the dynamical equations and the variational equations used, we refer to Peters (1981) and Lainey et al. (2004).

A possible perturbation that may significantly decrease the accuracy of our model is the spin librations of the Martian

² Former simulations introducing the Martian gravity field up to order 12 revealed no significant differences with respect to simulations introducing this potential only up to degree 10.

³ A preliminary study by Lainey & Tanga (2005) in the context of the GAIA mission studied the small influence of the mutual perturbations of the Martian moons. In the present work, these forces have been introduced only for completeness.

⁴ The angles (α_0 , δ_0 , W) are defined in Seidelmann et al. (2002).

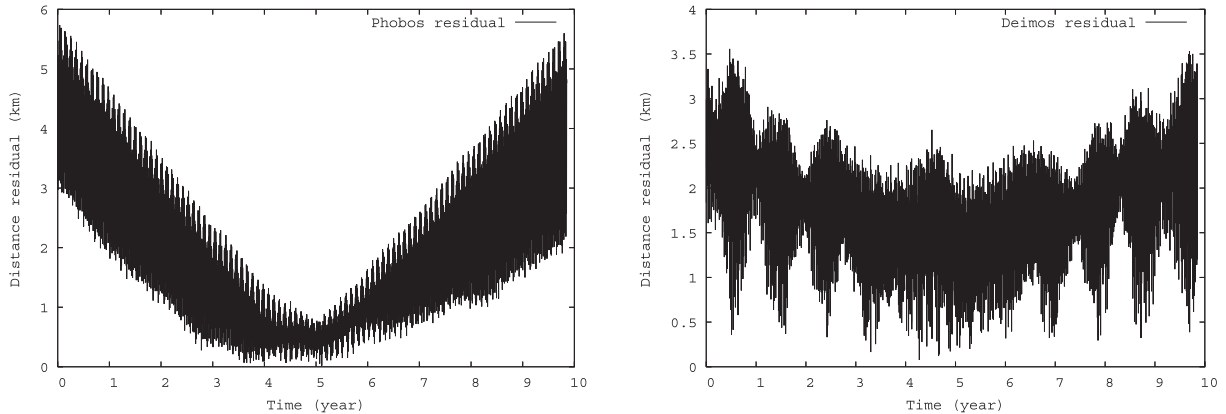


Fig. 1. Differences in distance after fitting the numerical model to the JPL ephemerides for Phobos (*left panel*) and Deimos (*right panel*). The satellite's initial positions and velocities and the Martian dissipation quality factor Q have been fit here. The horizontal axes are in years relative to Julian day 2 445 053.5 (25/03/1982).

moons. As both moons are in a spin-orbit resonance, induced librations affect the evolution of the satellite longitudes. So far, this perturbation has only been considered in the extensive work of Chapront-Touze (1990). However, the introduction of this resonance would need to consider the phase angle and its derivative at initial epoch as unknown parameters. As no observations of such an angle can be used easily, the fit of these parameters would be done on the basis of its influence on the orbital motion. Moreover, this sort of perturbation would require a good estimate of the C_{20} parameter for both moons, which is not available, in particular after the still controversial value of the Phobos mass itself (Andert et al. 2004). Hence, the introduction of spin orbit librations in our model will be postponed to future work.

The integrator subroutine is from Everhart (1985) and called RA15. It was chosen for its computation speed and accuracy. During the different integrations, a constant step size of $\Delta t = 0.025$ day was used. To increase the numerical accuracy during the fitting procedure (see Sect. 5), we performed forward and backward integrations starting at an initial Julian epoch of 2 445 053.5 (25/03/1982 TDB). This epoch was chosen to keep high precision during the spacecraft era. The numerical accuracy of our simulation is at the level of a few tens of meters over 10 years and a few hundreds of meters over one century.

4. Fit to JPL ephemerides

To obtain good first estimates of the initial satellite positions and velocities, we fit the model to the JPL ephemerides of the Martian moons, which are based on the Jacobson et al. (1989) ephemerides. These computations were done over a time span of 3600 days with a rate of one value per day. The initial epoch was Julian day 2 445 053.5 (TDB time). The global modeling already described in Sect. 3 was considered. Differences in Cartesian positions for all satellites and the Martian dissipation factor Q have been fit, with no weights assigned. The residuals after applying the least-square procedures are shown in Fig. 1. The resulting differences do not exceed a few kilometers and are distributed around a non-zero mean of the same order. In particular, the long-scale trends may be explained by the use of a different Martian gravity potential and precession rate. In addition, the assumed modeling precision of the JPL ephemerides is also one to two kilometers (Jacobson et al. 1989). This good agreement is sufficient to start a fitting procedure to the observations directly.

5. Fit to the observations

5.1. The fitting procedure

During the fitting procedure, time scale and light time corrections for each satellite-observer distance were introduced. The weights were computed by preliminary residuals, except for the spacecraft observations where the published weights were used. The only exception were the MOLA observations for which no weights are available. Hence, we used the published time offset given in Bills et al. (2005) for each shadow event and added an empirical uncertainty of 1.5 s to weight each event. All spacecraft observations were used, except the early Mariner 9 observations from the approach to Mars. The uncertainty in Mariner 9's position was about 50 km during this phase instead of only 4 km during the orbital phase (Duxbury & Callahan 1989). These observations were used, however, for computing all rms post fit residuals to be in agreement with former published works. A three-sigma rejection criterion was used for Earth-based observations, but considering the low accuracy of early observations (pre-50 s observations) this criterion was reduced to two-sigma in this last case.

Earth-based observations involve just one satellite (absolute or relative positions to Mars) or intersatellite observations (Deimos relative to Phobos). In the first case, it is sometimes possible to deduce intersatellite positions when both satellites are present. We tried two possibilities, either always converting satellite positions as intersatellite positions or not, when fitting the data. Intersatellite positions increase the correlations between Phobos and Deimos initial state. In particular, observational error on one satellite can potentially be absorbed in changes in the orbital evolution of the second satellite. Intersatellite positions have not been considered in this paper when relative positions to Mars were available⁵.

The normal system was inverted by the least-square method (singular value decomposition). The fit parameters were the initial state vectors and the dissipation factor Q . After a few iterations, however, the solution quickly diverged. Actually, this problem was also encountered by Taylor (1998) with the Uranian satellites. He solved the problem by fitting initial elliptical

⁵ Intersatellite positions are often a powerful way to avoid the center of mass determination and ephemeris errors of the planet. It only makes sense if all satellites have the same magnitude (and so the same observational error). Moreover, the number of satellites must be high enough to avoid correlations.

elements instead of initial Cartesian coordinates. As all former models were analytic so developed in elliptical elements, this problem has not occurred with the Martian moons so far. More details concerning the fit of the elliptical elements can be found in Taylor (1998). An alternative way is to introduce constraints on the initial Cartesian coordinates to prevent high values that would induce a divergence in the solution. Both approaches using the same preliminary observational sets were tested. The data set was based on spacecraft observations only and covered 34 years. When fitting elliptical initial elements, the convergence was reached after only a few iterations. On the other hand, the constraint method was far less efficient and much more empirical. First, the magnitude of the uncertainties needed to be chosen carefully. A high value produced a diverging process, while a low value made the convergence very slow. After several trials, we finally found optimal uncertainties of 4×10^{-9} AU and 10^{-8} AU/day for the position and velocity components, respectively. The constraint method needed around ten iterations where the former method needed only three or four. Therefore, only the elliptical fitting method was finally considered. Throughout the rest of this work, no constraints have been applied in the least-square process. All unknowns have been fit all together at each iteration, which includes the initial state vectors, the dissipation parameter Q , and the C_{20} and C_{22} coefficients of Phobos (see next section).

5.2. Fit to spacecraft observations

The spacecraft observations number in the hundreds and cover more than three decades. One should expect an accurate solution for both the Phobos and Deimos orbits using only those observations. The numerical model was fit to the spacecraft observations considering only the initial state vectors (by fit of the elliptical elements) of the two moons and the Martian dissipation factor Q as unknown parameters. A first fit only used Mariner 9, Viking 1-2, and Phobos 2 observations. This fit was extended by introducing MOLA and SRC observations. Unfortunately, their introduction significantly increased the residuals of the former observations (essentially Mariner 9 and Viking). If the estimated accuracy of the spacecraft observations is correct (no biases in the position and the orientation of the spacecrafts), this effect indicates something lacking in the modelling of the perturbation. The most probable reason⁶ that may introduce this discrepancy would be the triaxiality of Phobos. In particular, the use of the actual known Martian gravity field (deduced only from spacecraft tracking) no longer introduces significant correlations with Phobos. The Phobos gravity coefficients C_{20} and C_{22} by Borderies & Yoder (1990) were then used, which were computed from Phobos' topography and mass (assuming a constant density). After another trial, the residuals increased again by the same order of magnitude. It was thus decided to add Phobos' C_{20} and C_{22} coefficients as unknown parameters for the fit process. We found surprisingly very good residuals for all observations, with a consistent order of magnitude for the C_{20} and C_{22} values (without constraints). This result will be commented in Sect. 5.4 and in Sect. 8.

5.3. Fit to modern ground-based observations

Earth-based observations during the spacecraft era were added to the already considered spacecraft observations in the last run. Because discrepancies exist among the various observational

sets, only the most accurate Earth-based observations were considered. These consist of 267 astrometrical observations done by Pascu at the Flagstaff and the Washington observatories between 1967 and 1971 (2 oppositions) and between 1982 and 1988 (4 oppositions). From the opposition of 1988, 813 intersatellite observations by Colas at Pic du Midi (Colas 1992), and 88 and 78 observations of Phobos and Deimos, respectively, done at La Palma by Jones et al. (1989), and 660 and 639 observations of Phobos and Deimos, respectively, done by Kudryavtsev et al. (1992) were included. Further 196 observations by Rohde, Ries, and Pascu at Flagstaff in 2003 were also added.

The post-fit residuals increased slightly compared to the former fit presented in Sect. 5.2. An explanation is that some observations by Pascu from 1982 to 1988 were probably biased, as found in the past by a comparison with other ephemeris sources (Pascu, priv. com.). These observations were reduced with regard to separation and position angle (s, p), while the systematical bias probably affected only one of these two variables. Unfortunately, the software used in this work automatically converts (s, p) variables into $(\Delta\alpha \cos \delta, \Delta\delta)$ coordinates, so no control of systematical errors could be done. As such a former correction had not been applied in the first step, this bias contaminates the results and compromises the quality of the fit. In the future, this treatment will be done in order to improve the final residuals. Despite this point, Pascu's observations are highly accurate and in addition provide satellite positions relative to Mars.

5.4. Introducing the pre-50 s observations

Earth-based observations made before 1950 were then introduced into the database. Although less accurate than modern observations, they cover a long time span before the spacecraft era (the oldest observations were made in 1877). For practical reasons, we did not introduce all observations, but only those that do not depend on the (s, p) variables. The latter will be considered in a future work. Only very few iterations were required starting from the fit performed in Sect. 5.2, and the residuals did not change much. As this fit includes observations covering almost 130 years, this fit was chosen as the final solution for the ephemerides. Figure 2 shows Phobos and Deimos' post fit residuals from spacecraft observations. Figure 3 shows Phobos and Deimos from Earth-based observations (old and modern one). Tables 2 and 3 present the final rms post-fit residuals for each observational set. In particular, these tables can be compared to a similar table published in Chapront-Touze (1990). The MEX residuals clearly fit the expected accuracy of these observations. The MGS residuals are significantly larger, but a close look at Fig. 2 also shows periodic behavior. This may come from the use of former ephemerides models in the reduction process. Indeed, during the shadow-event reduction, only a time shift is fit. Hence, the satellite coordinates relative to Mars are computed from the JPL ephemerides. The other spacecraft residuals are the same order of magnitude as those published by Chapront-Touze (1990). Another method of comparison can directly compute the differences between both ephemerides. This is done in Sect. 7 with the JPL ephemerides.

The Martian dissipation factor Q was found to be not very sensitive to the different sets of observations used. It was found to be equal to 79.61, 78.70, and 79.91 with similar error bars. The reference value chosen in this paper is $Q = 79.91 \pm 0.69$, which derived from the last fit, assuming $k_2 = 0.152$ for the Martian Love number and $Gm_{\text{Ph}} = 0.68012569 \times 10^6 \text{ m}^3/\text{s}^2$ for the mass of Phobos. There is also a suspicion of a non

⁶ Consideration of other perturbations will be in Sect. 8.

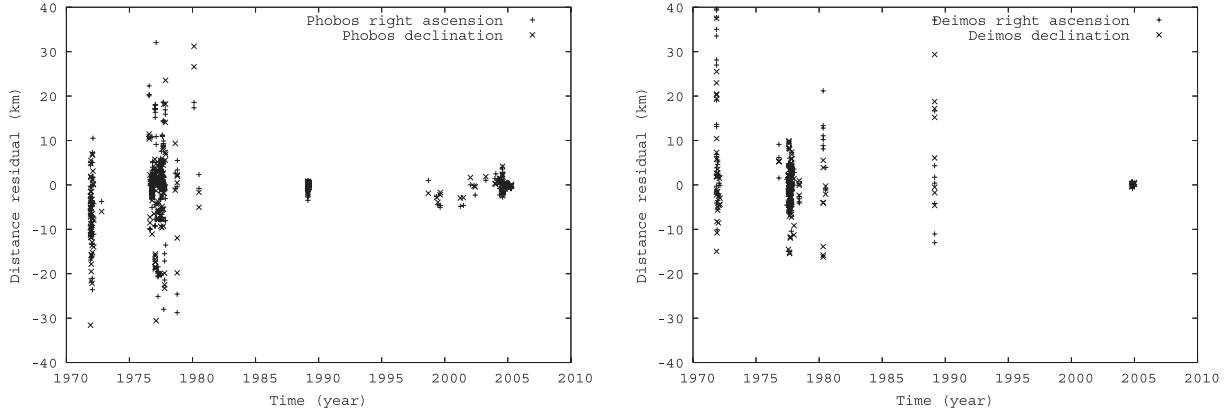


Fig. 2. Differences in distance after fit between the model and the spacecrafts observations for Phobos (*left panel*) and Deimos (*right panel*). The satellite initial positions, velocities and the Martian dissipation quality factor Q and Phobos' C_{20} and C_{22} have been fit here.

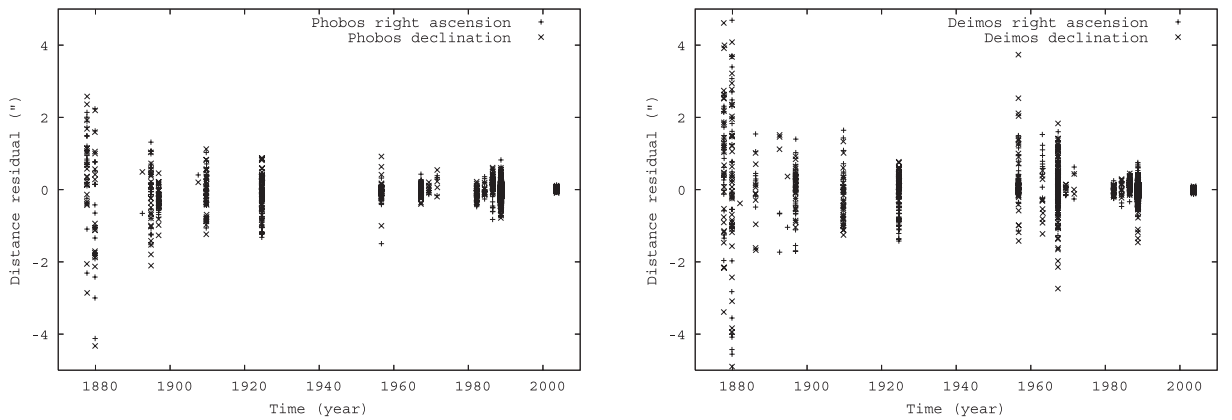


Fig. 3. Differences in distance after fit between the model and the ground observations for Phobos (*left panel*) and Deimos (*right panel*). The satellite initial positions, velocities and the Martian dissipation quality factor Q and Phobos' C_{20} and C_{22} have been fit here.

Table 2. Mean (ν) and standard deviation (σ) on right ascension and declination in seconds of degrees for each satellite.

Observations	ν_α (")	σ_α (")	ν_δ (")	σ_δ (")	N^a	satellite
Pascu (1995)*	0.00003	0.23234	0.04658	0.17103	217	Phobos
	0.06439	0.20355	0.00943	0.22216	223	Deimos
Rohde, Ries, and Pascu (2003)*	0.00876	0.02901	0.00803	0.02826	196	Phobos
	-0.00876	0.02901	-0.00803	0.02826	196	Deimos
Colas (1992)	-0.02147	0.05460	-0.00226	0.06345	813	Phobos
	0.02147	0.05460	0.00226	0.06345	813	Deimos
Jones et al. (1989)	-0.00213	0.11990	0.04983	0.11411	154	Phobos
	-0.06034	0.10228	-0.02699	0.09801	78	Deimos
Kudryavtsev et al. (1992)	0.09592	0.15067	-0.12893	0.15058	660	Phobos
	0.08342	0.15197	-0.11304	0.14451	639	Deimos
Old Observations – Morley (1989)	-0.29783	4.01389	-0.01730	1.60815	223	Phobos
Christie et al. (1878), Young (1880)	0.00314	5.54741	0.35150	4.56567	340	Deimos

* Unpublished observations.

^a Number of observations by satellite.

homogeneous density for Phobos. The estimate of the satellite gravity field is $C_{20} = -0.072 \pm 0.013$ and $C_{22} = -0.048 \pm 0.002$. This clearly conflicts with a constant density assumption that would imply the values $C_{20} = -0.10058$ and $C_{22} = +0.01591$ (Borderies & Yoder 1990). The negative sign of C_{22} , however, may suggest the signature of a remaining unmodeled perturbation, the use of a biased Martian gravity field, or the introduction of biased observations (see the discussion in Sect. 8).

The correlation of all the fit parameters are given in Table 4. The highest correlation is equal to 0.91 between C_{20} and C_{22} .

These coefficients are not completely correlated, because the orbit of Phobos has a small inclination, and the orientation of its northern pole is assumed to be equal to the Martian one. For more details concerning the correlation of the C_{20} and C_{22} coefficients, one can refer to Jacobson & Rush (2006) or Lainey (2002).

Table 5 presents a comparison between former Phobos' secular acceleration determinations. The result of this work is in good agreement with Jacobson et al. (1989) and Chapront-Touze (1990). The most recent determination by Bills et al. (2005) by

Table 3. Mean (ν) and standard deviation (σ) on right ascension and declination for each satellite.

Observations	ν_α (km)	σ_α (km)	ν_δ (km)	σ_δ (km)	N	satellite
MOLA (MGS)	-3.038	6.726	0.190	4.777	17	Phobos
Bills et al. (2005)	–	–	–	–	–	Deimos
Mariner 9	-6.441	6.669	-7.412	7.858	49	Phobos
Duxbury & Callahan (1989)	15.080	19.992	5.008	13.677	31	Deimos
SRC (MEX)	0.077	1.474	0.168	1.485	26	Phobos
Oberst et al. (2006)	0.002	0.517	0.044	0.322	10	Deimos
Viking 1-2	1.193	9.820	-0.856	8.969	166	Phobos
Duxbury & Callahan (1988)	0.477	4.443	-2.433	11.539	109	Deimos
Phobos 2	-0.350	0.967	-0.032	0.594	37	Phobos
Kolyuka et al. (1991)	3.991	15.248	9.959	11.224	8	Deimos

The angles have been multiplied by the distance between the point of observation and the two satellites to provide values in kilometers.

Table 4. Table of the correlations between all the fit parameters, including the initial elliptical elements, the dissipation factor Q , and the Phobos gravity coefficients C_{20} and C_{22} .

	a_1	L_1	k_1	h_1	q_1	p_1	a_2	L_2	k_2	h_2	q_2	p_2	C_{20}	C_{22}	Q
a_1	1.00	0.23	0.18	0.86	0.00	-0.11	0.00	0.00	0.00	0.00	0.00	0.00	0.13	0.38	0.45
L_1	0.23	1.00	0.68	0.15	-0.23	0.20	0.00	0.00	0.00	0.00	0.00	0.00	0.20	0.37	0.18
k_1	0.18	0.68	1.00	0.43	-0.12	-0.03	0.00	0.00	0.00	0.00	0.00	0.00	0.07	0.40	-0.39
h_1	0.86	0.15	0.43	1.00	0.04	-0.17	0.00	0.00	0.00	0.00	0.00	0.00	0.12	0.42	0.08
q_1	0.00	-0.23	-0.12	0.04	1.00	-0.45	0.00	0.00	0.00	0.00	0.00	0.00	-0.20	-0.23	0.04
p_1	-0.11	0.20	-0.03	-0.17	-0.45	1.00	0.00	0.00	0.00	0.00	0.00	0.00	0.82	0.68	-0.01
a_2	0.00	0.00	0.00	0.00	0.00	0.00	1.00	0.66	-0.61	-0.52	0.51	0.56	0.00	0.00	0.00
L_2	0.00	0.00	0.00	0.00	0.00	0.00	0.66	1.00	-0.42	-0.56	0.00	0.10	0.00	0.00	0.00
k_2	0.00	0.00	0.00	0.00	0.00	0.00	-0.61	-0.42	1.00	-0.06	0.12	0.11	0.00	0.00	0.00
h_2	0.00	0.00	0.00	0.00	0.00	0.00	-0.52	-0.56	-0.06	1.00	-0.17	-0.26	0.00	0.00	0.00
q_2	0.00	0.00	0.00	0.00	0.00	0.00	0.51	0.00	0.12	-0.17	1.00	0.86	0.00	0.00	0.00
p_2	0.00	0.00	0.00	0.00	0.00	0.00	0.56	0.10	0.11	-0.26	0.86	1.00	0.00	0.00	0.00
C_{20}	0.13	0.20	0.07	0.12	-0.20	0.82	0.00	0.00	0.00	0.00	0.00	0.00	1.00	0.91	0.02
C_{22}	0.38	0.37	0.40	0.42	-0.23	0.68	0.00	0.00	0.00	0.00	0.00	0.00	0.91	1.00	-0.05
Q	0.45	0.18	-0.39	0.08	0.04	-0.01	0.00	0.00	0.00	0.00	0.00	0.00	0.02	-0.05	1.00

Elliptical elements have been taken under the regularized form (a, L, k, h, q, p), where a denotes the semi-major axis, L denotes the mean longitude, (k, h) are the real and imaginary component of $z = e \exp^{i\varpi}$ and (q, p) are the real and imaginary component of $\zeta = \sin \frac{1}{2} \exp^{i\Omega}$, where ϖ is the longitude of the periape, e is the excentricity and I is the inclination. Subscript 1 denotes the Phobos' elements and subscript 2 denotes the Deimos' elements. The correlations higher than 0.8 are shown in boldface.

Table 5. Phobos secular acceleration ($\frac{1}{2} \frac{dn}{dt}$) deduced from Martian moons ephemerides.

source	secular acceleration $\frac{1}{2} \frac{dn}{dt}$ (10^{-5} deg/yr ²)
Jacobson et al. (1989)	124.9 ± 1.8
Chapront-Touze (1990)	127.0 ± 0.8
Emelyanov et al. (1993)	129.0 ± 1.0
Bills et al. (2005)	136.7 ± 0.6
This work	127.0 ± 1.5

fitting MOLA observations is the most contrasting one. An explanation could be that in the work of Bills et al. (2005), only three terms arising in the expression of Phobos longitude were fit, and only MOLA observations used. Table 6 gives the initial state vectors at Julian epoch 2445 053.5 computed as the initial state in the model.

6. Signal processing and final representation

The usual way to derive an ephemeris from numerical integration of a Solar system body in practical form is to fit Chebychev polynomials over the related numerical sampling. However,

the difference between Chebychev polynomials and an analytical series (developed by means of analytical integration) is the size of the files involved. For slow objects like external satellites of Giant planets, Chebychev representations are quite convenient, but become inconvenient for fast satellites like Phobos. In order to avoid large volume files that may increase the computing time, we decided to perform a spectral analysis instead of fitting Chebychev polynomials. This will make our final ephemerides file smaller in size and easier to provide via the internet. Moreover, this will simplify further comparison between our ephemerides and the others, once each frequency is recognized. Last but not least, the frequency representation is defined far beyond the numerical integration time span.

The method and the software used for spectral analysis are very similar to the software presented in Vienne & Duriez (1992) and based on the method presented in Laskar et al. (1992). The sampling step size was chosen after analyzing some small arcs at a very high step size. It appeared that no short periods with amplitudes higher than a few tens of meters were present for less than 0.1 day for Phobos and 0.4 day for Deimos. This allows use of a final step size of 0.05 and 0.2 day for Phobos and Deimos, respectively. To improve the algorithm, Chebychev polynomial (especially in the satellites longitude) were sometimes introduced.

Table 6. Initial state vectors at the Julian epoch 2 445 053.5 (25/03/1982 TDB).

Satellite	x	y	z
position of Phobos (AU)	-5.275254348561059E-005	4.940685958944592E-006	3.208377735462846E-005
velocity of Phobos (AU/day)	-3.419274688341861E-004	-1.145431373878196E-003	-3.624022104187871E-004
position of Deimos (AU)	5.339886204059241E-005	-1.211337469486434E-004	-8.411522628553895E-005
velocity of Deimos (AU/day)	6.576371605012466E-004	3.927174026111411E-004	-1.484537310476662E-004

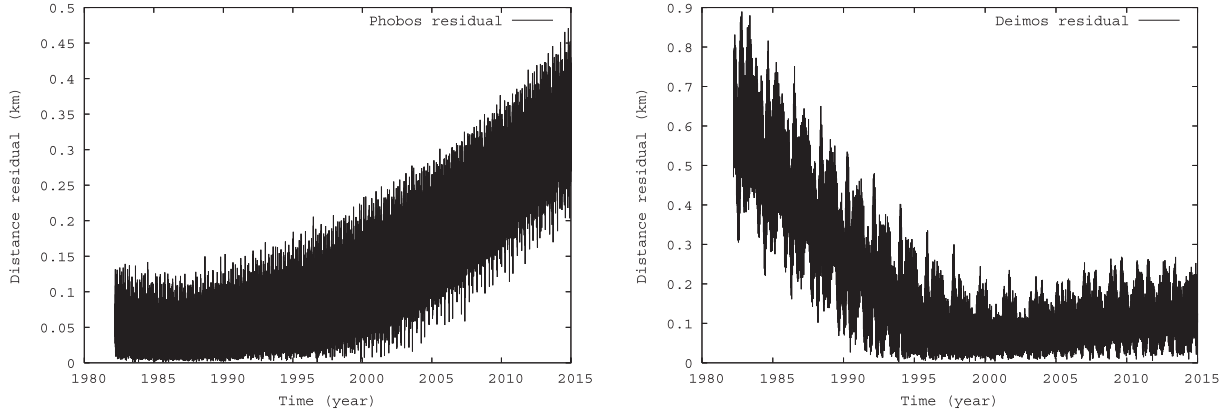
**Fig. 4.** The internal precision of the ephemerides reflects the differences between the numerical integration and the frequency reconstruction for Phobos (*left panel*) and Deimos (*right panel*).

Figure 4 shows the differences between our final frequency representation and the initial sampled time series produced by numerical integration. The differences reveal the internal precision of the final ephemerides, which is a few hundred meters during the period 1990–2015. The frequency analysis may be improved in the future when new spacecraft observations are available.

7. Comparison with JPL and ESOC ephemerides

Finally, the ephemerides were compared with the JPL and ESOC ephemerides. Both are available as SPICE kernels and defined over the time span 1976–2025 and 2004–2006, respectively. Figure 5 presents the related differences, which agree with the results found by Bills et al. (2005), Bell et al. (2005), and Oberst et al. (2006) using the MOLA, MER, and SRC instruments. In particular, JPL ephemerides are drifting compared to the ephemerides presented here, while ESOC’s ephemerides show a higher but periodic scattering and a shift of 9 km and 15 km with respect to Phobos and Deimos. It shall be noted that the ephemerides from the model of this paper agree with the JPL ephemerides during the Viking and Phobos 2 era. This leads to the conclusion that the spacecrafts residuals shown in Table 3 are mainly observational errors.

8. Consideration of non introduced perturbations

As explained in Sect. 1, the introduction of the Phobos’ C_{20} and C_{22} gravity field coefficients mainly induce some linear drifts in the angular elements (Borderies & Yoder 1990). An easy way to quantify them is to perform the difference between a first simulation involving the C_{20} and C_{22} coefficients, and a second simulation without them. This difference was performed over 3 years, and is presented in Fig. 6. The initial conditions and forces involved in the physical modeling are exactly the same as the ones used in the last fit of the present ephemerides. The Phobos’ C_{20} and C_{22} coefficients introduce a secular drift

of roughly 200 km over 3 years. A possible explanation for the negative (and so unphysical) sign of C_{22} could be that a perturbation at the same order of magnitude has been neglected in the present model. To verify such an eventuality, three perturbations not introduced in the former force model were checked. The differences between one simulation with and one simulation without each perturbation tested are presented in Fig. 6. The first perturbation tested is the influence of the temporal variation of the Martian C_{20} coefficient. The numerical values for the expression of the temporal signature were taken from Konopliv et al. (2006). The simulations indicate that this perturbation introduces some periodic terms with an amplitude of only a few tens of meters. The second perturbation that has been tested is the presence of the Solar tidal bulge raised on Mars. The main related effect is a secular trend of 60 m over three years. The last perturbation tested was the Martian nutation missing in the present model. As the Martian nutation is unobserved so far, the presumed nutation was taken from the numerical model of the Martian rotation provided by Rambaux (priv. com.). The numerical model called SONYR was applied to Mercury (Rambaux & Bois 2004). The global effect of the nutation is a secular trend of 300 m over 3 years on the Phobos’ longitude.

It appears that none of the three perturbations considered in this section reaches the order of magnitude of the perturbation associated with Phobos’ C_{20} and C_{22} coefficients. Although some other perturbations have not been tested (Phobos’ libration, radiation pressure, and Yarkovsky effect thought to be small), it seems, however, more likely that the Martian gravity field used or some of the spacecraft observations are biased. More importantly, it has been shown that Phobos’ oblateness gravity field contributes at an observable level to the Martian moon dynamics and could be, in principle, fit from astrometric observations.

9. Conclusion

New ephemerides of the Martian moons have been developed on the basis of MEX, MGS, Phobos 2, Viking 1-2, Mariner 9, and ground based observations. The recent observed differences

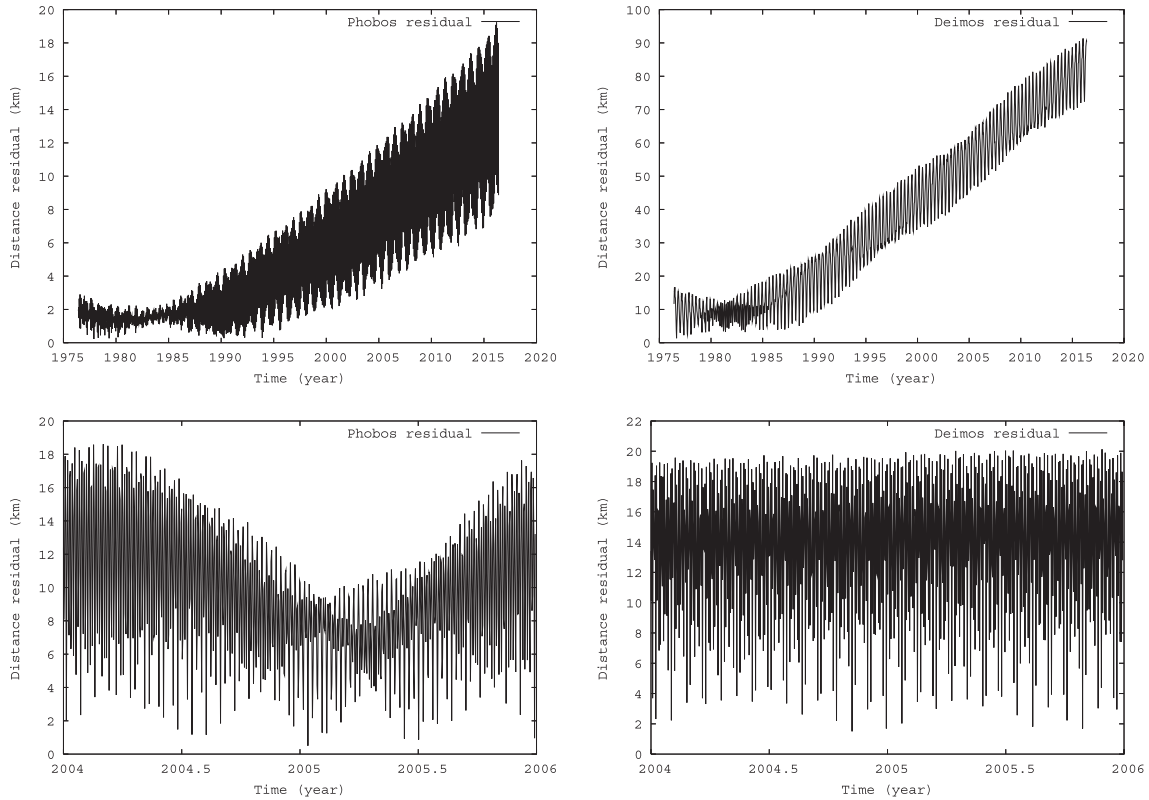


Fig. 5. Comparison between the computed ephemerides and ephemerides from other sources. The graphs present the differences in distance between the position of Phobos (*left*) and Deimos (*right*) using the model with respect to the JPL (*top*) model and the ESOC (*bottom*) model.

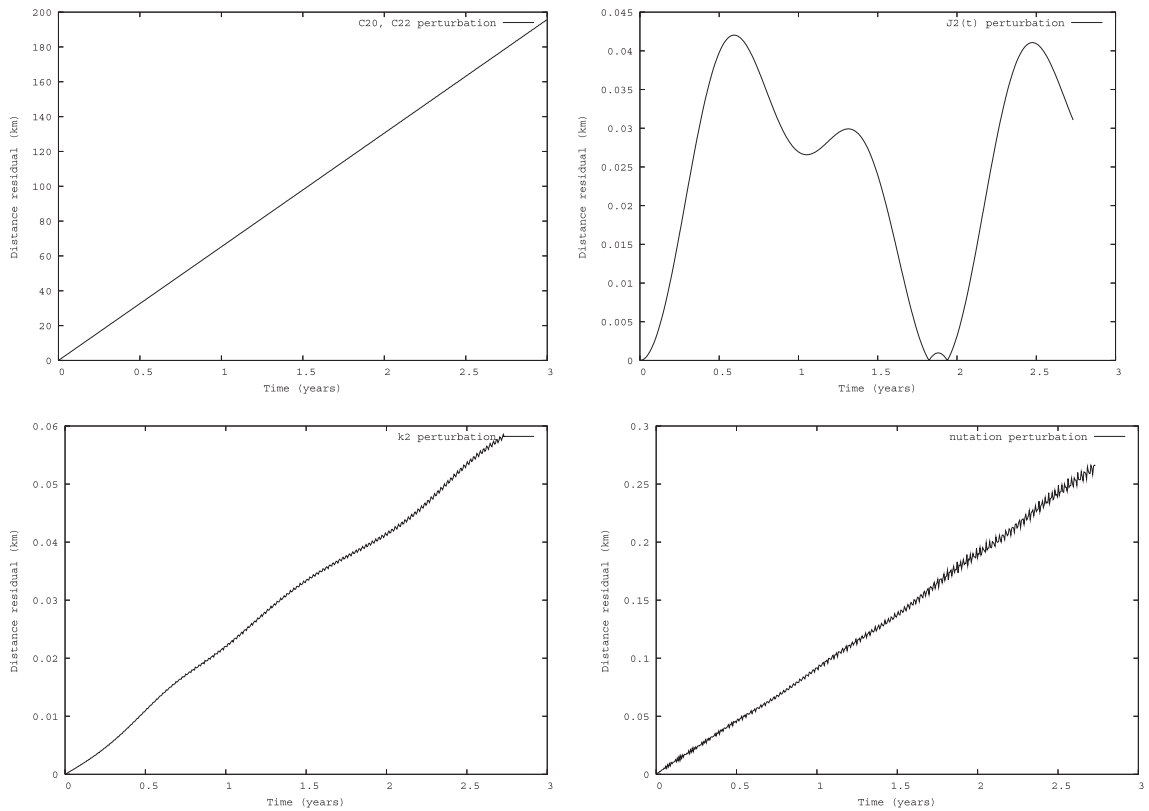


Fig. 6. Differences between one numerical simulation introducing the force modeling of reference in this paper and other simulations adding one perturbation to be tested. The perturbations tested are the Phobos' C_{20} and C_{22} coefficients (*upper left panel*), the temporal variation of the Martian C_{20} coefficient (*upper right panel*), the Solar tidal bulge raised on Mars (*lower left panel*), and the Martian nutation (*lower right panel*).

of up to ten kilometers between the prediction and the true satellite locations observed by MGS and MEX do not appear in this solution. Two different fitting methods were tested during the adjustment of the model to the observations. The use of elliptical elements during the fit process is by far more efficient than fitting Cartesian coordinates (even introducing constraints). This is also the first completely numerical ephemerides of Phobos and Deimos. The physical formulation of the tidal effects of the Mars/moon systems has been successfully introduced. The high Martian internal dissipation quantified at the time of Phobos 2 mission is confirmed. This dissipation factor is found to be $Q = 79.91 \pm 0.69$, assuming $k_2 = 0.152$ for the Martian Love number and $Gm_{\text{Ph}} = 0.68 \times 10^6 \text{ m}^3/\text{s}^2$ for the Phobos mass. The uncertainties of the last two values constrain the determination of Q . Unexpectedly, there is suspicion of a non-uniform density of Phobos. The solution for the Phobos gravity field is indeed found to be $C_{20} = -0.0719 \pm 0.013$ and $C_{22} = -0.0481 \pm 0.002$ and is different from a gravity field derived by a shape model assuming uniform density. If the solution in the present paper is not completely satisfying, at least it demonstrates the sensitivity of the Martian moon ephemerides to Phobos' gravity field.

The Mars Express mission has been extended for two more years and will provide many more precise astrometric observations of the Martian satellites. The present model will be regularly updated by introducing these new observations, as well as new MOLA observations (Bills, personal communication) in the future.

The Phobos libration has not been included in the model so far. It is a perturbation that will be introduced in further improvements. This will affect the previous determination of the Phobos gravity coefficients somewhat and will further improve the ephemerides residuals.

The accuracy of the computed ephemerides is expected to be roughly one kilometer over the presented period. A FORTRAN subroutine computing the Martian moons ephemerides is available on request.

While writing this paper, new JPL ephemerides have been released (Jacobson & Rush 2006). A comparison done there demonstrates a good agreement between our ephemerides and the new JPL ones.

Acknowledgements. The authors are grateful to D. Pascu for providing them all of his already reduced observations done at USNO and to J. Oberst for providing the SRC observations (Mars Express) of the Martian moons. The authors would also like to thank F. Lemoine for directing our attention to the possibility of improving the Mariner 9 and Viking 1-2 spacecraft positions. Our thanks go to S. Le Maistre and G. Pfyffer for computing the SPICE kernel. The authors are grateful to P. Rosenblatt, T. Van Hoolst, and N. Emelianov for fruitful discussions. This work benefited from the support of the European Community's Improving Human Potential Programme under contract RTN2-2001-00414, MAGE. M.P. acknowledges support from BMFT via DLR under grant 50QP9909.

References

Andert, T. P., Pätzold, M., Lainey, V., et al. 2004, AGU Fall Meeting Abstracts, A802

- Bell, J. F., Lemmon, M. T., Duxbury, T. C., et al. 2005, *Nature*, 436, 55
- Bills, B. G., Neumann, G. A., Smith, D. E., & Zuber, M. T. 2005, *J. Geophys. Res. (Planets)*, 110, 7004
- Bobylev, V. V., Evdokimov, A. E., Kalinichenko, O. A., et al. 1991, *Izvestiya Glavnoj Astronomicheskoy Observatorii v Pulkove*, 207, 37
- Borderies, N., & Yoder, C. F. 1990, *A&A*, 233, 235
- Chapront-Touze, M. 1990, *A&A*, 240, 159
- Christie, W., Erck, W., & Pritchard, C. 1878, *MNRAS*, 38, 361
- Colas, F. 1992, *A&AS*, 96, 485
- Duxbury, T., & Callahan, J. D. 1988, *A&A*, 201, 169
- Duxbury, T. C., & Callahan, J. D. 1989, *A&A*, 216, 284
- Emelyanov, N. V., Vashkovyakov, S. N., & Nasonova, L. P. 1993, *A&A*, 267, 634
- Everhart, E. 1985, in *Dynamics of Comets: Their Origin and Evolution*, ASSL 115: IAU Colloq. 83, 185
- Izhakevich, R., Kaltygina, S., Ledovskaya, I. V., Sereda, E., & Shatkhina, S. 1990, Scientific paper deposited in All-russian institute of scientific and technical information, 1
- Jacobson, R., & Rush, B. 2006, *JPL IOM*, 225, 1
- Jacobson, R., Synnott, S. P., & Campbell, J. K. C. 1989, *A&A*, 225, 548
- Jones, D. H. P., Sinclair, A. T., & Williams, I. P. 1989, *MNRAS*, 237, 15P
- Kalinichenko, O. A., Kiseleva, T. P., Salukvadze, G. N., & Chanturiia, S. M. 1990, *Abastumanskaia Astrofizicheskaia Observatoriia Biulleten*, 68, 99
- Kiselev, A. A., Kiseleva, T. P., Bobylev, V. V., et al. 1989, *Izvestiya Glavnoj Astronomicheskoy Observatorii v Pulkove*, 206, 33
- Kiseleva, T. P., & Chanturiia, S. M. 1988, *Abastumanskaia Astrofizicheskaia Observatoriia Biulleten*, 63, 31
- Kolyuka, Y., Tikhonov, V., Ivanov, N., et al. 1991, *A&A*, 244, 236
- Konopliv, A. S., Yoder, C. F., Standish, E. M., Yuan, D., & Sjogren, W. L. 2006, *Icarus*, 182, 23
- Kudryavtsev, S. M., Shokin, Y. A., & Yevstigneeva, N. M. 1992, Preprint, Sternberg State Astronomical Institute, 24, 1
- Lainey, V. 2002, Thèse de l'Observatoire de Paris, 1
- Lainey, V., & Tanga, P. 2005, AAS/Division for Planetary Sciences Meeting Abstracts, 37
- Lainey, V., Duriez, L., & Vienne, A. 2004, *A&A*, 420, 1171
- Laskar, J., Froeschlé, C., & Celletti, A. 1992, *Physica D Nonlinear Phenomena*, 56, 253
- Lemoine, F. G., Smith, D. E., Rowlands, D. D., et al. 2001, *J. Geophys. Res.*, 106, 23359
- Mignard, F. 1980, *Moon and Planets*, 23, 185
- Morley, T. 1989, *A&AS*, 77, 209
- Morley, T. A. 1990, *A&A*, 228, 260
- Neumann, G. A., Bills, B. G., Smith, D. E., & Zuber, M. T. 2004, in *Lunar and Planetary Institute Conference Abstracts*, 1820
- Nikonov, O. V., Zhilinskii, E. G., Bobylev, V. V., & Nikonova, E. S. 1991, *Izvestiya Glavnoj Astronomicheskoy Observatorii v Pulkove*, 207, 52
- Oberst, J., Matz, K., Roatsch, T., et al. 2006, *A&A*, 447, 1145
- Peters, C. F. 1981, *A&A*, 104, 37
- Rambaux, N., & Bois, E. 2004, *A&A*, 413, 381
- Seidemann, P. K., Abalakin, V. K., Bursa, M., et al. 2002, *Celestial Mechanics and Dynamical Astronomy*, 82, 83
- Sharpless, B. P. 1945, *AJ*, 51, 185
- Shor, V. 1989, Preprint of Sternberg Astronomical Institute, 13
- Shor, V. A. 1975, *Celestial Mechanics*, 12, 61
- Sinclair, A. 1978, *Vistas Astron.*, 22, 133
- Sinclair, A. T. 1972, *MNRAS*, 155, 249
- Standish, E. 1998, *JPL IOM*
- Taylor, D. B. 1998, *A&A*, 330, 362
- Tel'nyuk-Adamchuk, V., Churyumov, K. I., Pikalo, N., et al. 1990, Manuscript deponat at the Ukrainian science and technical information institute, 1
- Tyler, G., Balmino, G., Hinson, D., et al. 2003, *USA_NASA_JPL_MORS_1021*
- Vienne, A., & Duriez, L. 1992, *A&A*, 257, 331
- Young, C. A. 1880, *The Observatory*, 3, 270
- Yuan, D.-N., Sjogren, W. L., Konopliv, A. S., & Kucinkas, A. B. 2001, *J. Geophys. Res.*, 106, 23377

Strong tidal dissipation in Io and Jupiter from astrometric observations

Valéry Lainey¹, Jean-Eudes Arlot¹, Özgür Karatekin² & Tim Van Hoolst²

Io is the volcanically most active body in the Solar System and has a large surface heat flux^{1–3}. The geological activity is thought to be the result of tides raised by Jupiter⁴, but it is not known whether the current tidal heat production is sufficiently high to generate the observed surface heat flow^{5,6}. Io's tidal heat comes from the orbital energy of the Io–Jupiter system (resulting in orbital acceleration), whereas dissipation of energy in Jupiter causes Io's orbital motion to decelerate. Here we report a determination of the tidal dissipation in Io and Jupiter through its effect on the orbital motions of the Galilean moons. Our results show that the rate of internal energy dissipation in Io ($k_2/Q = 0.015 \pm 0.003$, where k_2 is the Love number and Q is the quality factor) is in good agreement with the observed surface heat flow^{5,6}, and suggest that Io is close to thermal equilibrium. Dissipation in Jupiter ($k_2/Q = (1.102 \pm 0.203) \times 10^{-5}$) is close to the upper bound of its average value expected from the long-term evolution of the system⁷, and dissipation in extrasolar planets may be higher than presently assumed⁸. The measured secular accelerations indicate that Io is evolving inwards, towards Jupiter, and that the three innermost Galilean moons (Io, Europa and Ganymede) are evolving out of the exact Laplace resonance.

The orbital evolution of the Galilean system due to tidal dissipation can be determined from astrometrically observed positions of the Galilean satellites over an extended period of time^{9,10} by using an accurate model of the orbital motion. Most orbital models are based on elaborate analytical methods and include the complex dynamics induced by the interactions of the Galilean moons. In particular, because the three innermost Galilean moons are in the Laplace resonance characterized by the relation

$$L_1 - 3L_2 + 2L_3 \approx \pi$$

where L_1 , L_2 and L_3 denote the mean longitudes of Io, Europa and Ganymede, respectively, changes in orbital energy and angular momentum are distributed between the three moons. Unfortunately, some long-period terms are lacking in such models, which explains why previous studies show large and widely different, even contradictory, results (see Table 1 and Supplementary Information for details). Here we use a method that numerically integrates the full equations of motion (Supplementary Information) for the satellite centres of mass instead of using an approximate analytical solution. Moreover, the tidal effects are directly included in the orbital model through the appearance of the Love number, k_2 , and the quality factor, Q , in the combination k_2/Q for Io and Jupiter. The orbital effects due to the dissipation in the Galilean satellites other than Io are neglected, but we take into account the tidal bulges raised by each moon on Jupiter using a constant Jupiter quality factor (Supplementary Information).

An extensive set of astrometric observations starting in 1891 and ending in 2007 has been considered in the fitting process. A long,

detailed set of observations such as this is necessary to reveal the long-term effects of dissipation on the orbits. We use a weighted least-squares inversion procedure and minimize the differences between the observed and computed positions of the satellites to determine the parameters of the model, in particular the respective dissipation ratios, k_2/Q , of Io and Jupiter. Our solution for the tidal dissipation yields $k_2/Q = 0.015 \pm 0.003$ (formal error bar, 1σ) for Io and $k_2/Q = (1.102 \pm 0.203) \times 10^{-5}$ for Jupiter. The Io–Jupiter interaction dominates the orbital evolution and is responsible for a large correlation coefficient of 0.983 between the dissipation ratios of Io and Jupiter. The almost 2% difference with respect to unity is due to the evolution of the Laplace resonance and is sufficient to separate the dissipation in Io from that in Jupiter (see Supplementary Information for a complete analysis of this correlation).

The dissipation values correspond to orbital acceleration values, \dot{n}/n (a dot denoting differentiation with respect to time), of $(0.14 \pm 0.01) \times 10^{-10} \text{ yr}^{-1}$, $-(0.43 \pm 0.10) \times 10^{-10} \text{ yr}^{-1}$ and $-(1.57 \pm 0.27) \times 10^{-10} \text{ yr}^{-1}$ (formal error bars, 1σ) for Io, Europa and Ganymede, respectively. These accelerations represent a shift in the satellite orbital positions of respectively 55 km, -125 km and -365 km over the 116 years considered. Surprisingly, the most external moon Ganymede shows the largest drift, as a consequence of the Laplace resonance. The 1σ post-fit astrometric residuals range essentially between 0.02 and 0.15 arcsec (Fig. 1, Supplementary Table 2 and Supplementary Table 3), which corresponds to 60 to 450 km at the distance of Jupiter. Owing to the long time span considered, such accuracy is enough to allow the tidal accelerations to be discerned from the observations.

Table 1 | A selection of secular mean-motion accelerations published for the three inner Galilean moons

Ref.	Secular mean-motion acceleration (\dot{n}/n) (10^{-10} yr^{-1})		
	Io	Europa	Ganymede
9	$+3.3 \pm 0.5$	$+2.7 \pm 0.7$	$+1.5 \pm 0.6$
10	-0.074 ± 0.087	-0.082 ± 0.097	-0.098 ± 0.153
24	$+4.54 \pm 0.95$	$+5.6 \pm 5.7$	$+2.8 \pm 2.0$
25	$+2.27 \pm 0.70$	-0.67 ± 0.80	$+1.06 \pm 1.00$
26	$+3.6 \pm 1.0$	—	—
This paper	$+0.14 \pm 0.01$	-0.43 ± 0.10	-1.57 ± 0.27

Refs 9, 24 used a simple orbital model, whereas refs 10, 25, 26 used the much more accurate Sampson–Lieske theory. Nevertheless, this orbital model has internal errors on the order of a few hundred kilometres (Supplementary Information), explaining the lack of agreement between all acceleration values. In particular, most of the tidal acceleration values found (see also Supplementary Table 1) are quite large except for those of ref. 10, in which data from over a very long time span (old eclipses) were used, partly averaging the missing long-period terms. Because our dynamical model fits the k_2/Q ratios, our solution uncertainties in \dot{n} have been derived for each satellite from the comparison of the two simulations that produced the minimum and maximum values of k_2/Q , respectively. As the k_2/Q ratios of Io and Jupiter are highly correlated, we could assume the minimum bound for Io's ratio when introducing the minimum bound of Jupiter's ratio, and vice versa.

¹IMCCE-Observatoire de Paris, UMR 8028 du CNRS, 77 Avenue Denfert-Rochereau, 75014 Paris, France. ²Royal Observatory of Belgium, Avenue Circulaire 3, Uccle, 1180 Bruxelles, Belgium.

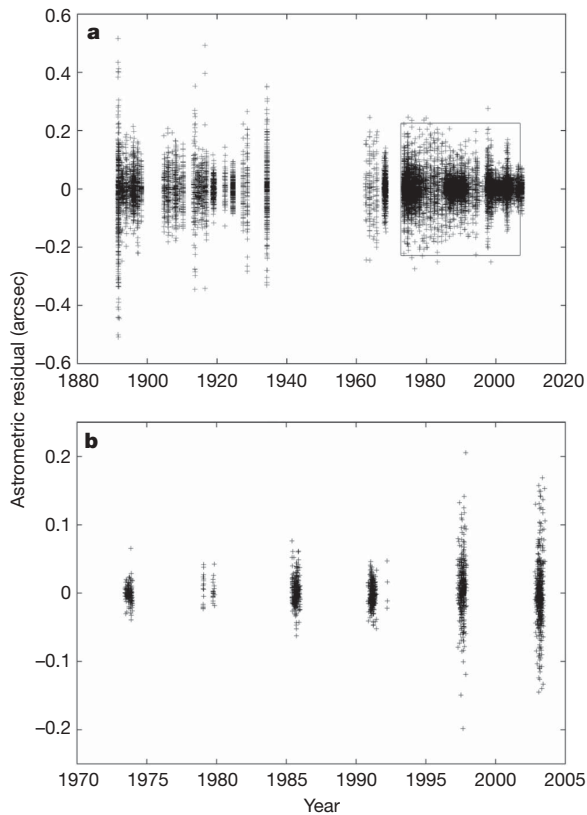


Figure 1 | Astrometric residuals. Residuals between the astrometric observations and our numerical model, after fitting the initial state vectors of each moon and the k_2/Q ratios of Jupiter and Io. We used an extensive set of astrometric observations that started in 1891, with heliometer measurements and the first photographic plates, and continued until 2007, with the most recent observations from the FASTT survey²⁷. **b**, Observations of the mutual events (occultation or eclipse of one satellite by another occurring every six years) from 1973 to 2003 (Supplementary Information; boxed region in **a**). The global 1σ accuracy is better than 0.1 arcsec (Supplementary Tables 2 and 3) at the Jovian distance (1 arcsec corresponds to about 3,000 km). The observations of mutual events, known to be among the most accurate observations, have a 1σ accuracy of about 0.025 arcsec and provide the best constraint of the satellite orbits for the past decades. Moreover, instead of considering the position of each satellite as given on the celestial sphere (that is, in arcseconds), we have considered only the relative positions of the observed satellites in the fitting process. For example, for the declination coordinate δ_i we did not fit $\delta_i^{\text{observed}} - \delta_i^{\text{computed}}$ but instead the quantity $[(\delta_i/\delta')^{\text{observed}} - (\delta_i/\delta')^{\text{computed}}] \delta_i^{\text{computed}}$, where $\delta' = \sqrt{\sum_{j=1}^N \delta_j^2}$ and N is the number of Galilean moons present in an observation. This allowed us to remove systematic errors in the scale factor introduced by the observers during the astrometric calibration of their observations.

The global energy dissipation, \dot{E} , in Io can be determined from $k_2/Q = 0.015 \pm 0.003$ using¹¹

$$\dot{E} = -\frac{21}{2} \frac{k_2}{Q} \frac{n^5 R^5}{G} e^2$$

where R is the radius of Io, G the gravitational constant and e the orbital eccentricity. We obtain $\dot{E} = (9.33 \pm 1.87) \times 10^{13}$ W. If energy were transported out of Io at the same rate, the associated surface heat flux would be 2.24 ± 0.45 W m⁻², which is similar to the observed surface heat flux (Fig. 2). This suggests that Io's interior is close to thermal equilibrium and that Io's internal heat is not the remnant of a past highly dissipative orbital configuration^{12–15}.

Theoretical studies have not been able to reproduce in a consistent equilibrium model both the tidal energy dissipation and the transport of this internally generated energy to the surface by mantle convection at the observed high surface heat flux^{15,16}. It has been argued that mantle viscosities cannot be chosen to satisfy both

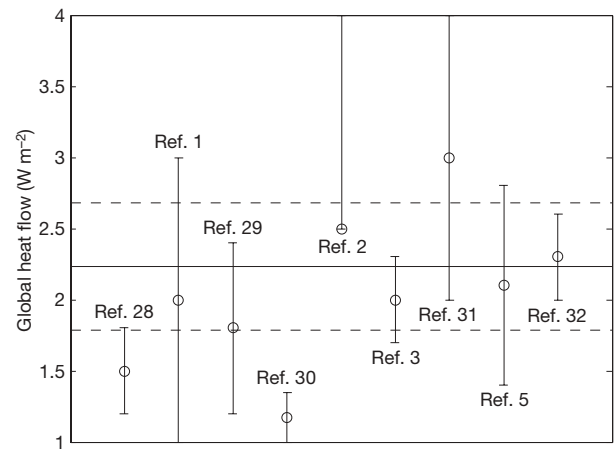


Figure 2 | Comparison of Io's thermal emission with the global dissipation determined in the present study. Io's intensive volcanic activity is associated with a large surface heat flow. The value determined by the present study (2.24 ± 0.45 W m⁻², shown by the horizontal lines) is in good agreement with the results of the remote observations^{1–3,5,28–32} of Io's thermal emission (the stated error bars mostly indicate ranges for the solutions rather than the standard deviations), suggesting that Io is close to thermal equilibrium. The average surface heat flow of Io is much larger than that of the Earth³³ (0.09 W m⁻²) and could be comparable to the high surface heat flow of the early Earth.

constraints: viscosities needed to generate the observed tidal dissipation (on the order of 10^{13} – 10^{16} Pa s; ref. 11) are too high to transport the produced heat to the surface by convection¹⁶. If Io is in thermal equilibrium as suggested here, a more efficient heat transport mechanism with a different viscosity dependence on temperature is required. The magma migration in Io's partially molten interior indicated by high eruption temperatures (larger than 1,300 K)¹⁷ is a possible mechanism¹⁸.

Plausible ranges for the quality factor of Io can be studied from the measured ratios k_2/Q by using limit values of the Love number. An upper limit of $Q = 82$ is found by considering Io as a body without strength, that is, by replacing the tidal Love number (k_2) by the fluid Love number, $k_2^f = 1.23$ (ref. 19). A much smaller quality factor is obtained for more realistic models in which Io is composed of a metallic core, a viscoelastic silicate mantle and an elastic lithosphere, depending on the viscosity and shear modulus of the mantle¹¹. A typical model with a core radius of 700 km, a core density of $6,944$ kg m⁻³, a mantle density of $3,375$ kg m⁻³ and a 40-km-thick lithosphere with a density of $2,600$ kg m⁻³, in agreement with the observations made by NASA's Galileo spacecraft¹⁹, yields $k_2 \approx 0.04$ and $Q \approx 3$ for a mantle rigidity of 50 GPa and viscosity of 4.1×10^{15} Pa s. However, if a low-viscosity asthenosphere exists in Io, the tidal Love number would increase to 0.7–0.8, resulting in a larger quality factor, of ~ 50 .

The dissipation in Jupiter (at the induced frequency of Io's tidal excitation) is determined to be $Q = (3.56 \pm 0.66) \times 10^4$ for the conventional value $k_2 = 0.379$ (ref. 20). This dissipation value is close to the lower limit over the age of the Solar System, $Q \geq 6 \times 10^4$, determined from the expansion of the orbits⁷, implying important dissipation in Jupiter. Estimates from numerical dissipation models of Jupiter suggest that Q undergoes large fluctuations as a function of tidal frequency^{21,22} and that the observed dissipation may be different from its long-term average (Supplementary Information).

Our results show that the mean motion of Io increases whereas those of Europa and Ganymede decrease. Therefore, Io moves inwards, towards Jupiter, and loses more orbital energy by dissipation of solid-body tides raised by Jupiter and by the Laplace resonance interaction than it gains from the exchange of angular momentum with Jupiter's rotational energy through tidal dissipation in Jupiter. The evolution of the Laplace resonance can be expressed in terms of the rate of change of the satellite mean motions, \dot{n}_1 , \dot{n}_2 and

\dot{n}_3 , where the subscripts correspond to Io, Europa and Ganymede, respectively^{7,13,23}. We have

$$\dot{v} = \dot{n}_1 - 2\dot{n}_2 = \dot{n}_2 - 2\dot{n}_3$$

The system is in stable equilibrium for $\dot{v} = 0$, which requires a balance between the dissipation rates in Jupiter and Io. With our rates of change of the mean motions, we have $\dot{v} = (0.74 \pm 0.24) \times 10^{-7} \text{ rad yr}^{-2}$, suggesting that the satellites are evolving away from exact resonance.

Received 12 January; accepted 30 April 2009.

- Matson, D. L., Ransford, G. A. & Johnson, T. V. Heat flow from Io. *J. Geophys. Res.* **86**, 1664–1672 (1981).
- Veeder, G., Matson, D., Johnson, T., Blaney, D. & Goguen, J. Io's heat flow from infrared radiometry: 1983–1993. *J. Geophys. Res.* **99**, 17095–17162 (1994).
- Spencer, J. R. et al. Io's thermal emission from the Galileo photopolarimeter-radiometer. *Science* **288**, 1198–1201 (2000).
- Peale, S. J., Cassen, P. & Reynolds, R. T. Melting of Io by tidal dissipation. *Science* **203**, 892–894 (1979).
- McEwen, A. S., Keszthelyi, P., Lopes, R., Schenk, P. M. & Spencer, J. R. in *Jupiter: The Planet, Satellites and Magnetosphere* (eds Bagenal, F., Dowling, T. E. & McKinnon, W. B.) 307–328 (Cambridge Univ. Press, 2004).
- Moore, B., Schubert, G., Anderson, J. D. & Spencer, J. R. in *Io After Galileo: A New View of Jupiter's Volcanic Moon* (eds Lopes, R. M. C. & Spencer, J. R.) 89–105 (Springer, 2007).
- Yoder, C. F. & Peale, S. The tides of Io. *Icarus* **47**, 1–35 (1981).
- Levrard, B. et al. Tidal dissipation within hot Jupiters: a new appraisal. *Astron. Astrophys.* **462**, L5–L8 (2007).
- De Sitter, W. Orbital elements determining the longitudes of Jupiter's satellites, derived from observations. *Leiden Ann.* **16**(2), 1–92 (1928).
- Lieske, J. H. Galilean satellite evolution - observational evidence for secular changes in mean motions. *Astron. Astrophys.* **176**, 146–158 (1987).
- Segatz, M., Spohn, T., Ross, M. N. & Schubert, G. Tidal dissipation, surface heat flow, and figure of viscoelastic models of Io. *Icarus* **75**, 187–206 (1988).
- Ojakangas, G. & Stevenson, D. Episodic volcanism of tidally heated satellites with application to Io. *Icarus* **66**, 341–358 (1986).
- Greenberg, R. Galilean satellites - evolutionary paths in deep resonance. *Icarus* **70**, 334–347 (1987).
- Fischer, H. J. & Spohn, T. Thermal-orbital histories of viscoelastic models of Io (J1). *Icarus* **83**, 39–65 (1990).
- Hussmann, H. & Spohn, T. Thermal-orbital evolution of Io and Europa. *Icarus* **171**, 391–410 (2004).
- Moore, W. Tidal heating and convection in Io. *J. Geophys. Res.* **108**, doi:10.1029/2002JE001943 (2003).
- Keszthelyi, L. et al. New estimates for Io eruption temperatures: implications for the interior. *Icarus* **192**, 491–502 (2007).
- Moore, W. The thermal state of Io. *Icarus* **154**, 548–550 (2001).
- Anderson, J. D., Jacobson, R. A. & Lau, E. L. Io's gravity field and interior structure. *J. Geophys. Res.* **106**, 32963–32969 (2001).
- Gavrilov, S. V. & Zharkov, V. N. Love numbers of the giant planets. *Icarus* **32**, 443–449 (1977).
- Ogilvie, G. I. & Lin, D. N. C. Tidal dissipation in rotating giant planets. *Astrophys. J.* **610**, 477–509 (2004).
- Wu, Y. Origin of tidal dissipation in Jupiter. II. The value of Q. *Astrophys. J.* **635**, 688–710 (2005).
- Yoder, C. F. How tidal heating in Io drives the Galilean orbital resonance locks. *Nature* **279**, 747–770 (1979).
- Goldstein, S. J. Jr & Jacobs, K. C. A recalculation of the secular acceleration of Io. *Astron. J.* **110**, 3054–3057 (1995).
- Vasundhara, R., Arlot, J.-E. & Descamps, P. in *Dynamics, Ephemerides and Astrometry of the Solar System* (eds Ferraz-Mello, S., Morando, B. & Arlot, J.-E.) 145–149 (Proc. 172nd Symp. Int. Astron. Union, IAU, 1996).
- Aksnes, K. & Franklin, F. A. Secular acceleration of Io derived from mutual satellite events. *Astron. J.* **122**, 2734–2739 (2001).
- Stone, R. C. Positions for the outer planets and many of their satellites. V. FASTT observations taken in 2000–2001. *Astron. J.* **122**, 2723–2733 (2001).
- Morrison, D. & Telesco, C. M. Io - observational constraints on internal energy and thermophysics of the surface. *Icarus* **44**, 226–233 (1980).
- Sinton, W. M. The thermal emission spectrum of Io and a determination of the heat flux from its hot spots. *J. Geophys. Res.* **86**, 3122–3128 (1981).
- Johnson, T. V. et al. Volcanic hotspots on Io - stability and longitudinal distribution. *Science* **226**, 134–137 (1984).
- Veeder, G. J., Matson, D. L., Johnson, T. V., Davies, A. G. & Blaney, D. L. The polar contribution to the heat flow of Io. *Icarus* **169**, 264–270 (2004).
- Rathbun, J. A. et al. Mapping of Io's thermal radiation by the Galileo photopolarimeter-radiometer (PPR) instrument. *Icarus* **169**, 127–139 (2004).
- Lay, T., Hernlund, J. & Bussett, B. A. Core-mantle boundary heat flow. *Nature Geosci.* **1**, 25–32 (2008).

Supplementary Information is linked to the online version of the paper at www.nature.com/nature.

Acknowledgements We thank D. Pascu for sharing his unpublished observations.

Author Contributions All authors contributed to the writing of the manuscript. V.L. developed and fitted to the observations the full numerical model presented in this work. J.-E.A. fitted to the observations the secular accelerations using L1 astrometric residuals (Supplementary Information). Theoretical calculations of the energy dissipation and Fig. 2 were made by Ö.K. T.V.H. and Ö.K. contributed to the geophysical interpretations of the secular accelerations.

Author Information Reprints and permissions information is available at www.nature.com/reprints. Correspondence and requests for materials should be addressed to V.L. (laine@imcce.fr).

STRONG TIDAL DISSIPATION IN SATURN AND CONSTRAINTS ON ENCELADUS' THERMAL STATE FROM ASTROMETRY

VALÉRY LAINEY¹, ÖZGÜR KARATEKIN², JOSSELIN DESMARS^{1,3}, SÉBASTIEN CHARNOZ⁴, JEAN-EUDES ARLOT¹,
NICOLAI EMELYANOV^{1,5}, CHRISTOPHE LE PONCIN-LAFITTE⁶, STÉPHANE MATHIS⁴, FRANÇOISE REMUS^{1,4,7},
GABRIEL TOBIE⁸, AND JEAN-PAUL ZAHN⁷

¹ IMCCE-Observatoire de Paris, UMR 8028 du CNRS, UPMC, 77 Av. Denfert-Rochereau, 75014 Paris, France; laine@imcce.fr

² Royal Observatory of Belgium, Avenue Circulaire 3, 1180 Uccle, Bruxelles, Belgium

³ Shanghai Astronomical Observatory, Chinese Academy of Sciences, 80 Nandan Road, 200030 Shanghai, China

⁴ Laboratoire AIM, CEA/DSM-CNRS-Université Paris Diderot, IRFU/SAP Centre de Saclay, 91191 Gif-sur-Yvette, France

⁵ Sternberg Astronomical Institute, 13 Universitetskij Prospect, 119992 Moscow, Russia

⁶ SyRTE-Observatoire de Paris, UMR 8630 du CNRS, 77 Av. Denfert-Rochereau, 75014 Paris, France

⁷ LUTH-Observatoire de Paris, UMR 8102 du CNRS, 5 place Jules Janssen, 92195 Meudon Cedex, France

⁸ Laboratoire de Planétologie et Géodynamique de Nantes, Université de Nantes, CNRS, UMR 6112, 2 rue de la Houssinière, 44322 Nantes Cedex 3, France

Received 2011 September 4; accepted 2012 March 23; published 2012 May 22

ABSTRACT

Tidal interactions between Saturn and its satellites play a crucial role in both the orbital migration of the satellites and the heating of their interiors. Therefore, constraining the tidal dissipation of Saturn (here the ratio k_2/Q) opens the door to the past evolution of the whole system. If Saturn's tidal ratio can be determined at different frequencies, it may also be possible to constrain the giant planet's interior structure, which is still uncertain. Here, we try to determine Saturn's tidal ratio through its current effect on the orbits of the main moons, using astrometric data spanning more than a century. We find an intense tidal dissipation ($k_2/Q = (2.3 \pm 0.7) \times 10^{-4}$), which is about 10 times higher than the usual value estimated from theoretical arguments. As a consequence, eccentricity equilibrium for Enceladus can now account for the huge heat emitted from Enceladus' south pole. Moreover, the measured k_2/Q is found to be poorly sensitive to the tidal frequency, on the short frequency interval considered. This suggests that Saturn's dissipation may not be controlled by turbulent friction in the fluid envelope as commonly believed. If correct, the large tidal expansion of the moon orbits due to this strong Saturnian dissipation would be inconsistent with the moon formations 4.5 Byr ago above the synchronous orbit in the Saturnian subnebulae. But it would be compatible with a new model of satellite formation in which the Saturnian satellites formed possibly over a longer timescale at the outer edge of the main rings. In an attempt to take into account possible significant torques exerted by the rings on Mimas, we fitted a constant rate da/dt on Mimas' semi-major axis as well. We obtained an unexpected large acceleration related to a negative value of $da/dt = -(15.7 \pm 4.4) \times 10^{-15}$ AU day⁻¹. Such acceleration is about an order of magnitude larger than the tidal deceleration rates observed for the other moons. If not coming from an astrometric artifact associated with the proximity of Saturn's halo, such orbital decay may have significant implications on the Saturn's rings.

Key words: astrometry – celestial mechanics – ephemerides – Planets and satellites: dynamical evolution and stability – Planets and satellites: interiors

Online-only material: color figures

1. INTRODUCTION

Starting with Huygens' observation of Titan in 1655, a little less than two centuries were needed to discover the so-called main moons of Saturn (defined by increasing distance to the primary, Mimas, Enceladus, Tethys, Dione, Rhea, Titan, Hyperion, and Iapetus). In common with the Galilean moons, astrometry of the Saturn satellites (consisting of measuring the moon positions in the sky) started in the middle of the 17th century, with the observations of eclipses by the primary. One has to wait until the end of the 19th century and the manufacturing of photographic plates, as well as large micrometer and heliometer instruments, for the gathering of reasonably accurate observations (Desmars et al. 2009b). Although previously used to probe the gravity fields of the system, astrometry has been replaced advantageously by radio-science data, since the spacecraft era. Nevertheless, the large time span covered by astrometric observations and number of observation sets available can still compensate for any possible lack of precision when one focuses on long-term dynamical effects, as, for example, in

the case of Mars (Laine et al. 2007) and Jupiter (Laine et al. 2009).

In Section 2, we present the observation set used in this study. Section 3 details the numerical model of the Saturnian satellite orbits that has been used to determine Saturn's tidal dissipation. In Sections 4 and 5, we present the fit of the orbit model to astrometric observations and demonstrate its robustness. The last section discusses possible interior models of Saturn and Enceladus in the light of our results.

2. THE OBSERVATION SET

To determine long-term effects in the mean motions of the satellites accurately, a set of astrometric observations covering a long time span is necessary. In this context, an extensive catalog of astrometric observations has been compiled. This catalog provides about 19,617 observations (counting one date as one observation even for several satellites observed simultaneously) and covers the period from 1886 to 2009. All observations are available in the NSDB natural satellites astrometric database (Arnot & Emelyanov 2009).

The main source of the catalog is COSS08 (Desmars et al. 2009b), yielding about 130,000 data (counting one coordinate of one satellite as one datum) from 1874 to 2007. For our set of data, only the “accurate” observations have been selected. To define “accurate” observations, we have first excluded those with a residual larger than 2 arcsec and then computed the rms of the residuals for all the observations corresponding to each bibliographic reference. Finally, for the purposes of the present paper, if the rms was larger than 0.3 arcsec for observations before 1950 and 0.25 arcsec for observations after 1950, the entire set issued from that particular bibliographic reference has been excluded. As a consequence, about 93% of COSS08 observations have been selected starting from 1886 until 2007.

Since 2007, other observations have become available. The USNO Flagstaff transit circle data, already included in COSS08, have been updated until 2009. Observations from Peng et al. (2008) have also been added. Moreover, the highly accurate astrometric observations provided by the observation of the mutual phenomena of Saturnian satellites during 1995 and 2009 have been added.

Finally, the extensive catalog contains about 19,000 observations made from 1886 to 2009.

Direct astrometric observations can be performed in several different ways: transit observations, photographic plates, and CCD imaging. They are reduced from the known position of reference stars visible in the field of view during the observation. Because of their small field of view, the CCD frames and some long focus photographic plates do not often allow the use of reference stars. To deal with such data, the authors generally use the position of specific well-known satellites (usually Titan, Rhea, Dione, and Tethys because of their accurate ephemerides) computed with a specific theory as a reference in order to deduce the astrometric positions of the other satellites. A drawback of this is that these observations may be biased by any limiting assumptions in the adopted theory. To deal with this problem, we preferred to consider only relative separation and position angle between the satellites using pixel positions. This method provides astrometric observations that do not depend on the theory. It has been applied for CCD observations when stars were not used in the astrometric reduction. The influence of such a bias is tested in Section 5.3.

Photometric observations of mutual occultations and eclipses of the Saturnian satellites provide very accurate astrometric relative positions of the satellites. These observations are possible during the Saturnian equinox, since the Sun and the Earth are then in the equatorial plane of Saturn, which is also the common orbital plane of the satellites. Campaigns of observations of such mutual occultations and eclipses were made in 1995 and 2009. We undertook the processing of the complete database of these photometric observations published by Thuillot et al. (2001). An accurate photometric model of mutual events using the scattering properties of the satellite surfaces (Buratti 1984) issued from *Voyager* data was used. A large analysis of the properties of Saturnian icy satellites is done in Pitman et al. (2010) using the observations of these bodies provided by the *Cassini* probe. Phase curves are given in the *V* and *R* bands for solar phase angles in the vast range up to 180° (but only for Rhea and Dione). Unfortunately, because of this wide range of phase angles, we could not rely on Pitman et al. (2010) for the satellite albedo in the range of 1°–6° and therefore did not use their data.

In order to extract astrometric positions from photometric data, we developed an original method (Emelyanov & Gilbert 2006). We have processed the 46 light curves obtained during

the international campaign of photometric observations of the Saturnian satellites in 1995 and the 17 light curves obtained during the international campaign in 2009. From these photometric observations 46 topocentric or heliocentric angular differences in right ascension and declination for satellite pairs on the time interval from 1995 December 16 to 1996 February 6 and 17 topocentric or heliocentric angular differences on the time interval from 2008 December 19 to 2009 July 7 were obtained. The errors due to random errors of photometry are from 1 to 15 mas in right ascension and declination and characterize the internal accuracy of the astrometric results. Nevertheless, due to the rather small number of observed events compared to other observation sets, the contribution of mutual events has turned out to be modest. This contrasts with the Jovian case (Lainey et al. 2009).

3. THE DYNAMICAL MODEL

The NOE (Numerical Orbit and Ephemerides) numerical code (Lainey et al. 2007, 2009; Lainey 2008) has been used to model the orbital motion of the Saturnian satellites. It is a gravitational *N*-body code that incorporates highly sensitive modeling and can generate partial derivatives needed to fit initial positions, velocities, and other parameters (like the ratio k_2/Q) to the observational data. The code includes (1) gravitational interaction up to degree two in the spherical harmonic expansion of the gravitational potential for the satellites and up to degree six for Saturn with the numerical values from Jacobson et al. (2006), (2) perturbations due to the Sun and Jupiter using DE406 ephemerides (with the inner planets and the Moon included by incorporating their masses in the solar value), (3) Saturnian precession from Jacobson (2007), and (4) tidal effects introduced by means of the Love number k_2 and the quality factor Q in the combination k_2/Q for Saturn and Enceladus. The orbital effects due to the dissipation inside Saturnian satellites other than Enceladus are neglected, since they are expected to be much less dissipative, less eccentric, or much farther away from Saturn. Nevertheless, the tidal bulges raised by each moon on Saturn are taken into account.

The dynamical equations are numerically integrated in a Saturn-centric frame with inertial axes (conveniently the Earth mean equator J2000). The equation of motion for a satellite P_i can be expressed in a general form as

$$\begin{aligned} \ddot{\mathbf{r}}_i = & -G(m_0 + m_i) \left(\frac{\mathbf{r}_i}{r_i^3} - \nabla_i U_{i0} + \nabla_0 U_{0i} \right) + \sum_{j=1, j \neq i}^N G m_j \\ & \times \left(\frac{\mathbf{r}_j - \mathbf{r}_i}{r_{ij}^3} - \frac{\mathbf{r}_j}{r_j^3} - \nabla_j U_{ji} + \nabla_i U_{ij} + \nabla_j U_{j0} - \nabla_0 U_{0j} \right) \\ & + \frac{(m_0 + m_i)}{m_i m_0} (\mathbf{F}_{i0}^T - \mathbf{F}_{0i}^T) - \frac{1}{m_0} \sum_{j=1, j \neq i}^N (\mathbf{F}_{j0}^T - \mathbf{F}_{0j}^T). \end{aligned} \quad (1)$$

Here, \mathbf{r}_i and \mathbf{r}_j are the position vectors of the satellite P_i and a body P_j (another satellite, the Sun, or Jupiter) with mass m_j , subscript 0 denotes Saturn, U_{ki} is the oblateness gravity field of body P_l at the position of body P_k , and \mathbf{F}_{lk}^T is the force received by P_l from the tides it raises on P_k . This force is equal to (Lainey

Table 1
 Statistics of the Astrometric Residuals Computed from Our Model (Enceladus Tidal Equilibrium Solution) in Arcsecond

Observation subset	$\nu_\alpha \cos(\delta)$	$\sigma_\alpha \cos(\delta)$	ν_δ	σ_δ	N_α, N_δ
All observations					
S1	-0.0057	0.0952	-0.0108	0.0725	371, 371
S2	0.0019	0.1040	0.0028	0.1101	822, 822
S3	-0.0199	0.1267	0.0122	0.1067	1972, 1972
S4	0.0020	0.1066	0.0113	0.1067	2271, 2271
S5	0.0047	0.0899	-0.0023	0.0863	2977, 2977
S6	0.0121	0.1060	-0.0171	0.1070	3271, 3271
S7	0.1098	0.2984	0.0036	0.2166	973, 973
S8	0.0140	0.1143	-0.0052	0.1155	2008, 2008
Alden & O'Connell (1928)					
S2	0.0193	0.0890	0.0394	0.0816	40, 40
S3	0.0267	0.0653	0.0066	0.0569	65, 65
S4	0.0218	0.0493	0.0119	0.0467	64, 64
S5	0.0007	0.0563	0.0204	0.0528	64, 64
S6	-0.0442	0.0681	-0.0076	0.0566	64, 64
S8	-0.0190	0.1538	-0.0609	0.1337	59, 59
Alden (1929)					
S2	0.0258	0.0819	0.0228	0.0794	34, 34
S3	0.0031	0.0420	0.0127	0.0526	38, 38
S4	0.0097	0.0349	0.0359	0.0352	34, 34
S5	-0.0233	0.0520	0.0306	0.0364	36, 36
S6	-0.0267	0.0516	-0.0132	0.0508	36, 36
S8	0.0135	0.0727	-0.0887	0.1006	35, 35
Sinclair (1974, 1977) 13s					
S3	0.0279	0.1090	-0.0107	0.1446	20, 20
S4	0.0317	0.1551	0.0350	0.1528	25, 25
S5	0.0040	0.1099	-0.0330	0.0952	25, 25
S6	-0.1788	0.1799	0.0310	0.0819	25, 25
S8	0.1258	0.1603	-0.0254	0.1186	24, 24
Sinclair (1974, 1977) 26s					
S3	0.0005	0.1069	0.0124	0.1011	40, 40
S4	0.0044	0.0592	0.0098	0.0626	46, 46
S5	0.0054	0.0698	-0.0122	0.0805	48, 48
S6	-0.0002	0.0823	-0.0079	0.0555	48, 48
S8	-0.0099	0.0563	0.0004	0.0821	48, 48
Abbot et al. (1975) PDS					
S1	-0.1707	0.0000	-0.0859	0.0000	1, 1
S2	-0.0472	0.0901	0.1828	0.1098	4, 4
S3	-0.0068	0.1408	0.1060	0.1260	10, 10
S4	-0.0476	0.1199	0.0084	0.0622	10, 10
S5	0.0344	0.0347	0.0109	0.0371	10, 10
S6	-0.0693	0.0702	-0.0587	0.0241	11, 11
S7	-0.2607	0.1166	0.3553	0.0757	6, 6
S8	0.0138	0.0739	0.0475	0.0274	10, 10
Abbot et al. (1975) Mann					
S1	0.0692	0.0000	-0.1231	0.0000	1, 1
S2	-0.1171	0.0981	0.3500	0.2047	5, 5
S3	0.0028	0.0888	0.0298	0.1325	11, 11
S4	-0.0321	0.1280	0.0584	0.1849	11, 11
S5	0.0393	0.0448	0.0136	0.0761	11, 11
S6	-0.0960	0.1324	-0.0234	0.0385	11, 11
S7	-0.2767	0.0599	0.4871	0.0485	6, 6
S8	0.0325	0.0941	0.0465	0.0559	11, 11
Voronenko et al. (1991)					
S3	0.0172	0.2064	-0.0056	0.1350	85, 85
S4	-0.0324	0.1675	0.0066	0.1712	96, 96
S5	-0.0034	0.1455	0.0214	0.0976	143, 143
S6	0.0179	0.1319	-0.0196	0.1084	153, 153
S8	0.0154	0.1679	-0.0263	0.1085	19, 19
D. Pascu (1982, private communication)					
S1	-0.0105	0.1620	-0.0393	0.1155	56, 56
S2	0.0041	0.0953	-0.0228	0.1208	107, 107

Table 1
(Continued)

Observation subset	$\nu_\alpha \cos(\delta)$	$\sigma_{\alpha \cos(\delta)}$	ν_δ	σ_δ	N_α, N_δ
S3	0.0148	0.0644	-0.0104	0.0775	138, 138
S4	-0.0001	0.0505	-0.0064	0.0608	165, 165
S5	0.0115	0.0502	-0.0041	0.0602	209, 209
S6	-0.0010	0.0529	0.0153	0.0644	228, 228
S7	0.0761	0.2466	-0.0564	0.1824	11, 11
S8	-0.0191	0.0886	0.0211	0.1071	213, 213
Tolbin (1991a)					
S1	-0.0297	0.1602	-0.0414	0.1813	21, 21
S2	0.0059	0.0884	0.0090	0.1327	57, 57
S3	0.0004	0.0697	-0.0180	0.0834	75, 75
S4	0.0127	0.0551	-0.0073	0.0856	81, 81
S5	0.0016	0.0526	0.0047	0.0684	88, 88
S6	0.0033	0.0758	-0.0022	0.0968	89, 89
S8	-0.0194	0.1521	0.0336	0.1261	62, 62
Tolbin (1991b)					
S1	0.0292	0.1520	0.0194	0.1375	7, 7
S2	-0.0120	0.1237	0.0266	0.1293	50, 50
S3	0.0003	0.0596	-0.0037	0.0767	89, 89
S4	0.0121	0.0587	-0.0006	0.0706	96, 96
S5	0.0012	0.0617	-0.0041	0.0817	102, 102
S6	0.0067	0.0674	-0.0354	0.1222	107, 107
S8	-0.0189	0.0740	0.0309	0.1920	80, 80
Seitzer & Ianna (1980)					
S3	-0.0879	0.0096	0.0504	0.0297	3, 3
S4	-0.0332	0.0198	-0.0141	0.0109	3, 3
S5	0.0654	0.0629	-0.1057	0.0739	10, 10
S6	0.0454	0.0849	-0.0381	0.0600	17, 17
S8	-0.0515	0.1236	0.0060	0.1843	24, 24
Taylor & Sinclair (1985)					
S2	0.0604	0.1549	0.0443	0.0569	10, 10
S3	0.0710	0.1993	0.0589	0.0852	20, 20
S4	-0.0485	0.1979	0.0097	0.1309	35, 35
S5	0.0250	0.1227	-0.0005	0.1180	38, 38
S6	-0.0078	0.0973	-0.0696	0.1138	45, 45
S7	0.2277	0.5327	0.0817	0.5884	38, 38
S8	-0.0152	0.1239	0.0405	0.1432	45, 45
Seitzer et al. (1979)					
S1	-0.1067	0.1613	-0.0564	0.0106	2, 2
S3	0.0055	0.0678	-0.0073	0.0849	49, 49
S4	0.0539	0.2094	-0.1229	0.1929	41, 41
S5	0.0082	0.0652	-0.0387	0.0756	49, 49
S6	0.0829	0.1042	-0.0467	0.1039	50, 50
S7	-0.3379	0.1333	0.0453	0.1124	4, 4
S8	-0.0430	0.0971	0.1102	0.1839	60, 60
Dourneau et al. (1986)					
S1	0.0686	0.2278	-0.0274	0.1042	11, 11
S2	0.0146	0.1244	-0.0151	0.0593	39, 39
S3	0.0249	0.0786	-0.0285	0.0488	39, 39
S4	-0.0259	0.0691	-0.0260	0.0570	56, 56
S5	0.0045	0.0644	-0.0097	0.0478	76, 76
S6	0.0101	0.0684	0.0549	0.0426	82, 82
S7	0.7665	0.1130	0.0276	0.0832	95, 95
S8	-0.0126	0.1165	-0.0019	0.0698	95, 95
Veillet & Dourneau (1992) 3.6					
S3	0.0037	0.0858	-0.0083	0.1542	20, 20
S4	0.0630	0.1749	-0.0281	0.1058	25, 25
S5	0.0651	0.0404	-0.0392	0.0561	14, 14
S6	-0.0164	0.1288	-0.1052	0.0773	17, 17
S7	0.1865	0.3238	-0.0286	0.0985	25, 25
S8	-0.0763	0.1239	0.1069	0.0649	30, 30
Veillet & Dourneau (1992) 1.5					
S1	-0.1346	0.1196	-0.0500	0.0749	10, 10
S2	-0.0014	0.1013	-0.0223	0.0880	57, 57

Table 1
(Continued)

Observation subset	$\nu_\alpha \cos(\delta)$	$\sigma_\alpha \cos(\delta)$	ν_δ	σ_δ	N_α, N_δ
S3	-0.0083	0.1103	0.0007	0.0807	78, 78
S4	0.0112	0.0689	-0.0032	0.0674	155, 155
S5	0.0028	0.0542	-0.0019	0.0495	195, 195
S6	-0.0015	0.0671	0.0167	0.0479	197, 197
S7	0.0006	0.1234	0.0118	0.0916	197, 197
S8	0.0004	0.0874	-0.0037	0.0976	196, 196
Kiseleva et al. (1996)					
S2	-0.0420	0.0940	0.0219	0.1574	10, 10
S3	-0.0168	0.0868	0.0413	0.1150	11, 11
S4	-0.0057	0.0507	-0.0251	0.0566	25, 25
S5	-0.0211	0.0623	-0.0188	0.0792	25, 25
S6	-0.0036	0.0592	-0.0081	0.0834	32, 32
S8	0.0662	0.0902	0.0325	0.1311	21, 21
Vass (1997)					
S2	0.0025	0.1647	-0.0132	0.1532	151, 151
S3	-0.0704	0.1494	0.0319	0.1246	654, 654
S4	-0.0039	0.1388	0.0480	0.1269	600, 600
S5	0.0061	0.1237	-0.0059	0.1135	948, 948
S6	0.0083	0.1163	-0.0203	0.1193	1287, 1287
S7	-0.0477	0.1564	0.0478	0.2366	94, 94
S8	0.1306	0.1505	-0.0654	0.1037	243, 243
Kiseleva & Kalinitchenko (2000)					
S1	-0.1235	0.0434	0.0449	0.0373	3, 3
S2	-0.0387	0.0923	0.0023	0.0716	10, 10
S3	-0.0165	0.0654	0.0182	0.0748	22, 22
S4	0.0239	0.0527	-0.0236	0.0686	23, 23
S5	0.0039	0.0532	0.0138	0.0594	27, 27
S6	0.0100	0.0564	0.0069	0.0768	27, 27
S8	0.0139	0.1079	-0.0410	0.1718	14, 14
Kiseleva & Kalinitchenko (1998)					
S2	-0.0768	0.1335	0.2952	0.1175	3, 3
S3	-0.0178	0.0415	-0.0342	0.1405	7, 7
S4	0.0509	0.0714	-0.0259	0.1535	4, 4
S5	-0.0124	0.0384	-0.0070	0.0762	10, 10
S6	0.0386	0.0718	-0.0818	0.2194	12, 12
S8	0.0117	0.0000	-0.0871	0.0000	1, 1
French et al. (2006) HST-WF4					
S1	-0.0002	0.0111	-0.0093	0.0104	39, 39
S2	0.0025	0.0132	0.0005	0.0157	53, 53
S3	0.0039	0.0167	0.0057	0.0160	63, 63
S4	0.0027	0.0196	0.0054	0.0269	33, 33
S5	-0.0011	0.0152	0.0014	0.0199	39, 39
S6	-0.0273	0.0401	-0.0107	0.0328	23, 23
S7	0.0856	0.0074	0.0009	0.0040	4, 4
French et al. (2006) HST-PC					
S1	0.0022	0.0076	0.0004	0.0098	154, 154
S2	-0.0027	0.0056	-0.0001	0.0087	82, 82
S3	0.0056	0.0124	0.0031	0.0077	24, 24
S4	-0.0112	0.0024	-0.0122	0.0013	5, 5
S5	0.0083	0.0060	0.0049	0.0081	10, 10
French et al. (2006) HST-WF3					
S1	0.0037	0.0079	-0.0030	0.0173	25, 25
S2	-0.0034	0.0117	-0.0026	0.0130	51, 51
S3	0.0011	0.0086	0.0007	0.0142	55, 55
S4	0.0024	0.0187	-0.0087	0.0193	99, 99
S5	-0.0022	0.0166	0.0012	0.0291	70, 70
S7	-0.0119	0.0095	-0.0148	0.0301	13, 13
French et al. (2006) HST-WF2					
S1	0.0022	0.0119	0.0034	0.0135	34, 34
S2	-0.0020	0.0160	0.0119	0.0111	35, 35
S3	0.0042	0.0111	-0.0073	0.0206	33, 33
S4	0.0089	0.0199	0.0074	0.0281	87, 87

Table 1
(Continued)

Observation subset	$\nu_\alpha \cos(\delta)$	$\sigma_\alpha \cos(\delta)$	ν_δ	σ_δ	N_α, N_δ
S5	-0.0127	0.0140	-0.0105	0.0223	35, 35
S7	0.0030	0.0509	0.0234	0.0189	30, 30
USNO Flagstaff ^a					
S3	-0.0034	0.1461	0.0164	0.1315	251, 251
S4	0.0059	0.0912	0.0089	0.1031	398, 398
S5	0.0040	0.0585	0.0008	0.0721	651, 651
S6	0.0458	0.1052	-0.0335	0.1124	682, 682
S7	0.0635	0.1851	-0.0299	0.2159	450, 450
S8	0.0094	0.0752	-0.0144	0.0801	705, 705
Kiseleva (unpublished)					
S1	-0.0225	0.0601	0.0618	0.0327	3, 3
S2	0.0428	0.0790	0.0009	0.0523	10, 10
S3	0.0061	0.0896	-0.0300	0.1058	19, 19
S4	-0.0152	0.0794	-0.0495	0.1321	20, 20
S5	0.0107	0.0581	-0.0109	0.0700	21, 21
S6	-0.0208	0.0822	-0.0323	0.0945	25, 25
S8	0.0093	0.0903	0.1847	0.1637	13, 13
PHESAT					
S1	-0.0653	0.0649	-0.0073	0.0099	4, 4
S2	0.0009	0.0203	0.0046	0.0103	14, 14
S3	-0.0021	0.0152	0.0027	0.0180	53, 53
S4	0.0002	0.0281	0.0024	0.0180	34, 34
S5	0.0072	0.0179	-0.0005	0.0289	23, 23
S6	0.0010	0.0018	0.0100	0.0272	3, 3

Notes. μ and σ denote, respectively, the mean and standard deviation of the residuals computed in right ascension $\alpha \cdot \cos(\delta)$ and declination δ . N_α and N_δ are the number of observations considered for the respective coordinate. We recall that 0.1 s of arc corresponds to about 600 km at the Saturn distance.

^a <http://www.nofs.navy.mil/data/plansat.html>

et al. 2007)

$$\mathbf{F}_{ik}^T = -\frac{3k_2 G m_l^2 R^5 \Delta t}{r_{kl}^8} \left(\frac{2\mathbf{r}_{kl}(\mathbf{r}_{kl} \cdot \mathbf{v}_{kl})}{r_{kl}^2} + (\mathbf{r}_{kl} \times \boldsymbol{\Omega} + \mathbf{v}_{kl}) \right), \quad (2)$$

where $\mathbf{r}_{kl} = \mathbf{r}_k - \mathbf{r}_l$ and $\mathbf{v}_{kl} = d\mathbf{r}_{kl}/dt$, with $\boldsymbol{\Omega}$, R , and Δt being the instantaneous rotation vector, equatorial radius, and time potential lag of P_k , respectively. The usual tidal term independent of Q (and so only dependent on k_2) that arises in the tidal potential development has been neglected here. This is justified for two reasons: it is pretty small (a typical drift of a few tens of km in longitude after 100 years), and most importantly, since it provides only secular drift (but not secular acceleration) on longitudes, it can easily be absorbed in a tiny change of the initial conditions without any significant consequences. While it was considered only for completeness in Lainey et al. (2009), it has been neglected here.

The time lag Δt is defined by (Lainey et al. 2007)

$$\Delta t = T \arctan(1/Q)/2\pi, \quad (3)$$

where T is the period of the main tidal excitation. For the tides raised on Enceladus, T is equal to $2\pi/n$ (n being Enceladus' mean motion) as we only considered the tide raised by Saturn. For Saturn's tidal dissipation, T is equal to $2\pi/2(\Omega - n_i)$, where Ω is the spin frequency of Saturn and n_i is the mean motion of the tide raising Saturnian moon P_i . Δt depends on the tidal frequency and on Q ; therefore, it is not a constant parameter.

It is clear from the second term on the right-hand side of Equations (2) and (3) that k_2 and Q are completely correlated.

In practice, we considered the commonly used value $k_2 = 0.341$ (Gavrilov & Zharkov 1977) and fitted only Q .

Because of a 2:1 resonance located at the outer edge of the B-ring, Saturn's rings are expected to interact significantly with Mimas (Lissauer & Cuzzi 1982). However the magnitude of this effect is unknown, because of large uncertainties about the ring structures and surface densities. To take into account such an interaction, we had to introduce a supplementary force in the system modeling a constant rate da/dt on Mimas' semi-major axis (denoted by a) and considered as an additional free parameter in the model. As a consequence, no information on tidal dissipation inside Saturn may be obtained directly from Mimas' orbital motion, since the latter is mixed with the estimation of the ring dynamical effects. Moreover, because of the Mimas–Tethys resonant interaction, such a da/dt rate should not be compared with a possible observed kinematic rate. To introduce a da/dt constant term as a supplementary force in the model, we used the Gauss equations. We recall that this differential system provides the variation of Keplerian elements as a function of disturbing forces expressed in the local base. Introducing a constant variation in the semi-major axis (and no variations in the other Keplerian elements), this system can easily be inverted to provide the proper expression of the force.

For an unspecified parameter c_l of the model that shall be fitted (e.g., $\mathbf{r}(t_0)$, $d\mathbf{r}/dt(t_0)$, Q , ...), a useful relation is

$$\frac{\partial}{\partial c_l} \left(\frac{d^2 \mathbf{r}_i}{dt^2} \right) = \frac{1}{m_i} \left[\sum_j \left(\frac{\partial \mathbf{F}_i}{\partial \mathbf{r}_j} \frac{\partial \mathbf{r}_j}{\partial c_l} + \frac{\partial \mathbf{F}_i}{\partial \dot{\mathbf{r}}_j} \frac{\partial \dot{\mathbf{r}}_j}{\partial c_l} \right) + \frac{\partial \mathbf{F}_i}{\partial c_l} \right], \quad (4)$$

Table 2
 Statistics of the Astrometric Residuals Computed from Our Model (Enceladus Tidal Equilibrium Solution) in Arcseconds

Observation subset	ν_s	σ_s	ν_p	σ_p	N_s, N_p
All Observations					
S1	0.0140	0.1027	0.0131	0.1152	1285, 1298
S2	-0.0032	0.0988	0.0048	0.1069	2640, 2643
S3	0.0157	0.1130	-0.0003	0.1152	4702, 4700
S4	0.0150	0.1045	0.0023	0.1096	3775, 3776
S5	0.0113	0.1088	0.0030	0.1151	4471, 4489
S6	0.0238	0.0937	-0.0049	0.1084	2842, 2836
S7	0.0017	0.3275	0.1068	0.4838	138, 113
S8	0.0179	0.0766	0.0076	0.1246	1098, 1101
Struve (1898) 61/62					
S1	0.0076	0.1756	0.0394	0.1810	105, 119
S2	-0.0011	0.1129	-0.0215	0.1170	218, 226
S3	0.0617	0.1363	-0.0185	0.1190	276, 281
S4	0.0671	0.1367	-0.0242	0.1252	167, 170
S8	0.0531	0.0562	-0.0140	0.1181	6, 6
Struve (1898) 21/22					
S7	0.0017	0.3275	0.1068	0.4838	138, 113
S8	-0.0930	0.2411	-0.0063	0.5614	4, 4
Struve (1898)					
S5	-0.1310	0.1191	0.1167	0.0953	44, 42
S6	0.0339	0.1579	0.1721	0.1457	57, 54
Stone (1895)					
S2	-0.0725	0.1892	-0.0533	0.1717	5, 5
S3	-0.0654	0.1987	-0.0908	0.1791	16, 18
S4	-0.0730	0.1514	0.0623	0.1837	17, 19
S5	0.0051	0.0761	-0.0449	0.2588	6, 6
S6	0.0750	0.0000	0.0126	0.0998	1, 2
Stone (1896)					
S5	-0.0569	0.2756	-0.0047	0.1999	54, 75
Stone (1898a, 1898b)					
S3	-0.1127	0.2733	-0.0086	0.2037	12, 12
S4	-0.1519	0.2589	-0.0089	0.2315	30, 28
S5	-0.1048	0.2048	0.0396	0.1578	15, 15
S6	0.0450	0.4001	0.1994	0.2881	4, 4
Morgan (1900)					
S3	0.2297	0.2526	0.0193	0.1762	7, 6
S4	0.3666	0.3065	0.0112	0.1027	6, 4
S5	0.5270	0.2765	0.0594	0.1558	6, 6
Aitken (1905)					
S2	-0.0412	0.2110	0.0744	0.1370	13, 13
S3	0.2097	0.2004	0.0387	0.2382	13, 12
S4	0.2498	0.1967	0.0827	0.2026	13, 13
Barnard (1910)					
S1	-0.0255	0.0989	0.0462	0.1269	6, 3
S2	-0.0721	0.1794	0.0584	0.0769	18, 8
S3	0.0411	0.2075	-0.0668	0.0723	12, 6
S4	0.0642	0.1755	0.0328	0.0913	7, 4
S5	0.0491	0.1116	0.1287	0.2496	8, 6
Aitken (1909)					
S2	-0.0910	0.1515	0.0621	0.0837	7, 8
S3	0.2377	0.2044	0.0678	0.1255	6, 9
S4	0.0847	0.1824	0.0562	0.1178	8, 8
USNO (1929)					
S2	0.0442	0.1108	0.0701	0.0363	2, 2
S3	0.0755	0.1692	-0.0128	0.1869	187, 191
S4	0.0521	0.1356	0.0074	0.1511	158, 157
S5	0.0649	0.1719	0.0174	0.1573	318, 320
S6	0.0996	0.1719	0.0106	0.1482	370, 372
S8	0.1215	0.1606	-0.0088	0.2598	117, 120
Barnard (1913)					
S1	0.1750	0.1093	0.0451	0.0186	3, 3

Table 2
(Continued)

Observation subset	ν_s	σ_s	ν_p	σ_p	N_s, N_p
S2	0.0726	0.1589	0.1242	0.2092	23, 23
S3	0.0804	0.2407	0.0768	0.3137	45, 44
S4	0.0519	0.1929	0.0711	0.3099	33, 33
S5	0.0718	0.2587	0.1386	0.2770	11, 11
Barnard (1915)					
S1	0.1383	0.0890	0.2791	0.3066	3, 4
S2	0.0943	0.1738	0.0023	0.2385	13, 13
S3	0.1256	0.1983	0.0580	0.2757	26, 28
S4	0.1291	0.2024	0.2029	0.2359	23, 23
S5	-0.0554	0.1118	0.0968	0.1420	11, 11
S8	0.3823	0.0000	0.1694	0.0000	1, 1
Barnard (1916)					
S1	0.1941	0.1928	0.0563	0.1434	13, 13
S2	0.0822	0.1972	0.1071	0.2209	19, 19
S3	0.1344	0.1686	0.0225	0.1796	42, 41
S4	0.1946	0.1835	0.0077	0.3271	21, 20
S5	0.1185	0.2452	0.0232	0.2104	12, 12
Barnard (1918)					
S1	-0.0194	0.1599	0.0703	0.0947	7, 6
S2	0.0826	0.2060	0.1282	0.2910	23, 23
S3	0.1649	0.1274	-0.0272	0.1748	36, 35
S4	0.1739	0.1307	-0.0074	0.2939	28, 30
S5	0.2478	0.1294	0.0212	0.3503	10, 9
Barnard (1927)					
S1	0.0125	0.2915	0.1242	0.2063	17, 19
S2	0.0116	0.2274	0.0690	0.2099	65, 66
S3	0.1270	0.1866	0.0215	0.1839	133, 125
S4	0.0936	0.1778	0.0155	0.2015	61, 63
S5	0.1839	0.1887	0.0147	0.3278	45, 43
S8	0.0901	0.2952	0.0284	0.2628	8, 8
Struve (1933) Johannesb					
S1	-0.0016	0.1646	-0.0010	0.1896	115, 115
S2	0.0429	0.1265	-0.0113	0.1324	187, 190
S3	0.0459	0.1249	0.0309	0.1298	127, 130
S4	0.0331	0.1229	0.1023	0.1136	54, 54
S5	-0.0166	0.0268	-0.0740	0.1009	2, 2
USNO (1954) 61/62					
S1	0.0000	0.0000	0.0000	0.0000	0, 0
S2	0.0827	0.1310	-0.0510	0.1843	18, 18
S3	0.0478	0.2775	-0.0200	0.2730	278, 276
S4	0.0732	0.2193	-0.0071	0.1963	283, 284
S5	0.0591	0.2203	0.0175	0.2220	455, 457
S6	0.0572	0.1785	-0.0466	0.1737	194, 188
S8	-0.0839	0.0000	-0.0360	0.0000	1, 1
Struve (1933) Yerkes					
S2	-0.1751	0.2256	0.0512	0.2054	48, 48
USNO (1954)					
S5	-0.0007	0.1547	0.0172	0.0857	32, 32
S6	0.0007	0.1547	-0.0172	0.0857	32, 32
Harper et al. (1997)					
S3	-0.0079	0.0377	0.0090	0.0602	184, 184
S4	-0.0024	0.0318	-0.0053	0.0580	193, 193
S5	0.0016	0.0281	-0.0025	0.0545	202, 202
S6	0.0062	0.0213	-0.0157	0.0682	118, 118
S8	-0.0023	0.0451	0.0049	0.0708	51, 51
Qiao et al. (1999)					
S1	-0.0448	0.1181	0.0086	0.0174	15, 15
S2	-0.0454	0.0802	0.0060	0.0645	47, 47
S3	-0.0065	0.0423	0.0050	0.0564	82, 82
S4	-0.0037	0.0296	-0.0017	0.0423	147, 147
S5	0.0088	0.0368	-0.0050	0.0477	151, 151
S6	-0.0017	0.0265	-0.0076	0.0578	164, 164

Table 2
(Continued)

Observation subset:	ν_s	σ_s	ν_p	σ_p	N_s, N_p
Veiga et al. (2003)					
S1	-0.0046	0.0534	-0.0059	0.0704	329, 329
S2	0.0069	0.0613	-0.0038	0.0720	414, 414
S3	-0.0041	0.0430	0.0103	0.0710	489, 489
S4	0.0055	0.0522	-0.0064	0.0721	527, 527
S5	-0.0106	0.0451	-0.0106	0.0947	480, 480
S6	0.0293	0.0583	0.0270	0.0932	219, 219
S8	-0.0339	0.0217	-0.1685	0.0502	7, 7
Vienne et al. (2001)					
S1	0.0439	0.0347	0.0103	0.0345	216, 216
S2	-0.0017	0.0421	0.0051	0.0513	860, 860
S3	-0.0050	0.0264	-0.0052	0.0396	1747, 1747
S4	0.0033	0.0247	0.0060	0.0377	1029, 1029
S5	-0.0018	0.0230	-0.0046	0.0507	1587, 1587
S6	0.0001	0.0153	-0.0006	0.0405	731, 731
S8	0.0036	0.0291	0.0061	0.0643	523, 523
Harper et al. (1999)					
S3	-0.0017	0.0272	-0.0106	0.0497	245, 245
S4	-0.0222	0.0400	0.0114	0.1133	205, 205
S5	0.0055	0.0423	0.0059	0.0856	238, 238
S6	0.0133	0.0351	-0.0135	0.0534	242, 242
S8	0.0076	0.0243	0.0083	0.0383	188, 188
Peng et al. (2002)					
S1	-0.0139	0.0302	0.0390	0.0485	54, 54
S2	-0.0181	0.0273	0.0062	0.0438	161, 161
S3	0.0093	0.0226	0.0053	0.0281	145, 145
S4	-0.0006	0.0182	-0.0022	0.0304	161, 161
S5	0.0068	0.0237	0.0055	0.0295	199, 199
S6	-0.0010	0.0126	-0.0005	0.0505	145, 145
S8	-0.0027	0.0191	-0.0281	0.0527	126, 126
Qiao et al. (2004)					
S1	-0.0400	0.1096	0.0466	0.1996	44, 44
S2	-0.0682	0.1322	-0.0005	0.2055	141, 141
S3	-0.0091	0.0866	0.0189	0.1497	236, 236
S4	-0.0175	0.0733	-0.0230	0.0987	246, 246
S5	0.0174	0.0571	-0.0001	0.1237	227, 227
S6	0.0232	0.0401	-0.0514	0.1428	207, 207
S8	0.0291	0.0274	0.1340	0.1958	66, 66
Peng et al. (2008)					
S1	0.0256	0.0712	0.0082	0.0912	358, 358
S2	-0.0009	0.0260	-0.0003	0.0383	358, 358
S3	-0.0051	0.0234	0.0007	0.0296	358, 358
S4	-0.0056	0.0237	-0.0003	0.0325	358, 358
S5	-0.0082	0.0245	0.0021	0.0418	358, 358
S6	0.0074	0.0209	-0.0200	0.1202	358, 358

Notes. μ and σ denote, respectively, the mean and standard deviation of the residuals computed in separation s and position angle p . N_s and N_p are the number of observations considered for the respective coordinate. We recall that 0.1 s of arc corresponds to about 600 km at the Saturn distance.

where F_i is the right-hand side of Equation (1) multiplied by m_i .

Partial derivatives of the solutions with respect to initial positions and velocities of the satellites and dynamical parameters are computed from simultaneous integration of Equation (4) and Equation (1). For an explicit formulation of the dynamical equations and the variational equations used, we refer to Lainey et al. (2007, 2009), Lainey (2008), and references therein.

The RA15 numerical integrator is used with a constant step size of 0.075 days. To increase the numerical accuracy, we performed forward and backward integrations starting at an

initial Julian epoch of 2,433,291.0 (1950 January 9, TDB). The numerical accuracy of our simulation is at the level of a few hundreds of meters over the whole 123 years (see also Appendix A.1.1).

During the fitting procedure, timescale and light-time corrections for each satellite-observer distance were introduced (Lainey et al. 2007). Corrections for phase, aberration, and differential refraction were applied when they were not already included in the observation astrometric reductions (Lainey et al. 2007). Observational subsets (related to different observational campaigns or publications) have been considered with a

relative weight computed by preliminary residuals (Lainey et al. 2007) and corresponding to their rms error for deriving formal errors. Least-squares iterations have been applied to solve for the fitted parameters. In particular, despite the development of new techniques, least squares is still one of the most efficient methods available to solve for the parameters of dynamical systems (Desmars et al. 2009a), as long as the studied system has been observed over a sufficiently long period of time to allow for rather accurate initial conditions (which is the case for the main planetary satellites of the solar system). No constraints have been applied in the least-squares inversion. Only a few iterations have been required to reach an optimal solution.

In all this work, the fitted parameters are the initial state vectors of the main Saturnian moons (actually their equivalent form as Keplerian elements) of all Saturnian moons, the extra parameter da/dt for Mimas and the ratio k_2/Q for Saturn. In particular, Enceladus' tidal dissipation could not be fitted due to significant correlations. To solve this issue, we considered two extreme scenarios for each solution: (1) Enceladus is at thermal equilibrium and (2) Enceladus is not dissipative at all. Then we merged both solutions into one, providing one global solution with higher error bars, but independent of Enceladus' internal state (see Section 4). Hence, the total number of fitted parameters considered is between 50 and 53 (depending on whether Q is assumed constant or dependent on the tidal frequency).

4. FITTING THE MODEL TO ASTROMETRIC OBSERVATIONS

The dependence of Q on tidal frequency is a matter for debate. While it is traditionally approximated by a constant for long timescales (Goldreich & Soter 1966; Sinclair 1983), recent developments in the numerical simulation of giant planet interiors have revealed a possible erratic frequency dependence of Q (Wu 2005). In this work we investigate both possibilities.

4.1. Constant Q Model

In a first inversion, we neglect dissipation in Enceladus and fit the initial state vectors of all eight moons including Saturn's ratio k_2/Q and Mimas' da/dt . We thus obtain $k_2/Q = (2.0 \pm 0.4) \times 10^{-4}$ and $da/dt = -(13.7 \pm 2.4) \times 10^{-15}$ AU day $^{-1}$. Saturn's dissipation ratio corresponds to orbital acceleration values \dot{n}/n (in yr $^{-1}$ units) of $-(2.67 \pm 0.57) \times 10^{-10}$, $-(4.26 \pm 0.91) \times 10^{-10}$, $-(1.52 \pm 0.33) \times 10^{-10}$, and $-(3.56 \pm 0.76) \times 10^{-11}$ for Enceladus, Tethys, Dione, and Rhea, respectively. This translates into semi-major axis variation da/dt (in au day $^{-1}$ units) of $(7.77 \pm 1.67) \times 10^{-16}$, $(1.53 \pm 0.33) \times 10^{-15}$, $(7.02 \pm 1.50) \times 10^{-16}$, and $(2.29 \pm 0.49) \times 10^{-16}$. Over the 123 years covered by the observation set we used, this corresponds to an orbital shift in longitude of 799 ± 172 km (0.129 ± 0.028 arcsec), 1152 ± 246 km (0.186 ± 0.040 arcsec), 365 ± 78 km (0.059 ± 0.013 arcsec), and 72 ± 15 km (0.012 ± 0.002 arcsec), respectively. In a second case, we introduce dissipation in Enceladus, which is expected to counterbalance its orbital acceleration, thereby modifying our global estimation of Saturn k_2/Q obtained from the satellite tidal accelerations. As already stated in Section 3, we do not have a sufficient number of observations to invert independently the k_2/Q values for Saturn and Enceladus. Hence, to introduce Enceladus' tidal dissipation, we assume that Enceladus is in a dynamical equilibrium state, which locks Enceladus' eccentricity as the result of dissipation in both Saturn and Enceladus inside the 2:1 resonance with Dione (Meyer & Wisdom 2007). In this case, we obtain

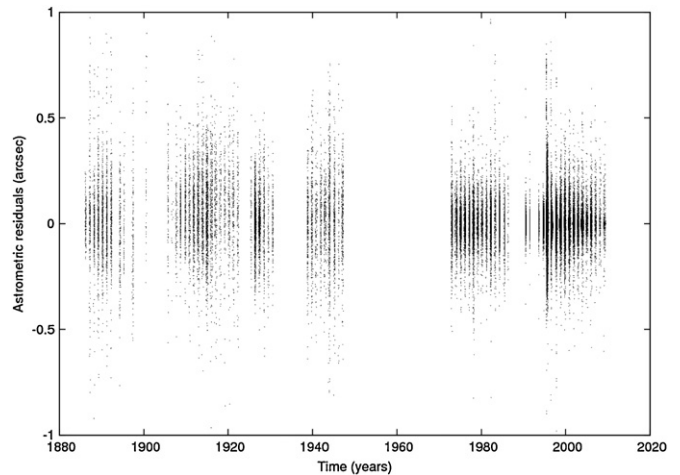


Figure 1. Astrometric residuals. Residuals between the astrometric observations and our numerical model (assuming eccentricity equilibrium for Enceladus), after fitting the initial state vectors of the eight main Saturnian moons, the ratio k_2/Q of Saturn and a constant rate da/dt on Mimas' semi-major axis. The global 1σ accuracy is about 0.1 arcsec (we recall that at the Saturnian distance 1 arcsec corresponds to about 6000 km). It can be noted that no clear differences between old and modern observations are obvious due to (1) selective criteria in precision for all subsets (see Section 2 for details) and (2) limitations inherent in graphical resolution (see Tables 1 and 2 for a detailed analysis of each observation subset).

$k_2/Q = (2.6 \pm 0.4) \times 10^{-4}$ and $da/dt = -(17.0 \pm 2.4) \times 10^{-15}$ AU day $^{-1}$. The associated secular accelerations related to Saturn's and Enceladus' tides are $-(2.06 \pm 0.57) \times 10^{-10}$, $-(5.61 \pm 0.91) \times 10^{-10}$, $-(2.09 \pm 0.32) \times 10^{-10}$, $-(4.69 \pm 0.76) \times 10^{-11}$. This translates into semi-major axis variation da/dt (in AU day $^{-1}$ units) of $(6.00 \pm 1.66) \times 10^{-16}$, $(2.02 \pm 0.33) \times 10^{-15}$, $(9.65 \pm 1.49) \times 10^{-16}$, and $(3.02 \pm 0.49) \times 10^{-16}$. This corresponds to 619 ± 171 km (0.100 ± 0.028 arcsec), 1516 ± 245 km (0.245 ± 0.040 arcsec), 501 ± 78 km (0.081 ± 0.013 arcsec), and 95 ± 15 km (0.015 ± 0.002 arcsec), as well. Even though both inversions provide the same orbital trends, acceleration values for each satellite are somewhat different. This arises from the use of only one global k_2/Q value for Saturn, while fitting several independent accelerations. Thanks to the long time span considered, astrometric accuracy is enough to detect tidal accelerations for Enceladus, Tethys, Dione, and Rhea from the observations (see Figure 1 and Tables 1–3). Combining the two fits, our nominal solution for the Saturn tidal dissipation (here assumed to be independent of the tidal frequency) yields $k_2/Q = (2.3 \pm 0.7) \times 10^{-4}$.

4.2. Non-constant Q Model

To check the assumption of a constant Q model considered in our nominal solution, we release simultaneously several Q values (with and without Enceladus' dissipation), one Q value being related to each tide-raising satellite. We succeed in obtaining Saturn's Q at four different tidal frequencies, related to Enceladus, Tethys, Dione, and Rhea (see Figure 2), respectively. Correlations between the four tidal ratios are below 0.2 (as shown in Table 4). However, a high correlation of 0.935 is found between Saturn's tidal ratio associated with Tethys' tidal frequency and Mimas' da/dt (equal to $-(16.3 \pm 3.7) \times 10^{-15}$ AU day $^{-1}$), as a consequence of the 2:4 mean motion resonance between Mimas and Tethys.

Implications of these results are discussed in Section 6.

Table 3
Correlation between k_2/Q and da/dt with All Our Fitted Parameters (Enceladus Tidal Equilibrium Solution)

	a_1	l_1	k_1	h_1	q_1	p_1	a_2	l_2	k_2	h_2	q_2	p_2
k_2/Q	-0.116	0.142	0.103	-0.012	-0.031	-0.309	-0.035	0.705	0.000	0.484	0.000	-0.010
da/dt	0.085	-0.020	-0.125	-0.044	0.082	0.375	0.027	-0.588	-0.005	-0.415	0.011	0.008
	a_3	l_3	k_3	h_3	q_3	p_3	a_4	l_4	k_4	h_4	q_4	p_4
k_2/Q	-0.043	0.169	0.014	-0.037	-0.199	0.219	-0.170	0.372	0.088	-0.070	0.036	-0.027
da/dt	0.087	0.241	-0.054	0.046	0.247	-0.290	0.157	-0.303	-0.076	0.066	-0.045	0.042
	a_5	l_5	k_5	h_5	q_5	p_5	a_6	l_6	k_6	h_6	q_6	p_6
k_2/Q	0.032	0.136	0.028	-0.030	-0.016	0.022	0.052	0.014	-0.004	0.018	0.014	-0.019
da/dt	0.007	-0.106	-0.026	0.009	0.012	-0.017	0.035	-0.011	-0.001	-0.014	-0.010	0.012
	a_7	l_7	k_7	h_7	q_7	p_7	a_8	l_8	k_8	h_8	q_8	p_8
k_2/Q	-0.001	0.005	0.001	0.000	-0.004	-0.014	-0.016	-0.014	0.000	0.008	0.001	-0.031
da/dt	0.001	-0.004	-0.002	0.000	0.003	0.009	0.023	0.013	0.001	-0.024	-0.002	0.024
	k_2/Q	da/dt										
k_2/Q	1.000	-0.838										
da/dt	-0.838	1.000										

Notes. Where a is the semi-major axis, l is the mean longitude, $k = e \cos(\Omega + \omega)$, $h = e \sin(\Omega + \omega)$, $q = \sin(i/2) \cos(\Omega)$ and $p = \sin(i/2) \sin(\Omega)$ (with e denoting the eccentricity, Ω denoting the longitude of the node, and ω denoting the argument of the periapsis). Numbers 1, ..., 8 refer to Mimas (S1), ..., Iapetus (S8), respectively.

Table 4
Correlation between All Four k_2/Q Ratios Estimated at the Tidal Frequency of Enceladus, Tethys, Dione, and Rhea, and da/dt (Enceladus' Eccentricity Equilibrium Solution)

	$k_2/Q(S_2)$	$k_2/Q(S_3)$	$k_2/Q(S_4)$	$k_2/Q(S_5)$	da/dt
$k_2/Q(S_2)$	1.000	0.020	-0.197	0.003	-0.012
$k_2/Q(S_3)$	0.020	1.000	0.001	0.000	-0.935
$k_2/Q(S_4)$	-0.197	0.001	1.000	0.024	0.004
$k_2/Q(S_5)$	0.003	0.000	0.024	1.000	0.006
da/dt	-0.012	-0.935	0.004	0.006	1.000

5. ROBUSTNESS OF THE SOLUTION

In this section, we present various tests that assess the robustness of our solution. During these tests, we considered as a reference solution the Enceladus equilibrium scenario with a constant Saturn Q model, that is, $k_2/Q = (2.6 \pm 0.4) \times 10^{-4}$ and $da/dt = -(16.9 \pm 2.4) \times 10^{-15}$ AU day $^{-1}$.

5.1. Random Holdout Method

This method considers the change in fitted parameters when a constant percentage of observations is removed. We have performed a test, with a percentage of 10% of observations that are not used. The number of observations in the full nominal least-squares inversion is 19,616 (all moon coordinates at a given time considered as one observation). One hundred different subsets were generated and used to check the robustness of the fitted parameters. We obtained the k_2/Q -value in the interval $[1.8 \times 10^{-4}, 3.3 \times 10^{-4}]$ for Saturn and the Mimas da/dt value in the interval $[-21.9 \times 10^{-15}, -9.1 \times 10^{-15}]$ AU day $^{-1}$ (even though most values were in agreement with the nominal error bars). This suggests that factors of two and four could be introduced in our nominal error bars in k_2/Q and da/dt , respectively. However, it must be remembered that Mimas and Tethys are hard to observe from the ground. Hence,

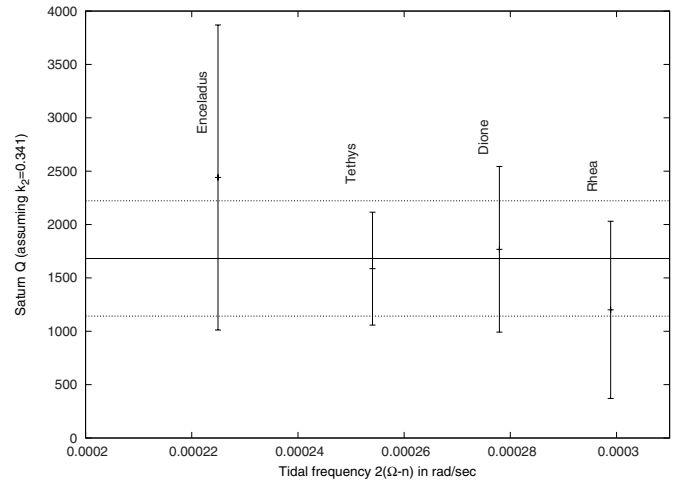


Figure 2. Determination of the Saturn tidal dissipation factor Q vs. the tidal frequency $2(\Omega - n)$, where Ω and n denote its rotation rate and the moon mean motion, respectively. The Love number is assumed to be $k_2 = 0.341$. The horizontal line shows the nominal solution (constant Q model) equal to $Q = 1682 \pm 540$, with error bars as dashed lines. The vertical values with error bars are derived from a variable Q model. The large error bar associated with Enceladus is a consequence of the uncertain tidal dissipation in that satellite (whether one assumes no dissipation or eccentricity equilibrium). Presumably, the small value of Q is the signature of a rock-ice core or its boundary in Saturn.

significantly decreasing the number of observations of Mimas will automatically increase the chance of losing the da/dt signal.

5.2. Removing Successively the Five Largest Observation Subsets

In this test, we completely removed several observation subsets among the most dense ones: (1) Vienne et al. (2001), (2) Vass (1997), (3) FASTT observations (see Stone & Harris 2000, and references therein), (4) Struve (1898), and (5) USNO

Table 5
Fitted Value of k_2/Q and da/dt after Removing Observation Subsets

Subset Removed	k_2/Q	da/dt (AU day ⁻¹)	Observations
Vienne et al. (2001)	$(2.0 \pm 0.4) \times 10^{-4}$	$-(11.0 \pm 2.4) \times 10^{-15}$	6693
Vass (1997)	$(2.6 \pm 0.4) \times 10^{-4}$	$-(16.9 \pm 2.3) \times 10^{-15}$	3977
FASTT	$(2.6 \pm 0.4) \times 10^{-4}$	$-(16.9 \pm 2.3) \times 10^{-15}$	3137
Struve (1898)	$(4.2 \pm 0.6) \times 10^{-4}$	$-(20.8 \pm 2.9) \times 10^{-15}$	796
USNO (1929)	$(2.6 \pm 0.5) \times 10^{-4}$	$-(12.9 \pm 2.5) \times 10^{-15}$	1162

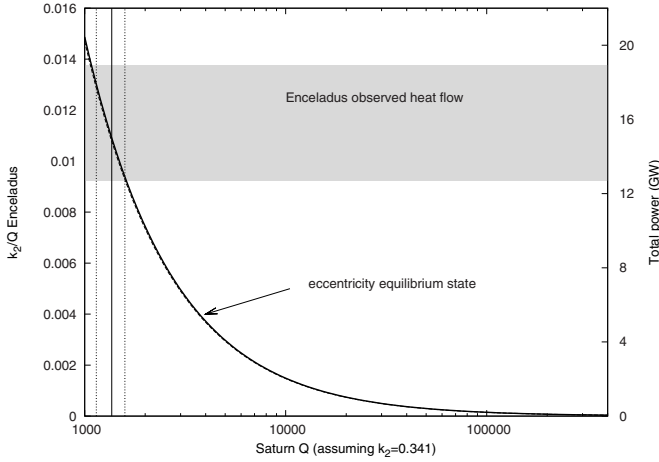


Figure 3. Comparison of Enceladus' thermal emission power with the Saturn tidal dissipation determined in the present study. The solid curve indicates the k_2/Q ratio and total dissipated power (in GW) in Enceladus for which the current orbital configuration of Enceladus and Dione is at eccentricity equilibrium as a function of Q in Saturn. Assuming such equilibrium in our fit, the value of Saturn's Q that we derive ($Q = 1363 \pm 221$; see the vertical line with associated dashed lines for error bars) shows that the expected total heat production rate is close to the observed emitted power. Hence, tidal heating equilibrium is a possible mechanism for maintaining Enceladus' thermal activity at its currently observed rate.

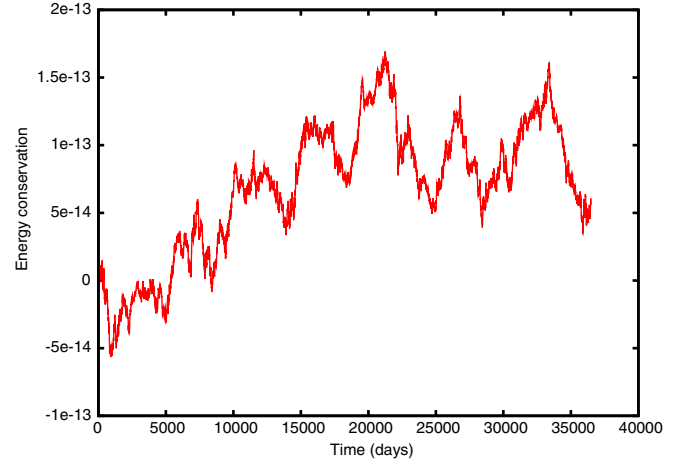


Figure 5. Energy conservation within our model (see the text for details).
(A color version of this figure is available in the online journal.)

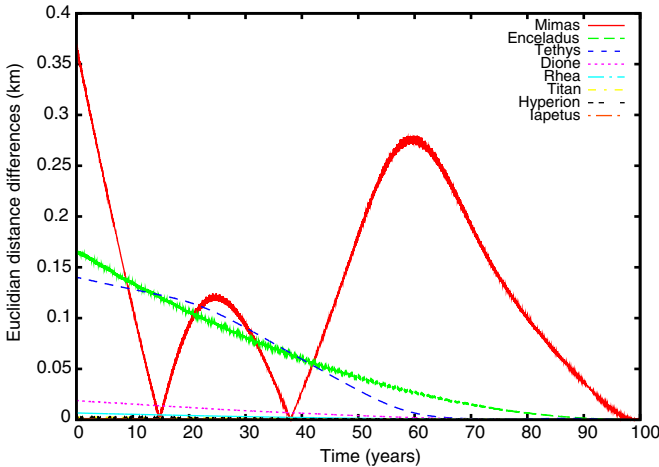


Figure 4. Test of the numerical precision of our model using the forward-backward method.
(A color version of this figure is available in the online journal.)

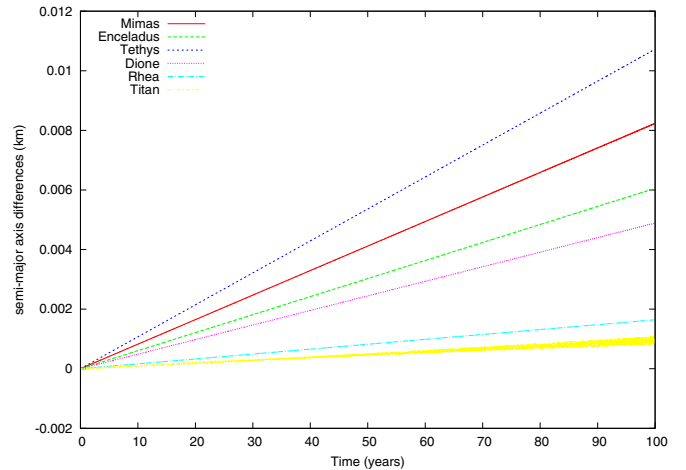


Figure 6. Semi-major axis variation test under the effect of tides raised in the planet (two-body problem).
(A color version of this figure is available in the online journal.)

(1929). The first three observation subsets are associated with the modern era, while the last two consist of observations from the end of the 19th century and beginning of the 20th century, respectively. We provide in Table 5 the fitted value of k_2/Q and da/dt after having removed the mentioned subset.

With the exception of removing the Struve data, all solutions above are very close to (though not in full agreement with) our nominal solution. The Struve data even indicate a slightly higher tidal dissipation ratio. We conclude that removing any observational subsets (old or modern) still confirms the high Saturnian dissipation obtained in our nominal solution.

5.3. On the Use of Pixel Positions

As already mentioned in Section 2, the ephemerides of the outermost Saturnian moons are sometimes used to determine the scale and orientation of the observations (because of the lack of stars in the observed fields). This can be justified since outermost

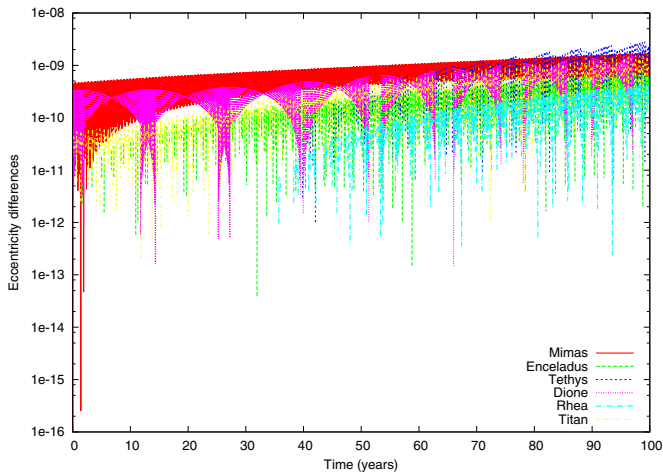


Figure 7. Eccentricity variation test under the effect of tides raised in the planet (two-body problem).

(A color version of this figure is available in the online journal.)

moons (Dione, Rhea, Titan, and sometimes Iapetus) are easier to observe (entailing a more accurate ephemeris). Moreover, an error on the scale factor and orientation is expected to have a smaller influence on the innermost moons that are close to the center of the observation. Nevertheless, introducing possibly an external orbital model in the reduction of the observations is not fully satisfactory. This is why we decided, when available, to use pixel positions instead of (α, δ) or (s, p) coordinates. Under this form, the observations are not corrupted by any external dynamical model, but their significance in the fit is lower, since information on the scale and orientation is no longer present.

We have checked the difference between our nominal solution (using pixel positions) and a fit using the usual astrometric coordinates (α, δ) or (s, p) . We obtained the following result: $k_2/Q = (1.8 \pm 0.4) \times 10^{-4}$ for Saturn and $da/dt = -(13.0 \pm 2.4) \times 10^{-15}$ for Mimas. This is in agreement with our nominal solution (taking into account the error bars).

5.4. Scale Factor Biases

One of the crucial systematic errors in astrometric observations is related to scale factors. Scale factors express the equivalence between an observed distance on a field (measured in micrometer on a photographic plate, or pixel on a CCD image) and its related angular separation on the celestial sphere. In principle, a scale factor should be an isotropic quantity. Nevertheless, stellar positions used to calibrate the observations are rarely corrected for atmospheric differential refraction. Hence, scale factors along equatorial and polar directions are different. Most of the time, old observations used a constant scale factor, which introduced systematic errors in the satellite positions. In particular, such errors produce higher residuals for the distant satellites than for the closer ones, which are much less affected by a small error in the field scale.

To check the influence of scale factor errors on our results, we have performed another fit of our model using this time the relative distance of the satellites between each other (instead of the absolute distance derived from the scale factor estimation), when at least three satellites were observed simultaneously. We obtained the following result: $k_2/Q = (2.7 \pm 0.3) \times 10^{-4}$ for Saturn and $da/dt = -(17.9 \pm 1.8) \times 10^{-15}$ for Mimas. These two values agree with our nominal solution within the error bars.

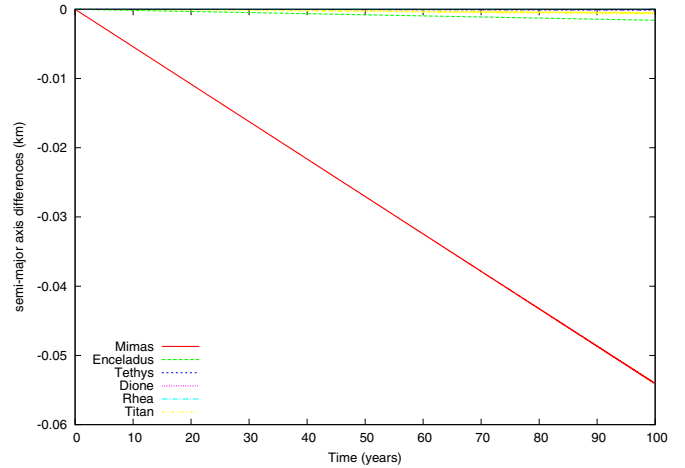


Figure 8. Semi-major axis variation test under the effect of tides raised in the satellites (two-body problem).

(A color version of this figure is available in the online journal.)

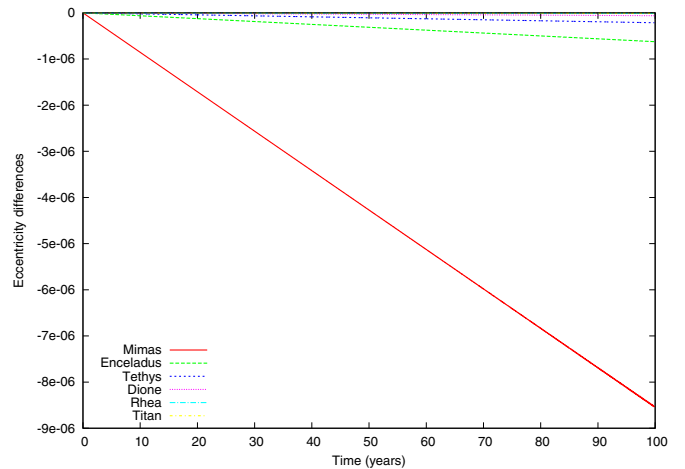


Figure 9. Eccentricity variation test under the effect of tides raised in the satellites (two-body problem).

(A color version of this figure is available in the online journal.)

5.5. Releasing More Parameters in the Fit (Saturn's Pole and Precession)

While the gravity field parameters we are using are accurate thanks to *Cassini* data, the IAU expression for Saturn's pole coordinates and precession frequency dates back to 1994 (Davies et al. 1996; Archinal et al. 2011). Here, we investigate the influence of fitting the pole coordinates and precession frequency of Saturn on our results. Starting from our nominal solution (the Enceladus equilibrium model), we performed a new fit that added four more parameters in the fitting process. These parameters refer to the IAU formulation for the pole coordinates of planets (Archinal et al. 2011):

$$\begin{aligned} \alpha &= \alpha_0 + \dot{\alpha}T \\ \delta &= \delta_0 + \dot{\delta}T \end{aligned} ,$$

where (α_0, δ_0) are the pole coordinates in the ICRF at epoch J2000.0 and $(\dot{\alpha}, \dot{\delta})$ introduces the precession/nutation of the primary. Releasing the 50+4 parameters simultaneously, we obtain after iterations the following solution: $k_2/Q = (2.63 \pm 0.41) \times 10^{-4}$, $da/dt = -(16.7 \pm 2.4) \times 10^{-15}$ AU day⁻¹, $\alpha_0 = 40.5915 \pm 0.0055^\circ$, $\dot{\alpha} = -0.131 \pm 0.022^\circ/\text{Julian century}$,

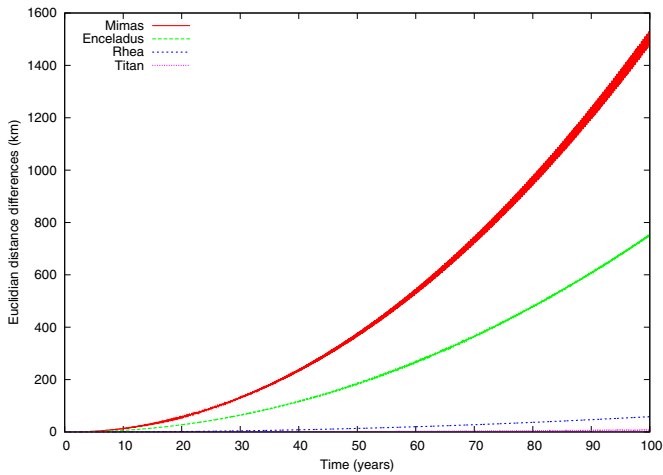


Figure 10. Semi-major axis variation test under the effect of tides raised in the planet (full model).

(A color version of this figure is available in the online journal.)

$\delta_0 = 83.54163 \pm 000053^\circ$, $\dot{\delta} = 0.0219 \pm 0.0025^\circ/\text{Julian century}$.

Clearly k_2/Q and da/dt are poorly affected by adding to the fit Saturn’s pole coordinates and precession frequency. Moreover, the post-fit residuals are highly similar to those from the nominal solutions (in the limit of one-tenth of a mas). Hence, our results are expected to be poorly sensitive to possible IAU errors in the expression of Saturn’s pole coordinates and precession frequency.

5.6. Neglecting General Relativity

Here we focus on the influence of general relativity. Since the influence of these effects is pretty small (Iorio & Lainey 2005), they have been neglected in our nominal fits. To demonstrate the validity of such an assumption, we have introduced these effects in the model (we considered relativistic effects associated to both Saturn and the Sun) and performed a new solution. After fitting, we obtained $k_2/Q = (2.54 \pm 0.42) \times 10^{-4}$, $da/dt = -(16.9 \pm 2.4) \times 10^{-15} \text{ AU day}^{-1}$.

Here again, the post-fit residuals are highly similar to the nominal solution ones (in the limit of one-tenth of a mas).

In conclusion, the envelope of all the tests performed in this whole section provides $k_2/Q = (3.1 \pm 1.7) \times 10^{-4}$ and $da/dt = -(16.2 \pm 7.6) \times 10^{-15} \text{ AU day}^{-1}$. In particular, our different tests confirm that the present estimation of the k_2/Q ratio of Saturn is reliable.

6. DISCUSSION

We can see from Section 4.2 that all k_2/Q values lie in the same range and show smooth frequency dependence. To understand the implications of this result, let us recall what is presently known about the physical mechanisms that convert into heat the kinetic energy of the tides, thus driving the secular evolution of the system. Saturn has a hydrogen–helium fluid envelope, which may be partially or entirely convective, and an expected rock–ice core (Guillot 1999) (ignoring here the role of a possible outer radiative layer). The fluid equilibrium tide is damped mainly in the convective part of the envelope, and its amplitude depends smoothly on frequency (Zahn 1966, 1989). In contrast, the dynamical tide in this region, which consists of excited inertial modes (Ogilvie & Lin 2004; Wu 2005; Goodman & Lackner 2009), varies considerably with

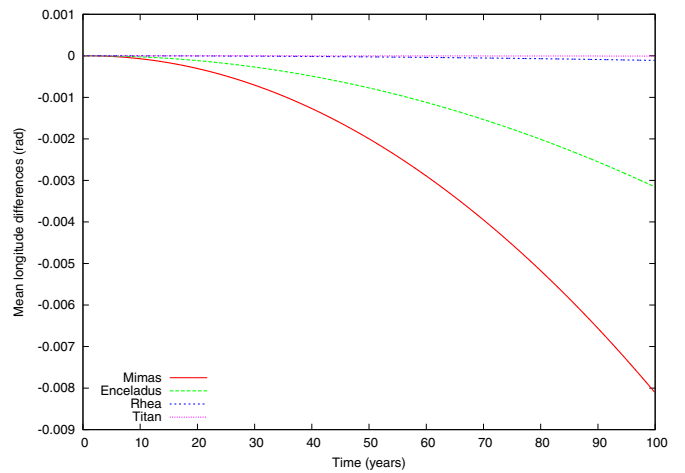


Figure 11. Eccentricity variation test under the effect of tides raised in the planet (full model).

(A color version of this figure is available in the online journal.)

frequency, particularly in the presence of a dense core (Rieutord & Valdetaro 2010). Although both of these fluid tides are damped through turbulent friction, they yield a relatively low value of the dissipation parameter: $k_2/Q \sim 10^{-6}$ at most (Ogilvie & Lin 2004). Therefore, one has to turn to other mechanisms to explain the high tidal dissipation in Saturn’s system that we report here, with k_2/Q ranging from 1.4×10^{-4} to 3.4×10^{-4} . For instance, the contribution to tidal dissipation of a stably stratified layer surrounding the core, due to the settling of helium when it ceases to be soluble in metallic hydrogen (Morales et al. 2009; Fortney & William 2003), remains to be evaluated. Another possibility could be the presence of a dense core, as predicted by most models (Guillot 1999). In Saturn, this core is expected to be relatively larger than in Jupiter, which would be consistent with the relatively lower tidal dissipation in that planet: $k_2/Q = (1.102 \pm 0.203) \times 10^{-5}$, as determined by the same method (Lainey et al. 2009).

So far, the averaged lower bound of Saturn’s Q was derived from theoretical considerations, assuming that all main moons formed above the synchronous orbit 4.5 Byr ago (Goldreich & Soter 1966). Considering Mimas, the innermost mid-sized satellite, and using the averaged equations for a tidally evolving system, Sinclair (1983) derived a present-day reference value of $Q \geq 18,000$ (assuming $k_2 = 0.341$ from Gavrilov & Zharkov 1977). If the observed high value of Saturn’s k_2/Q determined in this work represents well the long-term averaged value, then a very large tidal expansion of the moon orbits should have occurred. In particular, the conventional assumption of Saturnian satellites forming contemporaneously with their parent planet has to be dismissed. Recently, Charnoz et al. (2011) suggested a new mechanism of formation of Saturnian satellites at the outer edge of the rings. While the satellites evolve outward in their model due to exchange of angular momentum with the rings and tides that rose in the primary, they noticed, however, that a strong tidal dissipation in Saturn is mandatory to place the satellites at their current observed positions. It is noteworthy that the tidal dissipation quantification presented here allows their model to form and place the Saturnian satellites at the proper distance to their primary.

Since the discovery of the very active province at Enceladus’ south pole by the *Cassini* spacecraft in 2005 (Spencer et al. 2009; Porco et al. 2006), a variety of theoretical models have

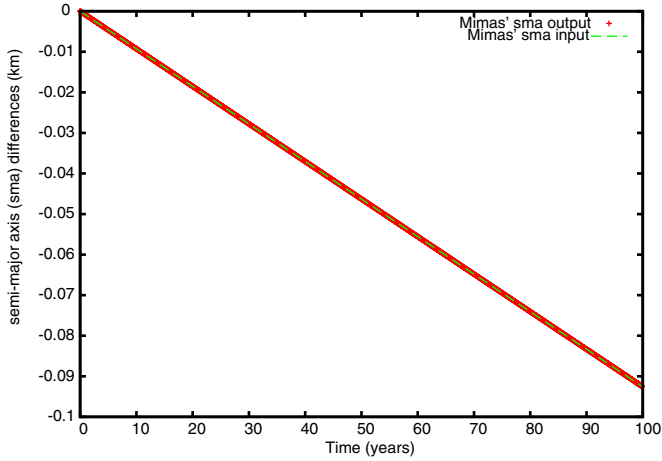


Figure 12. Test of the da/dt perturbation in the two-body problem case.
(A color version of this figure is available in the online journal.)

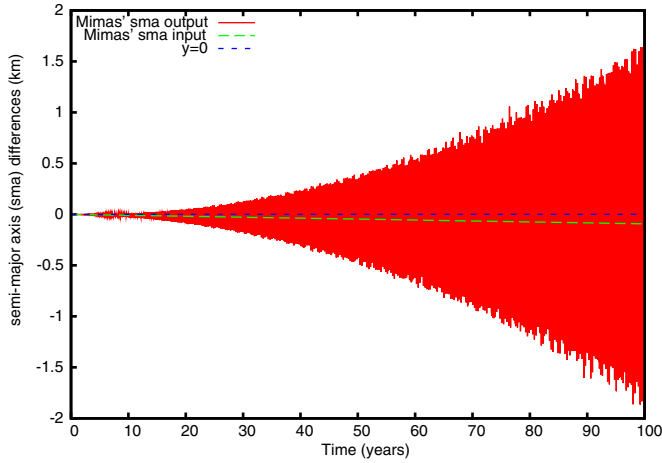


Figure 13. Mimas' semi-major axis variation under the influence of da/dt perturbation (full model).

(A color version of this figure is available in the online journal.)

been proposed to explain the huge thermal emission and the associated eruptions of water vapor and ice particles (Meyer & Wisdom 2007; Nimmo et al. 2007; Tobie et al. 2008; O'Neill & Nimmo 2010; Howett et al. 2011). The amount of energy produced at present by radioactive decay in the rocky core of Enceladus contributes less than 2% to the total emitted power (15.8 ± 3.1 GW; Howett et al. 2011), suggesting another internal energy source such as tidal dissipation. Previous studies based on the former estimation of Saturn's Q ($\geq 18,000$) (Sinclair 1983) showed that tidal heating at orbital equilibrium, required to maintain the resonant Enceladus–Dione orbital configuration, could not account for more than 1.1 GW (Meyer & Wisdom 2007). This was suggesting that either the resonant system oscillates around equilibrium with dissipated power varying from almost zero to the observed value or more, or the satellite episodically releases the internal heat that is continuously produced at a rate compatible with orbital equilibrium (Tobie et al. 2008; O'Neill & Nimmo 2010). None of these solutions were fully satisfactory.

The new dissipation factor of Saturn reported here totally changes our understanding of Enceladus' heat production mechanism. As shown in Figure 3, with the new inferred Q value, equilibrium tidal heating can now account for the observed heat

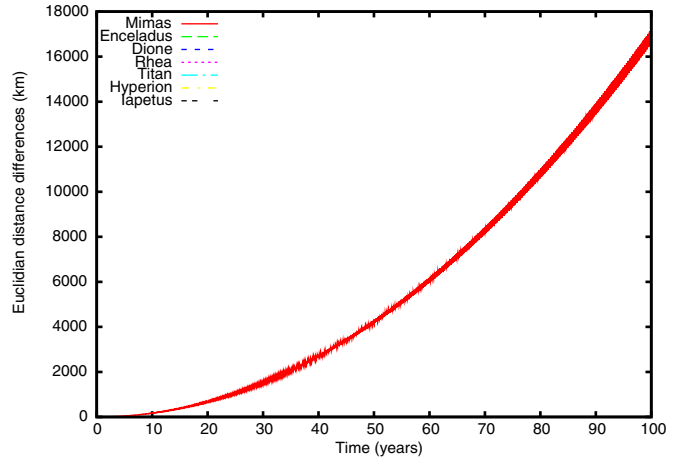


Figure 14. Mimas' orbital position differences under the influence of da/dt perturbation (full model).

(A color version of this figure is available in the online journal.)

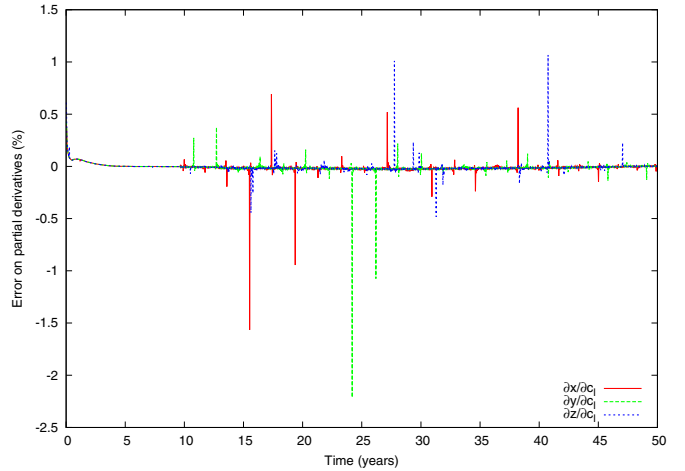


Figure 15. Variational equations test of da/dt parameter from Mimas position.

(A color version of this figure is available in the online journal.)

power. This indicates that Enceladus' interior could be close to thermal equilibrium at present, with surface heat loss being balanced by heat produced by tidal dissipation. Large tidal dissipation in Enceladus implies that the satellite probably possesses a liquid water layer decoupling the outer ice shell from the rocky core (Nimmo et al. 2007; Tobie et al. 2008). For Saturnian Q lower than 2000, Enceladus can remain highly dissipative during a very long period of time without damping its orbital eccentricity, and the long-term stability of a subsurface ocean would thus be possible.

7. CONCLUSION

We have quantified Saturn's tidal dissipation ratio k_2/Q to be $(2.3 \pm 0.7) \times 10^{-4}$ using astrometric observations spanning 123 years. Moreover, such a quantification directly derived from observations is provided here at various frequencies, for the first time in a giant planet. As a consequence, we conclude that tidal dissipation may mostly occur in Saturn's core and its boundary. Moreover, tidal heating equilibrium is now a possible state for Enceladus.

The present quantification of Saturnian tidal dissipation is incompatible with a satellite formation scenario in Saturn's

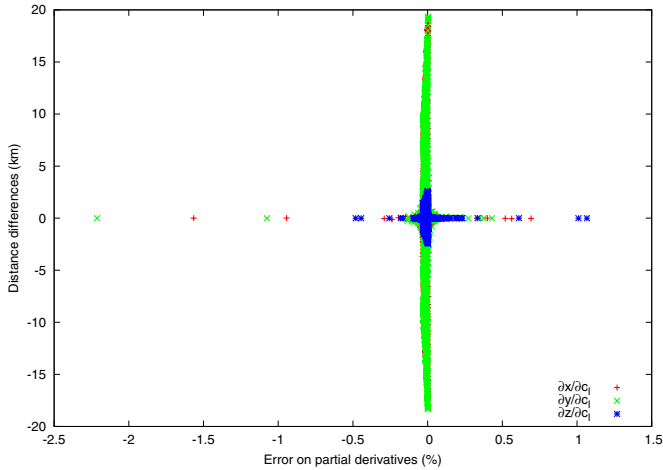


Figure 16. Distribution of distance differences as a function of error on partial derivatives using the test of da/dt parameter from Mimas position.

(A color version of this figure is available in the online journal.)

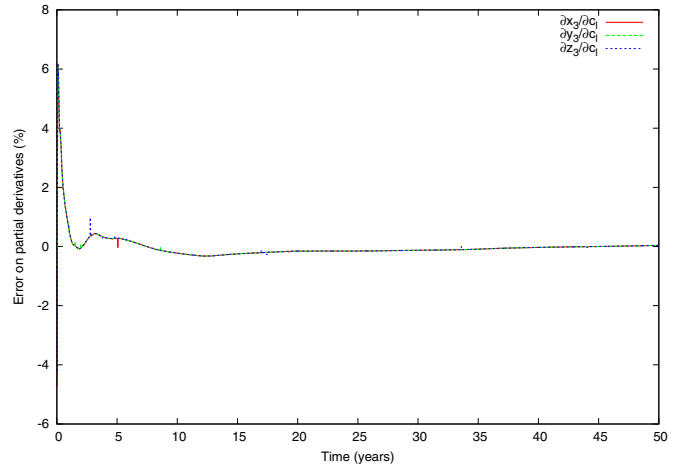


Figure 18. Variational equations test of Saturn’s Q parameter from Tethys position.

(A color version of this figure is available in the online journal.)

APPENDIX

A.1. Testing Our Numerical Model

It is not possible to show the very large amount of tests that have been performed over years when developing the NOE code. Nevertheless, in the following section we provide several tests that can be considered as fundamental to our study.

Unless explicitly mentioned, the tested model here introduces the Enceladus equilibrium scenario with constant Q .

A.1.1. Numerical Precision

To test the numerical precision of our integrations of the equations of motion, we performed backward and forward integrations (see also the conservation of energy test). Figure 4 shows the difference, for each moon, between backward and forward integration expressed as Euclidian distance in km, over one century. These variations are all below 400 m. Since our integrations have been performed over no longer than 64 years (we recall that our fit epoch is 1950, and we cover the period 1886–2009), we can conclude that the numerical precision of the satellite positions in our study is a few hundreds of meters.

A.1.2. Conservation of Energy

Checking the conservation of energy is quite important for two reasons:

1. It provides another way to quantify numerical error (here the numerical accuracy).
2. More importantly, it checks the validity of the force model.

Nevertheless, energy is not always conserved for “any” force model (nonconservative forces, use of planetary ephemerides, introduction of forced precession, and spin–orbit coupling). In the following test (see Figure 5), we did not introduce (1) da/dt “force,” (2) tidal dissipation, and (3) Saturn’s precession. Moreover, solar and Saturnian motions have been integrated explicitly (no use of planetary ephemerides) and the rotation of the moons has been frozen.

As one can see in Figure 5, energy is conserved up to 13 digits (use of double precision) over 100 years, in our model.

A.1.3. Testing the Tidal Model

Since conservation of energy cannot be used to check the validity of our tidal model, we have used analytical expression

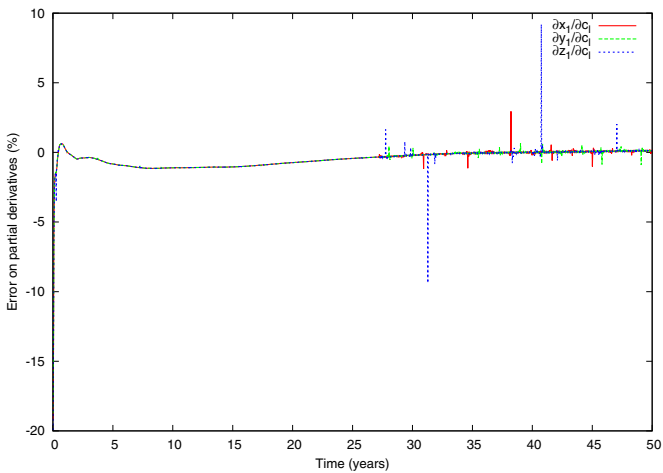


Figure 17. Variational equations test of Saturn’s Q parameter from Mimas position.

(A color version of this figure is available in the online journal.)

subnebulae for all moons below Titan. However, it is fully compatible with a formation at the edge of Saturn’s rings (Charnoz et al. 2011).

During all fitting procedures, we obtain an extra acceleration on Mimas’ orbital longitude, related to a negative value of $da/dt = -(15.7 \pm 4.4) \times 10^{-15}$ AU day $^{-1}$ (combination of all fit values). A possible source of error explaining such decay could be the proximity of Mimas to Saturn’s halo. But if confirmed in the future, Mimas’ orbital decay could have significant implications on Saturn’s rings.

This work has been supported by EMERGENCE-UPMC grant (contract number: EME0911), FP7 program Europlanet-RI, EC grant (228319), and PNP (CNRS/INSU). The authors are indebted to all participants of the French Encelade WG and to Chloé Michaut. V.L. thanks Nick Cooper, Carl Murray, Michael Efroimsky, Alain Vienne, and Laurène Beauvalet for fruitful discussions.

Table 6
Testing the Tidal Model (Tides in the Satellites/Two-body Problem)

Moon	Δa (km)	Δe
Mimas	-5.402801100992870E-002	-8.537669664267916E-006
Enceladus	-1.587689542119058E-003	-6.236475859717691E-007
Tethys	-1.229629000688473E-004	-2.139456833055286E-007
Dione	-8.724264672974581E-005	-6.140003928510260E-008
Rhea	-1.158774729219763E-005	-9.617269239444934E-009
Titan	-5.787519520775916E-004	-8.114568451206283E-009

of da/dt and de/dt to check the code. In particular, we recall that we have (as a first approximation) for the tides raised in the primary (Kaula 1964)

$$\frac{da}{dt} = \frac{3k_2 mn R^5}{Q M a^4} \left(1 + \frac{51}{4} e^2\right) \quad (\text{A1})$$

$$\frac{de}{dt} = \frac{57k_2 mn}{8QM} \left(\frac{R}{a}\right)^5 e$$

and for the tides raised in the 1:1 spin-orbit satellite (Peale & Cassen 1978)

$$\frac{da}{dt} = -\frac{21k_2^s Mn R_s^5}{Q^s m a^4} e^2$$

$$\frac{de}{dt} = -\frac{21k_2^s Mn}{2Q^s m} \left(\frac{R_s}{a}\right)^5 e \quad (\text{A2})$$

To make the comparison straightforward, we first considered a two-body problem for each moon. However, integrating the Saturnian system by modeling only two-body interactions requires considering a different eccentricity when using Equations (A1) and (A2). In particular, we have found that using our nominal solution as initial conditions, the eccentricity of each moon was changed to 0.017011, 0.00534, 0.000976, 0.00188, 0.00114, and 0.02895 for Mimas to Titan, respectively.

Tides in the Planet (Two-body Problem). Over 100 years, variations on a are expected to be 8.37, 6.08, 10.722, 4.889, 1.641, 0.952 m for, respectively, S1, . . . , S8 (Mimas, . . . , Titan). Similarly, variations on e are expected to be 1.81×10^{-9} , 3.24×10^{-10} , 8.46×10^{-11} , 5.78×10^{-11} , 8.42×10^{-12} , and 5.30×10^{-11} .

Comparing such estimations with our numerical simulation offers a good agreement (see Figures 6 and 7; numerical table is available on request).

Tides in the Satellites (Two-body Problem). Over 100 years and assuming arbitrarily $k_2^s/Q^s = 10^{-2}$ for all moons, variations on a are expected to be -54.607, -1.597, -0.124, -0.087, -0.012, -0.544 m for, respectively, S1, . . . , S8 (Mimas, . . . , Titan). Similarly, variations on e are expected to be -8.66×10^{-6} , -6.28×10^{-7} , -2.15×10^{-7} , -6.15×10^{-8} , -9.61×10^{-9} , and -7.68×10^{-9} .

Our numerical simulation offers a good match with analytical formulation (see Figures 8 and 9 and Table 6). In particular, the use of a quite simplified force model greatly decreases numerical errors during integration, making the comparison possible (up to two digits at least, which may be the accuracy of the analytical formulation we consider).

Tides in the Planet (Full Model). One can try checking the tidal model with the full model considered in this work,

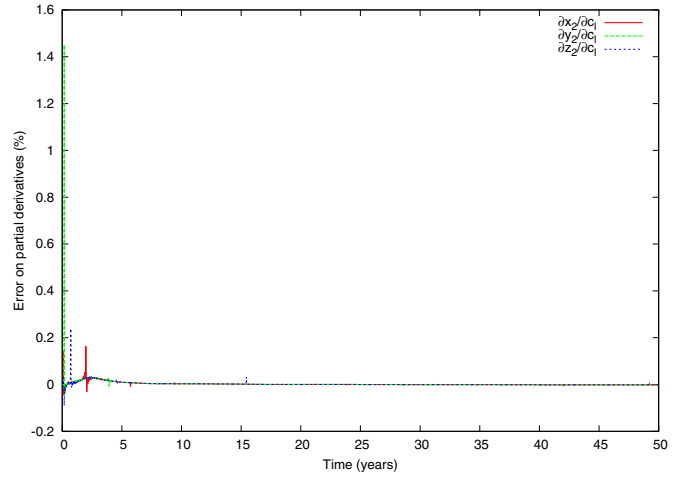


Figure 19. Variational equations test of Enceladus' Q parameter from Enceladus position.

(A color version of this figure is available in the online journal.)

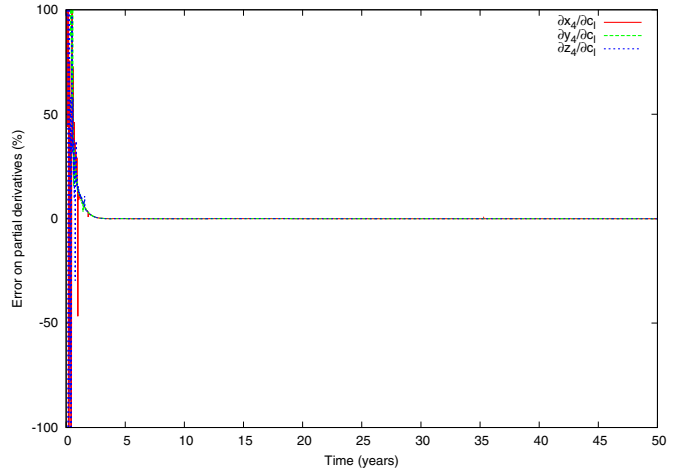


Figure 20. Variational equations test of Enceladus' Q parameter from Dione position.

(A color version of this figure is available in the online journal.)

even though perturbations will make the comparison with an analytical formulation more difficult. In particular, the expected drift on a and e may be masked by large short-period oscillations. Nevertheless, changes on a can still be checked by looking at the associated acceleration in longitude. Expected variations over 100 years in a from Equation (A1) are 8.38, 6.08, 10.72, 4.89, 1.64, and 0.95 m for Mimas to Titan, respectively. This translates to 1522, 761, 975, 306, 62, and 10 km in the mean longitudes.

In the simulations below, Tethys and Dione have been removed from the model to avoid resonances (which would make the analytic formulation of Equation (A1) invalid).

We obtain clearly a pretty good agreement (see Figures 10 and 11). A similar agreement can be found with the satellite case (full model).

A.1.4. Testing da/dt Acceleration

As for the tidal model, the “ da/dt ” force cannot be tested by the conservation of energy. Using Gauss' equations, we recall that we have introduced a force on Mimas that affects only its semi-major axis by a constant drift da/dt . Checking the validity of this force can be done easily by checking Mimas' semi-major axis variations after integration.

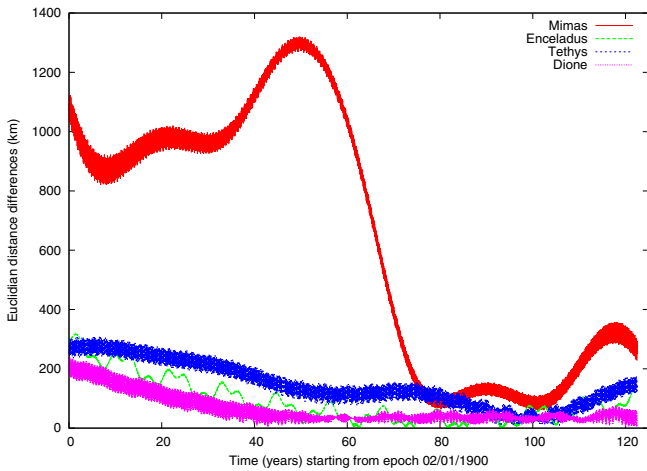


Figure 21. Position differences between JPL-SPICE sat317 ephemeris and the present work.

(A color version of this figure is available in the online journal.)

Here we consider the difference between two numerical simulations, with/without Mimas’ da/dt (Mimas’ semi-major axis input) equal to -16.9×10^{-15} AU day $^{-1}$.

Two-body Problem. We provide below such a test (Figure 12), assuming a two-body problem with only Saturn and Mimas. Clearly, the force acting on Mimas (input) and its expected effect on Mimas’ semi-major axis (output) are in full agreement.

The other elements are not affected by the da/dt force, in the limit of accuracy of our integration.

Full Model. As for tidal effects, one may expect the comparison between input/output to be more difficult using the full model (Enceladus equilibrium scenario and constant Saturn’s Q). Nevertheless, we can still use the mean longitude drift for the test and have a pretty good agreement with the two figures (Figures 13 and 14; Tethys has been removed from the simulation to avoid the Mimas–Tethys resonance). In particular, $da/dt = -16.9 \times 10^{-15}$ AU day $^{-1}$ translates to 16,776 km in Mimas’ mean longitude after 100 years. Figures 13 and 14 show the variations in semi-major axis and in positions (which corresponds essentially to the mean longitude variations).

A.1.5. Testing the Variational Equations

Partial derivatives of the moon state vectors as functions of initial conditions and physical parameters are computed by solving the so-called variational equations (see Equation (4)). Having accurate partial derivatives is a fundamental requirement when fitting a dynamical model to astrometric data. Solutions of the variational equations are routinely tested in our code. To check the accuracy of such computations, we compared our numerical solutions with their approximations using the centered difference method (i.e., $f'(x) \simeq [f(x+h) - f(x-h)]/2h$).

It is not possible to provide here the tests of all partial derivatives. Hence, we will restrict the number of figures by showing the computation of partial derivatives related to da/dt (Figures 15 and 16), Saturn’s Q (Figures 17 and 18), and Enceladus’ Q (denoted hereafter by Q^{s2} ; Figures 19 and 20), only. Any other plots are available on request.

We recall that c_l denotes an unspecified parameter of the model that shall be fitted. For more details on the method used, we refer to Lainey et al. (2004).

Plots for $c_l = da/dt$ on Mimas position are shown in Figures 15 and 16.

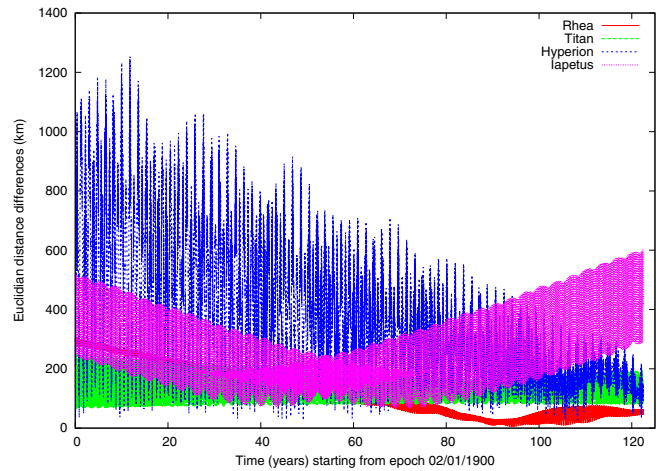


Figure 22. Position differences between JPL-SPICE sat317 ephemeris and the present work.

(A color version of this figure is available in the online journal.)

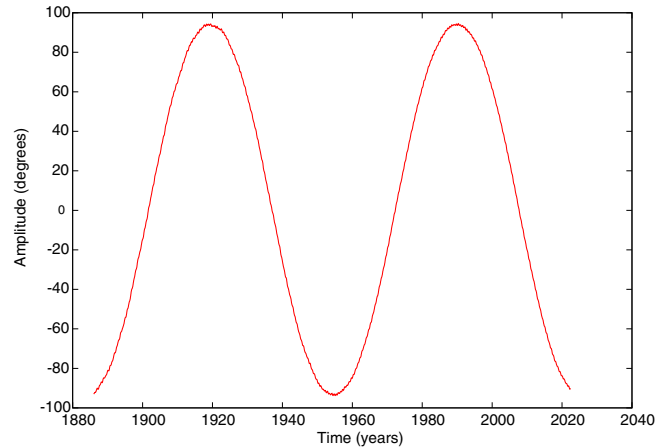


Figure 23. Mimas–Tethys resonant angle variation obtained with our model.

(A color version of this figure is available in the online journal.)

As can be seen in Figures 15 and 16, numerical computation of $\partial \mathbf{r} / \partial c_l$, where $\mathbf{r} = \mathbf{r}_1$ and $c_l = da/dt$, is in agreement with its approximation derived from the center difference method. The scattering behavior evident in Figure 15 is usual and corresponds to a nonlinear configuration occurring when the satellite reaches its maximum value along one Cartesian axis. As shown in Figure 16, these configurations occur when the distance differences (on the considered axis) are pretty small. Hence, this does not affect the fitting procedure. See also Lainey et al. (2004) for more details.

Plots for $c_l = Q$ on Mimas position and Tethys position are shown in Figures 17 and 18, respectively.

As can be seen in Figures 17 and 18, numerical computation of $\partial \mathbf{r} / \partial c_l$, where $\mathbf{r} = \mathbf{r}_1$ or $\mathbf{r} = \mathbf{r}_3$ and $c_l = Q$, is in agreement with its approximation derived from the center difference method.

Plots for $c_l = Q^{s2}$ on Enceladus position and Dione position are shown in Figures 19 and 20, respectively.

As can be seen in Figures 19 and 20, numerical computation of $\partial \mathbf{r} / \partial c_l$, where $\mathbf{r} = \mathbf{r}_2$ or $\mathbf{r} = \mathbf{r}_4$ and $c_l = Q^{s2}$, is in agreement with its approximation derived from the center difference method.

A.2. SPICE Kernel NOE-6-2011-MAIN.bsp

We have derived ephemerides of the eight main Saturnian moons for the Enceladus equilibrium and constant Q scenario. Our ephemerides are available as a SPICE kernel on the

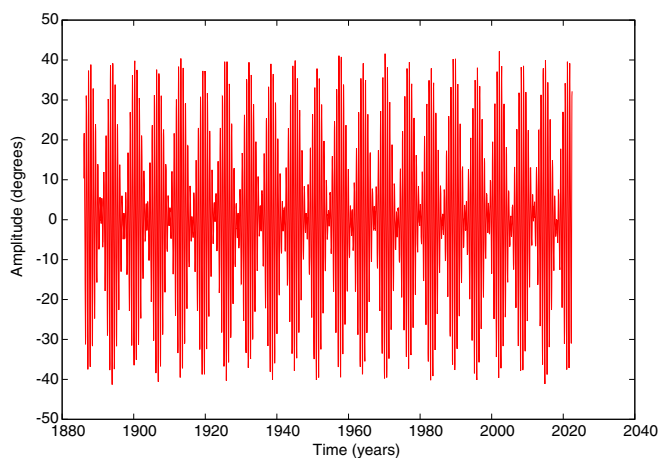


Figure 24. Enceladus–Dione resonant angle variation obtained with our model. (A color version of this figure is available in the online journal.)

FTP server of IMCCE: <ftp://ftp.imcce.fr/pub/ephem/satel/NOE/SATURNE/>.

Figures 21 and 22 show the Euclidian distance differences between our ephemerides and the JPL ones (kernel: sat317.bsp). Differences in the interval [1980, 2011] are between a few tens of km to less than 200 km, except for Hyperion and Iapetus, whose dynamics are less well constrained by the astrometric observations we used.

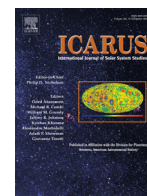
Since we have fitted a large da/dt term for Mimas, while JPL probably did not, one could expect large differences in Mimas' position. But as one can see, the large differences arise only before the 1970s. This suggests that it is the use of a large time span that makes possible the derivation of da/dt .

A.3. Resonances

While analytical developments require introducing explicitly orbital resonances, the latter are a simple consequence of initial conditions with numerical models. Figures 23 and 24 show the evolution of the resonant arguments associated with the Mimas–Tethys and Enceladus–Dione resonances, respectively.

REFERENCES

- Abbot, R. I., Mulholland, J. D., & Shelus, P. J. 1975, *AJ*, **80**, 723
- Aitken, R. G. 1905, *Lick Obs. Bul. No. 94*
- Aitken, R. G. 1909, *Lick Obs. Bul. No. 172*
- Alden, H. L., & O'Connell, W. C. 1928, *AJ*, **38**, 53
- Alden, H. L. 1929, *AJ*, **40**, 88
- Archinal, B. A., A'Hearn, M. F., Bowell, E., et al. 2011, *Celest. Mech. Dyn. Astron.*, **109**, 101
- Arlot, J.-E., & Emelyanov, N. V. 2009, *A&A*, **503**, 631
- Barnard, E. E. 1910, *AJ*, **26**, 79
- Barnard, E. E. 1913, *AJ*, **28**, 1
- Barnard, E. E. 1915, *AJ*, **29**, 33
- Barnard, E. E. 1916, *AJ*, **30**, 33
- Barnard, E. E. 1918, *AJ*, **31**, 49
- Barnard, E. E. 1927, *AJ*, **37**, 157
- Buratti, B. J. 1984, *Icarus*, **59**, 392
- Charnoz, S., Crida, A., Castillo-Rogez, J. C., et al. 2011, *Icarus*, **216**, 535
- Davies, M. E., Abalakin, V. K., Bursa, M., et al. 1996, *Celest. Mech. Dyn. Astron.*, **63**, 127
- Desmars, J., Arlot, S., Arlot, J.-E., Lainey, V., & Vienne, A. 2009a, *A&A*, **499**, 321
- Desmars, J., Vienne, A., & Arlot, J. E. 2009b, *A&A*, **493**, 1183
- Dourneau, G., Veillet, C., Dulou, M. R., & Le Campion, J. F. 1986, *A&A*, **160**, 280
- Emelyanov, N. V., & Gilbert, R. 2006, *A&A*, **453**, 1141
- Fortney, J. F., & William, B. H. 2003, *Icarus*, **164**, 228
- French, R. G., McGhee, C. A., Frey, M., et al. 2006, *PASP*, **118**, 246
- Gavrilov, S. V., & Zharkov, V. N. 1977, *Icarus*, **32**, 443
- Goldreich, P., & Soter, S. 1966, *Icarus*, **5**, 375
- Goodman, J., & Lackner, C. 2009, *ApJ*, **696**, 2054
- Guillot, T. 1999, *Science*, **286**, 72
- Harper, D., Beurle, K., Williams, I. P., et al. 1999, *A&AS*, **136**, 257
- Harper, D., Murray, C. D., Beurle, K., et al. 1997, *A&AS*, **121**, 65
- Howett, C. J. A., Spencer, J. R., Pearl, J., & Segura, M. 2011, *J. Geophys. Res.*, **116**, E03003
- Iorio, L., & Lainey, V. 2005, *Int. J. Mod. Phys. D*, **14**, 2039
- Jacobson, R. A. 2007, The Orientation and Precession of the Pole of Saturn, American Astronomical Society, DDA Meeting 38, 13.06
- Jacobson, R. A., Antreasian, P. G., Bordi, J. J., et al. 2006, *AJ*, **132**, 2520
- Kaula, W. M. 1964, *Rev. Geophys. Space Phys.*, **2**, 661
- Kiseleva, T. P., & Kalinitchenko, O. A. 1998, *Pulkovo, Glavnaia Astronomicheskaja Observatoriia, Izvestiia*, **213**, 122
- Kiseleva, T. P., & Kalinitchenko, O. A. 2000, *Pulkovo, Glavnaia Astronomicheskaja Observatoriia, Izvestiia*, **214**, 344
- Kiseleva, T. P., Kiselev, A. A., Khrutskaya, E. V., & Kalinitchenko, O. A. 1996, *Pulkovo, Glavnaia Astronomicheskaja Observatoriia, Izvestiia*, **210**, 76
- Lainey, V. 2008, *Planet. Space Sci.*, **56**, 1766
- Lainey, V., Arlot, J. E., Karatekin, Ö., & Van Hoolst, T. 2009, *Nature*, **459**, 957
- Lainey, V., Dehant, V., & Pätzold, M. 2007, *A&A*, **465**, 1075
- Lainey, V., Duriez, L., & Vienne, A. 2004, *A&A*, **420**, 1171
- Lissauer, J. J., & Cuzzi, J. N. 1982, *AJ*, **87**, 1051
- Meyer, J., & Wisdom, J. 2007, *Icarus*, **188**, 535
- Morales, M. A., Schwegler, E., Ceperley, D., et al. 2009, *Proc. Natl Acad. Sci.*, **106**, 1324
- Morgan, H. R. 1900, *Astron. Nachr.*, **154**, 91
- Nimmo, F., Spencer, J. R., Pappalardo, R. T., & Mullen, M. E. 2007, *Nature*, **447**, 289
- Ogilvie, G. I., & Lin, D. N. C. 2004, *ApJ*, **610**, 477
- O'Neill, C., & Nimmo, F. 2010, *Nat. Geosci.*, **3**, 88, doi:10.1038/NGEO731
- Peale, S. J., & Cassen, P. 1978, *Icarus*, **36**, 245
- Peng, Q., Vienne, A., & Shen, K. X. 2002, *A&A*, **383**, 296
- Peng, Q., Vienne, A., Wu, X. P., Gan, L. L., & Desmars, J. 2008, *AJ*, **136**, 2214
- Pitman, K. M., Buratti, B. J., & Mosher, J. A. 2010, *Icarus*, **206**, 537
- Porco, C. C., Helfenstein, P., Thomas, P. C., et al. 2006, *Science*, **311**, 1393
- Qiao, R. C., Shen, K. X., Harper, D., & Liu, J. R. 2004, *A&A*, **422**, 377
- Qiao, R. C., Shen, K. X., Liu, J. R., & Harper, D. 1999, *A&AS*, **137**, 1
- Rieutord, M., & Valdetaro, L. 2010, *J. Fluid Mech.*, **643**, 363
- Seitzer, P., & Ianna, P. A. 1980, *AJ*, **85**, 1117
- Seitzer, P., Ianna, P. A., & Levinson, F. 1979, *AJ*, **84**, 877
- Sinclair, A. T. 1974, *MNRAS*, **169**, 591
- Sinclair, A. T. 1977, *MNRAS*, **180**, 447
- Sinclair, A. T. 1983, *IAU Colloq.* **74**, Dynamical Trapping and Evolution in the Solar System, ed. V. V. Markellos & Y. Kozai (Dordrecht: Reidel), **19**
- Spencer, J. R., Barr, A. C., Esposito, L. W., et al. 2009, in *Saturn from Cassini-Huygens*, ed. M. K. Dougherty, L. W. Esposito, & S. M. Krimigis (Berlin: Springer), **683**
- Stone, O. 1895, *AJ*, **15**, 110
- Stone, O. 1896, *AJ*, **16**, 62
- Stone, O. 1898a, *Astron. Nachr.*, **146**, 223
- Stone, O. 1898b, *AJ*, **19**, 118
- Stone, R. C., & Harris, F. H. 2000, *AJ*, **119**, 1985
- Struve, H. 1898, *Publ. Obs. Central Nicolas*, **11**, 2
- Struve, G. 1933, *Veroff. Berlin-Babelsberg* **6**, parts 2, 3 and 5
- Taylor, D. B., & Sinclair, A. T. 1985, *A&AS*, **61**, 221
- Thuillot, W., Arlot, J.-E., Ruatti, C., et al. 2001, *A&A*, **371**, 343
- Tobie, G., Cadek, O., & Sotin, C. 2008, *Icarus*, **196**, 642
- Tolbin, S. B. 1991a, Scientific paper deposited in All-russian institute of scientific and technical information, 3077-B91, 1
- Tolbin, S. B. 1991b, Scientific paper deposited in All-russian institute of scientific and technical information, 3078-B91, 1
- USNO 1929, *Publ. U.S. Naval Obs.*, **12**, 2
- USNO 1954, *Publ. U.S. Naval Obs.*, **17**, 2
- Vass, G. 1997, *Roman. Astron. J.*, **7**, 45
- Veiga, C. H., Vieira Martins, R., Vienne, A., Thuillot, W., & Arlot, J. E. 2003, *A&A*, **400**, 1095
- Veillet, C., & Dourneau, G. 1992, *A&AS*, **94**, 291
- Vienne, A., Thuillot, W., Veiga, C. H., Arlot, J. E., & Vieira Martins, R. 2001, *A&A*, **380**, 727
- Voronenko, V. I., Gorel, G. K., Gudkova, L. A., & Pozhalova, J. A. 1991, Scientific paper deposited in All-russian institute of scientific and technical information, 3167-B91, 1
- Wu, Y. 2005, *ApJ*, **635**, 688
- Zahn, J.-P. 1966, *Ann. Astrophys.*, **29**, 489
- Zahn, J.-P. 1989, *A&A*, **220**, 112



New constraints on Saturn's interior from Cassini astrometric data



Valéry Lainey^{a,*}, Robert A. Jacobson^b, Radwan Tajeddine^{c,a}, Nicholas J. Cooper^{d,a}, Carl Murray^d, Vincent Robert^{e,a}, Gabriel Tobie^f, Tristan Guillot^g, Stéphane Mathis^h, Françoise Remus^{i,a,h}, Josselin Desmars^{j,a}, Jean-Eudes Arlot^a, Jean-Pierre De Cuyper^k, Véronique Dehant^k, Dan Pascu^l, William Thuillot^a, Christophe Le Poncin-Lafitte^m, Jean-Paul Zahnⁱ

^aIMCCE, Observatoire de Paris, PSL Research University, CNRS, Sorbonne Universités, UPMC Univ. Paris 06, Univ. Lille, France

^bJet Propulsion Laboratory, California Institute of Technology, 4800 Oak Grove Drive, Pasadena, CA 91109-8099, United States

^cCenter for Astrophysics and Planetary Science, Cornell University, Ithaca, NY 14853, USA

^dQueen Mary University of London, Mile End Rd, London E1 4NS, United Kingdom

^eIPSA, 7-9 rue Maurice Grandcoing, 94200 Ivry-sur-Seine, France

^fLaboratoire de Planétologie et Géodynamique de Nantes, Université de Nantes, CNRS, UMR 6112, 2 rue de la Houssinière, 44322 Nantes Cedex 3, France

^gLaboratoire Lagrange, CNRS UMR 7293, Université de Nice-Sophia Antipolis, Observatoire de la Côte d'Azur, B.P. 4229, 06304 Nice Cedex 4, France

^hLaboratoire AIM Paris-Saclay, CEA/DRF - Université Paris Diderot - CNRS, IRFU/SAP Centre de Saclay, 91191 Gif-sur-Yvette, France

ⁱLUTH-Observatoire de Paris, UMR 8102 du CNRS, 5 place Jules Janssen, 92195 Meudon Cedex, France

^jObservatório Nacional, Rua José Cristino 77, São Cristovão, Rio de Janeiro CEP 20.921-400, Brazil

^kRoyal Observatory of Belgium, Avenue Circulaire 3, 1180 Uccle, Bruxelles, Belgium

^lUSNO, 3450 Massachusetts Avenue Northwest, Washington, DC 20392, United States

^mSYRTE, Observatoire de Paris, PSL Research University, CNRS, Sorbonne Universités, UPMC Univ. Paris 06, LNE, 61 avenue de l'Observatoire, 75014 Paris, France

ARTICLE INFO

Article history:

Received 4 October 2015

Revised 8 July 2016

Accepted 24 July 2016

Available online 3 August 2016

Keywords:

Astrometry

Interior

Saturn

ABSTRACT

Using astrometric observations spanning more than a century and including a large set of Cassini data, we determine Saturn's tidal parameters through their current effects on the orbits of the eight main and four coorbital Moons. We have used the latter to make the first determination of Saturn's Love number from observations, $k_2=0.390 \pm 0.024$, a value larger than the commonly used theoretical value of 0.341 (Gavrilov & Zharkov, 1977), but compatible with more recent models (Helled & Guillot, 2013) for which the static k_2 ranges from 0.355 to 0.382. Depending on the assumed spin for Saturn's interior, the new constraint can lead to a significant reduction in the number of potential models, offering great opportunities to probe the planet's interior. In addition, significant tidal dissipation within Saturn is confirmed (Lainey et al., 2012) corresponding to a high present-day tidal ratio $k_2/Q=(1.59 \pm 0.74) \times 10^{-4}$ and implying fast orbital expansions of the Moons. This high dissipation, with no obvious variations for tidal frequencies corresponding to those of Enceladus and Dione, may be explained by viscous friction in a solid core, implying a core viscosity typically ranging between 10^{14} and 10^{16} Pa.s (Remus et al., 2012). However, a dissipation increase by one order of magnitude at Rhea's frequency could suggest the existence of an additional, frequency-dependent, dissipation process, possibly from turbulent friction acting on tidal waves in the fluid envelope of Saturn (Ogilvie & Lin, 2004; Fuller et al. 2016).

© 2016 Elsevier Inc. All rights reserved.

1. Introduction

Tidal effects among planetary systems are the main driver in the orbital migration of natural satellites. They result from physical processes arising in the interior of celestial bodies, not observable necessarily from surface imaging. Hence, monitoring the Moons'

motions offers a unique opportunity to probe the interior properties of a planet and its satellites. In common with the martian and jovian systems (Lainey et al., 2007, 2009), the orbital evolution of the saturnian system due to tidal dissipation can be derived from astrometric observations of the satellites over an extended time period. In that respect, the presence of the Cassini spacecraft in orbit around Saturn since 2004 has provided unprecedented astrometric and radio-science data for this system with exquisite precision. These data open the door for estimating a potentially large

* Corresponding author.

E-mail address: lainey@imcce.fr (V. Lainey).

number of physical parameters simultaneously, such as the gravity field of the whole system and even separating the usually strongly correlated tidal parameters k_2 and Q .

The present work is based on two fully independent analyses (modeling, data, fitting procedure) performed at IMCCE and JPL, respectively. Methods are briefly described in Section 2. Section 3 provides a comparison between both analyses as well as a global solution for the tidal parameters k_2 and Q of Saturn. Section 4 describes possible interior models of Saturn compatible with our observations. Section 5 discusses possible implications associated with the strong tidal dissipation we determined.

2. Material and methods

Both analyses stand on numerical computation of the Moons' orbital states at any time, as well as computation of the derivatives of these state vectors (see Section 2.1) with respect to: (i) their initial state for some reference epoch; (ii) many physical parameters. Tidal effects between both the Moons and the planet are introduced by means of the amplitude of the tidal bulge and its time lag associated to dissipation processes. The gravitational effect of the tidal bulge is classically described by the tidal Love number k_2 and the tidal ratio k_2/Q . The Love number k_2 is defined as the ratio between the gravitational potential induced by the tidally-induced mass redistribution and the tide-generating potential. As the interior does not respond perfectly to the tidal perturbations, because of internal friction applied on tides, there is a time lag between the tide-raising potential and the tidally-induced potential. The torque created by this lag is proportional to the so-called tidal ratio k_2/Q . The amplitude and lag of the tide potential can also be described using a complex representation of the Love number, where the real part correspond to the part of the potential aligned with the tide-raising potential, while the imaginary part describes the dissipative part (see also Section 4). The factor Q , often called the quality factor (Kaula 1964), or the specific dissipation function, Q^{-1} , in its inverse form, is inversely proportional to the amount of energy dissipated by tidal friction in the deformed object. Coupled tidal effects such as tidal bulges raised on Saturn by one Moon and acting on another are considered. Besides the eight main Moons of Saturn, the coorbital Moons Calypso, Telessto, Polydeuces, and Helene are integrated in both studies.

Although the two tidal parameters k_2 and Q often appear independently in the equations of motion, the major dynamical effect by far is obtained when the tide raised by a Moon on its primary acts back on this same Moon. In this case, only the ratio k_2/Q is present as a factor for the major term, therefore preventing an independent fit of k_2 and Q . However, the small co-orbital satellites raise negligible tides on Saturn and yet react to the tides raised on the planet by their parent satellites (see Figure in Appendix A.1). This unique property allows us to make a fit for k_2 that is almost independent of Q (see Appendix A.1). In particular, we find that the modeling of such cross effects between the coorbital moons allows us to obtain a linear correlation between k_2 and Q of only 0.03 (Section 3 and Appendix A.4). Thanks to the inclusion of Telessto, Calypso, Helene and Polydeuces, we can estimate k_2 essentially around the tidal frequencies of Tethys and Dione.

2.1. IMCCE's approach

The IMCCE approach benefits from the NOE numerical code that was successfully applied to the Mars, Jupiter, and Uranus systems (Lainey et al., 2007, 2008, 2009). It is a gravitational N-body code that incorporates highly sensitive modeling and can generate partial derivatives needed to fit initial positions, velocities, and other parameters (like the ratio k_2/Q) to the observational data. The code includes (i) gravitational interaction up to degree two in

the spherical harmonics expansion of the gravitational potential for the satellites and up to degree 6 for Saturn (Jacobson et al. 2006); (ii) the perturbations of the Sun (including inner planets and the Moon by introducing their mass in the Solar one) and Jupiter using DE430 ephemerides; (iii) the Saturnian precession; (iv) the tidal effects introduced by means of the Love number k_2 and the quality factor Q .

The dynamical equations are numerically integrated in a Saturncentric frame with inertial axes (conveniently the Earth mean equator J2000). The equation of motion for a satellite P_i can be expressed as (Lainey et al. 2007)

$$\ddot{\vec{r}}_i = -\frac{G(m_0 + m_i)\vec{r}_i}{r_i^3} + \sum_{j=1, j \neq i}^N Gm_j \left(\frac{\vec{r}_j - \vec{r}_i}{r_{ij}^3} - \frac{\vec{r}_j}{r_j^3} \right) + G(m_0 + m_i)\nabla_i U_{i0} + \sum_{j=1, j \neq i}^N Gm_j \nabla_j U_{j0} + \frac{(m_0 + m_i)}{m_i m_0} (\vec{F}_{i0}^T - \vec{F}_{0i}^T) - \frac{1}{m_0} \sum_{j=1, j \neq i}^N (\vec{F}_{j0}^T - \vec{F}_{0j}^T) + GR \quad (1)$$

Here, \vec{r}_i and \vec{r}_j are the position vectors of the satellite P_i and a body P_j (another satellite, the Sun, or Jupiter) with mass m_j , subscript 0 denotes Saturn, U_{ij} is the oblateness gravity field of body P_i at the position of body P_j , GR are corrections due to General Relativity (Newhall et al. 1983) and \vec{F}_{ik}^T the force received by P_i from the tides it raises on P_k . This force is equal to (Lainey et al. 2007)

$$\vec{F}_{ik}^T = -\frac{3k_2 G m_i^2 R^5 \Delta t}{r_{kl}^8} \left(\frac{2\vec{r}_{kl}(\vec{r}_{kl} \cdot \vec{v}_{kl})}{r_{kl}^2} + (\vec{r}_{kl} \times \vec{\Omega} + \vec{v}_{kl}) \right) \quad (2)$$

where $\vec{r}_{kl} = \vec{r}_k - \vec{r}_l$, $\vec{v}_{kl} = d\vec{r}_{kl}/dt$, $\vec{\Omega}$, R , and Δt being the instantaneous rotation vector, equatorial radius and time potential lag of P_k , respectively. The time lag Δt is defined by

$$\Delta t = \text{Tarctan}(1/Q)/2\pi \quad (3)$$

where T is the period of the main tidal excitation. For the tides raised on Enceladus, T is equal to $2\pi/n$ (n being Enceladus' mean motion) as we only considered the tide raised by Saturn. For Saturn's tidal dissipation, T is equal to $2\pi/2(\Omega - n_i)$ where Ω is the spin frequency of Saturn and n_i is the mean motion of the tide raising saturnian Moon P_i . Δt depends on the tidal frequency and on Q , therefore it is not a constant parameter.

It is clear from the second term in the right hand side of Eqs. (2) and (3) that k_2 and Q are completely correlated. To separate both parameters, we consider the action on any Moon of the tides raised on Saturn by all other Moons (see also Appendix A.1). Neglecting tidal dissipation in that case provides the extra terms

$$\sum_{j=1, j \neq i}^N \frac{-T}{m_i} \vec{F}_{ij} = \frac{3k_2 G m_j R^5}{2r_i^5 r_j^5} \left[-\frac{5(\vec{r}_i \cdot \vec{r}_j)^2 \vec{r}_i}{r_i^2} + r_j^2 \vec{r}_i + 2(\vec{r}_i \cdot \vec{r}_j) \vec{r}_j \right]. \quad (4)$$

For an unspecified parameter c_i of the model that shall be fitted (e.g. $\vec{r}(t_0)$, $d\vec{r}/dt(t_0)$, Q ...), a useful relation is (Lainey et al. 2012 and references therein)

$$\frac{\partial}{\partial c_i} \left(\frac{d^2 \vec{r}_i}{dt^2} \right) = \frac{1}{m_i} \left[\sum_j \left(\frac{\partial \vec{F}_i}{\partial \vec{r}_j} \frac{\partial \vec{r}_j}{\partial c_i} + \frac{\partial \vec{F}_i}{\partial \dot{\vec{r}}_j} \frac{\partial \dot{\vec{r}}_j}{\partial c_i} \right) + \frac{\partial \vec{F}_i}{\partial c_i} \right], \quad (5)$$

where \vec{F}_i is the right hand side of Eq. (1) multiplied by m_i . Partial derivatives of the solutions with respect to initial positions and velocities of the satellites and dynamical parameters are computed from simultaneous integration of Eqs. (5) and (1).

Here, fourteen Moons of Saturn are considered all together, i.e. the eight main Moons and six coorbital Moons (Epimetheus, Janus, Calypso, Telesto, Helene, and Polydeuces). All the astrometric observations already considered in Lainey et al. (2012) and Desmars et al. (2009) are used, with the addition of a large set of ISS–Cassini data (Tajeddine et al., 2013, 2015; Cooper et al. 2014). We also include a new reduction of old photographic plates, obtained at USNO between the years 1974 and 1998. As part of the ESPaCE European project, the scanning and new astrometric reduction of these plates were performed recently at Royal Observatory of Belgium and IMCCE, respectively (Robert et al. 2011, 2016). We use a weighted least squares inversion procedure and minimize the squared differences between the observed and computed positions of the satellites in order to determine the parameters of the model. For each fit, the following parameters are released simultaneously and without constraints: the initial state vector and mass of each Moon, the mass, the gravitational harmonic J_2 , the orientation and the precession of the pole of Saturn as well as its tidal parameters k_2 and Q . Tidal dissipation within the Moons is neglected, except in Enceladus for which strong tides are believed to take place. No da/dt term is released for Mimas. In particular, it appears that the large signal obtained in Lainey et al. (2012) can be removed after fitting the gravity field of the Saturn system. Indeed, due to its long period libration (about 70 years), the 2:1 Mimas–Tethys resonance strongly affects the dynamical evolution of Mimas' orbit over the considered time span of observations. Due to exchange of angular momentum between the rings and Mimas, a quadratic effect on Mimas' longitude may be strongly correlated with the libration amplitude. Since the libration is conditioned by the mass of Mimas and Tethys, Lainey et al. (2012) fixed their value to former estimates that benefited from the first Cassini data (Jacobson 2006) to solve for da/dt . Unfortunately, even a small error on the mass of the two Moons was sufficient to generate erroneous behavior in the libration angle, strongly affecting the da/dt determination. In this work, and thanks to Cassini data, the mass of Saturn and all main Moons are fitted accurately.

2.2. JPL's approach

The second approach incorporates the tidal parameters into the ongoing determination of the satellite ephemerides and Saturnian system gravity parameters that support navigation for the Cassini Mission. Initial results from that work appear in Jacobson et al. (2006). For Cassini the satellite system is restricted to the eight major satellites, Phoebe, and the lagrangians Helene, Telesto, and Calypso. The analysis procedure is to repeat all of the Cassini navigation reconstructions but with a common set of ephemerides and gravity parameters. We combine these new reconstructions with other non-Cassini data sets to obtain the updated ephemerides and revised gravity parameters. The non-Cassini data include radiometric tracking of the Pioneer and Voyager spacecraft, imaging from Voyager, Earth-based and HST astrometry, satellite mutual events (eclipses and occultations), and Saturn ring occultations. We process the data via a weighted least-squares fit that adjusts our models of the orbits of the satellites and the four spacecraft (Pioneer, Voyager 1, Voyager 2, Cassini). Peters (1981) and Moyer (2000) describe the orbital models for the satellites and spacecraft, respectively. The set of gravity related parameters adjusted in the fit contains the GMs of the Saturnian system and the satellites (Helene, Telesto, and Calypso are assumed massless), the gravitational harmonics of Saturn, Enceladus, Dione, Rhea, and Titan, Saturn's polar moment of inertia, the orientation of Saturn's pole, and the tidal parameters k_2 and Q .

3. Results

Since tidal effects within Saturn and Enceladus have almost opposite orbital consequences, Lainey et al. (2012) could not solve for the Enceladus tidal ratio k_2^E/Q^E . Here, we face a similar strong correlation and follow their approach by considering two extreme scenarios for Enceladus' tidal state. In a first inversion, we neglect dissipation in Enceladus and obtain for Saturn k_2 , $k_2^{(I)}=0.371 \pm 0.003$, $k_2^{(J)}=0.381 \pm 0.011$ (formal error bar, 1σ) where the indices I and J refer to the IMCCE and JPL solutions, respectively. The Saturn tidal ratio that we obtain is $k_2/Q^{(I)}=(1.32 \pm 0.25) \times 10^{-4}$, $k_2/Q^{(J)}=(1.04 \pm 0.19) \times 10^{-4}$. In a second inversion, we assume Enceladus to be in a state of tidal equilibrium (Meyer & Wisdom, 2007), obtaining $k_2^{(I)}=0.372 \pm 0.003$, $k_2^{(J)}=0.402 \pm 0.011$ and $k_2/Q^{(I)}=(2.07 \pm 0.26) \times 10^{-4}$, $k_2/Q^{(J)}=(1.22 \pm 0.23) \times 10^{-4}$. If both studies are generally in good agreement within the uncertainty of the measurements (see also Tables 1 and 2), the last $k_2/Q^{(I)}$ value stands at 3σ of the JPL estimation. This possibly reflects the difference in the data sets, since JPL introduced radio-science data, while IMCCE introduced scanning data. Nevertheless, both estimates suggest strong tidal dissipation, at least about five times larger than previous theoretical estimates (Sinclair, 1983). Merging IMCCE's and JPL's results into one value by overlapping the extreme 1σ values, we get $k_2=0.390 \pm 0.024$ and $k_2/Q=(1.59 \pm 0.74) \times 10^{-4}$. These last error bars are not formal 1σ values anymore, but the likely interval of expected physical values.

Last, to assess a possibly large variation in Saturn's Q as function of tidal frequency, we followed Lainey et al. (2012) and released as free parameters four different Saturnian tidal ratios k_2/Q associated with the Enceladus', Tethys', Dione's, and Rhea's tides (see Tables 1 and 2). It turns out that no significant change for the k_2 estimation arises with an overall result of $k_2=0.390 \pm 0.024$. Moreover, global solutions for k_2/Q ratios are equal to $(20.70 \pm 19.91) \times 10^{-5}$, $(15.84 \pm 12.26) \times 10^{-5}$, $(16.02 \pm 12.72) \times 10^{-5}$, $(123.94 \pm 17.27) \times 10^{-5}$ at Enceladus', Tethys', Dione's and Rhea's tidal frequency, respectively. Increasing the number of frequencies to be tested may be problematic. If the tidal bulges raised by Titan on Saturn are much larger than those raised by the other Moons, their feedback on Titan's orbit is significantly smaller. This can easily be checked from analytical expression of orbital expansion of Moons raising tides on their primary (Kaula 1964). As a consequence, we did not release Saturn's k_2/Q at Titan's tidal frequency. Moreover, since Mimas and Tethys are locked in a mean motion resonance, they share their orbital energy and angular momentum. Hence, the action of tides raised on Saturn by Mimas and Tethys is distributed among the resonant pair. In the limit of our current measurements, this prevented solving simultaneously for Saturn's k_2/Q at Mimas and Tethys frequencies. Hence, Saturn's k_2/Q was kept fixed at its former constant estimation (see above) for Mimas as well as for all other Moons, with the exception of Enceladus, Tethys, Dione and Rhea. We provide in Fig. 1 a plot showing all global k_2/Q ratios associated with constant and non-constant assumptions.

4. Modeling Saturn's interior

To model the tidal response of Saturn's interior and to compare it to the k_2 and k_2/Q values inferred in the present study, we consider a wide range of interior models consistent with the gravitational coefficients measured using the Cassini spacecraft (Helled & Guillot 2013). In total, 302 interior models, corresponding to various core size and composition, helium phase separation and enrichment in heavy elements in the external envelope, have been tested. Each interior model is characterized by radial profiles of density, ρ , and bulk modulus, K .

Table 1Fitting k_2 and variable Saturnian Q at Enceladus (S2), Tethys (S3), Dione (S4) and Rhea (S5) frequencies.

	k_2	k_2/Q (S2)	k_2/Q (S3)	k_2/Q (S4)	k_2/Q (S5)
IMCCE	0.372 +/- 0.003	$(7.4 +/- 3.1) \times 10^{-5}$	$(10.9 +/- 6.1) \times 10^{-5}$	$(16.1 +/- 3.8) \times 10^{-5}$	$(122.3 +/- 15.0) \times 10^{-5}$
JPL	0.377 +/- 0.011	$(5.5 +/- 4.7) \times 10^{-5}$	$(6.0 +/- 2.4) \times 10^{-5}$	$(21.5 +/- 7.3) \times 10^{-5}$	$(125.8 +/- 14.9) \times 10^{-5}$

Table 2Fitting k_2 and variable Saturnian Q at Enceladus (S2), Tethys (S3), Dione (S4) and Rhea (S5) frequencies assuming Enceladus' tidal equilibrium.

	k_2	k_2/Q (S2)	k_2/Q (S3)	k_2/Q (S4)	k_2/Q (S5)
IMCCE	0.372 +/- 0.003	$(18.1 +/- 3.1) \times 10^{-5}$	$(11.9 +/- 6.1) \times 10^{-5}$	$(15.0 +/- 3.8) \times 10^{-5}$	$(121.6 +/- 15.0) \times 10^{-5}$
JPL	0.394 +/- 0.011	$(27.1 +/- 13.5) \times 10^{-5}$	$(21.5 +/- 6.6) \times 10^{-5}$	$(5.4 +/- 2.1) \times 10^{-5}$	$(127.9 +/- 13.3) \times 10^{-5}$

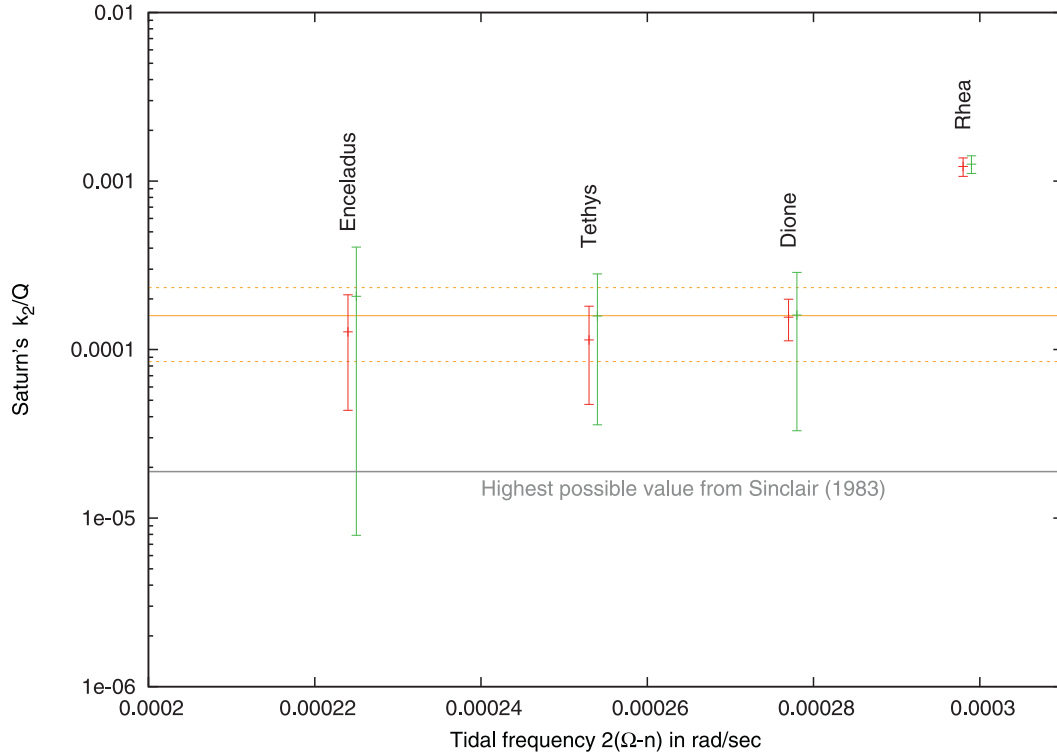


Fig. 1. Variation of the Saturnian tidal ratio k_2/Q as a function of tidal frequency $2(\Omega-n)$, where Ω and n denote its rotation rate and the Moon's mean motion, respectively. Four frequencies are presented associated with Enceladus', Tethys', Dione's and Rhea's tides. IMCCE and JPL solutions are in red and green, respectively. They are shown slightly shifted from each other along the X-axis for better visibility. Orange lines refer to the global estimation $k_2/Q = (15.9 \pm 7.4) \times 10^{-5}$. (For interpretation of the references to color in this figure legend, the reader is referred to the web version of this article).

In giant planets, two main mechanisms are invoked for tidal dissipation: the viscous dissipation associated to viscoelastic deformation of a solid core (as initially proposed by [Dermott \(1979\)](#) and further explored here) and the fluid friction applied on tidal waves propagating in the deep gaseous envelope (see e.g. [Ogilvie & Lin 2004](#) and the discussion hereafter). As demonstrated in [Guenel, Mathis and Remus \(2014\)](#), these two mechanisms may have comparable strengths and superpose.

Here, the tidal response of Saturn's interior is first computed from all the considered density profiles assuming that the core is solid and viscoelastic, with radius R_{core} (varying typically between 7000 and 16,000 km) overlaid by a thick non-dissipative fluid envelope (to explore the own effect of the core), similar to the approach of [Remus et al. \(2012, 2015\)](#). The envelope is only taken into account for the hydrostatic effects it applies on the core. The complex Love number k_2^c (including both the response aligned with tide-raising potential and the dissipative part in quadrature) is computed by integrating the 5 radial functions, y_i , describing the displacements, stresses, and gravitational potential from the planet

center to the surface, following the formalism initially introduced by [Alterman et al. \(1959\)](#). The viscoelastic deformation in the solid viscoelastic core is computed using the compressible elastic formulation of [Takeuchi & Saito \(1972\)](#), adapted to viscoelastic media (see [Tobie et al., 2005](#) for more details). For the fluid envelope, the static formulation of [Saito \(1974\)](#) is used. In this formalism, the fluid friction is not modeled. However, it allows us to take into account the gravitational effects of the fluid envelope on the solid core deformation, which has a strong impact in the case of very thick fluid envelope like in the case of Saturn as demonstrated by [Dermott \(1979\)](#) and [Remus et al. \(2012, 2015\)](#). The system of differential equations (6 in the core and 2 in the envelope) is solved by integrating from the center to the surface three independent solutions using a fifth order Runge-Kutta method with adaptive stepsize control, and by applying the appropriate condition at the solid core/fluid envelope interface and at the surface (see [Takeuchi & Saito 1972](#) and [Tobie et al. 2005](#) for more details). The complex Love number k_2^c is determined from the complex 5th radial function at the planet surface, $y_5^c(R_s)$, and the global dissipation

function by the ratio between the imaginary part and the modulus of k_2^c : $k_2^c = |k_2^c| = |y_5^c(R_s) - 1|$; $Q^{-1} = -\text{Im}(k_2^c) / |k_2^c|$.

For the solid core, a compressible Maxwell rheology, characterized by the bulk modulus K , the shear modulus μ , and the viscosity η , is assumed. As the mechanical properties of such a core are totally unknown, a wide range of parameter values is considered. As we will show hereafter, the Q factor of Saturn can be explained only for a limited range of viscoelastic parameters, thus providing useful constraints on Saturn's core structure and rheology. The shear modulus is determined from the bulk modulus assuming a constant μ/K ratio varying between 0.001 and 1, and the viscosity is assumed constant over a range varying between 10^{12} and 10^{18} Pa.s. For comparison, the μ/K ratio in the inner core of the Earth is about 0.12 (Dziewonski and Anderson, 1981), and its viscosity is estimated typically between 10^{14} and 10^{20} Pa.s (Karato, 2008). Obviously, Saturn's core is different from Earth's metallic inner core due to difference in pressure and composition. However, this comparison gives us an estimate of the typical parameter values we might expect in Saturn.

In order to test the validity of our numerical code, we compared our numerical solutions with the analytical solutions derived by Remus et al. (2012) for a viscoelastic core and a fluid envelope with constant density. As illustrated on Fig. A.2, we reproduce almost perfectly the analytical value of the tidal Love number. For the dissipation function, the agreement is also very good, the difference between the analytical and numerical solutions never exceed a few per cent. To further test our code, we also compared with the solution provided by Kramm et al. (2011) for a density distribution of a $n=1$ polytrope: we obtained $k_2=0.5239$, while the value reported by Kramm et al. (2011) is 0.5198, which corresponds to a difference of less than 0.8%.

Our calculations confirm that the real part of the tidal Love number (k_2) of the planet is almost entirely determined by the density profile; therefore it is a very close to the fluid Love number. For the 302 tested interiors models, corresponding to various core size and composition of the core and fluid envelope, we obtained values of k_2 ranging between 0.355 and 0.381. The lowest values are obtained for fast deep rotation (10h32') and high-density core (modeled with the EOS of pure rock), while the highest values correspond to slow deep rotation (10h39') and low-density core (modeled with the EOS of pure ice). All tested models are consistent with the equatorial radius and the gravitational coefficients (J_2 , J_4 and J_6) determined by Cassini, within error bars. Although we did not test all possible models, based on these results, we can reasonably conclude that a k_2 value as high as 0.39 is incompatible with the observed gravitational coefficient. For slow rotation cases, all models with a low density ice-rich core have a k_2 value above 0.366, the lower limit inferred from astrometric measurements, while only about half of the models with a high density core exceeds this value. For fast rotation cases, only four tested models exceed this limit: all of them have a low-density core and a helium separation occurring at 1 Mbar, in line with recent determinations of hydrogen-helium phase separation (Morales et al., 2009). Even if we can notice some tendencies as a function of core size (Fig. 2), the k_2 value is controlled by several other internal parameters (core composition, helium separation, enrichment in heavy elements in the external envelope), which precludes any simple interpretation of the measured k_2 value in term of internal structure. Tests performed for a wide range of mechanical parameters for the core show that they have only very minor effects on the k_2 value. Varying the μ/K ratio from 0.001 to 1 results in only 0.2% of variations on the amplitude of k_2 . Nevertheless, it strongly affects the imaginary part of k_2 , and hence the quality factor, Q .

As shown in Fig. 3a and b, the global Q factor depends on the assumed shear modulus (hence the μ/K ratio) and the viscosity in

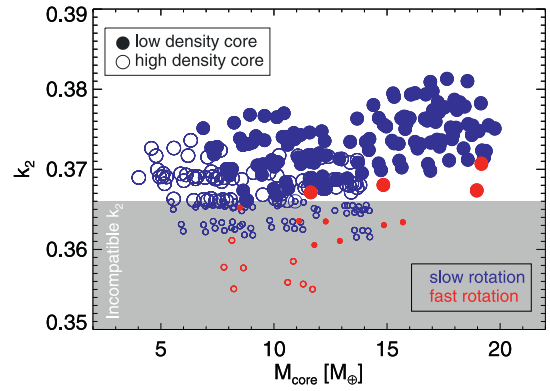


Fig. 2. Mass of the core and k_2 Love number for interior models of Saturn from Helled & Guillot (2013). Filled circles indicate models assuming a low density core (modeled using the equation of state of pure ice) while empty circles indicate models assuming a high density core (modeled using the EOS of rocks). Models in blue assume a “slow” deep rotation of 10h39m while models in red assume a “fast” deep rotation of 10h32m, more in line with the recent determination of Helled et al. (2015). The grey area indicates where values of k_2 are incompatible with our astrometric determination. (For interpretation of the references to color in this figure legend, the reader is referred to the web version of this article).

the core as well as on its size. The minimal values Q_{min} shown in Fig. 3a were obtained by systematically exploring the core viscosity for values comprised between 10^{12} and 10^{17} Pa.s. This shows that for $\mu/K \sim 0.1$ – 0.5 , $Q < 3000$ can be obtained for core size comprised between 8000 and 17,000 km, with values as low as 200–300 for the largest core size (corresponding to ice-rich core). Fig. 3b shows the range of viscosity values for which Q remains below 3000. For models with ice core, $Q < 3000$ for viscosity values ranging between about 2.10^{13} and 2.10^{16} Pa.s. For small core radii ($< 11,000$ km) corresponding to a rock core, Q values lower than 3000 can also be found, but for a more restricted range of viscosity values, between typically 10^{15} and 10^{16} Pa.s. For a very low μ/K ratio (0.01), $Q < 3000$ can be obtained for large ice-rich cores and viscosity values of the order of 5.10^{13} – 5.10^{14} Pa.s. These possible ranges of viscosity are compatible with those derived previously in Remus et al. (2012, 2015) where simplified two-layer planetary models were used.

As illustrated in Fig. 4, the computed k_2/Q values vary only very weakly with tidal frequency, when compared to the frequency dependence expected for dissipation due to dissipation of tidal waves in the fluid envelope (e.g. Ogilvie & Lin, 2004). We obtained a weak frequency dependence with logarithmic rate of change with frequency ranging between -1 and $+1$, depending on the shear modulus and viscosity of the core. The slope, negative or positive, is determined by the Maxwell time, which is defined as the ratio between the viscosity and the shear modulus: $\tau = \eta/\mu$, relative to the forcing period. As in our models, the shear modulus vary as a function of radius in the core, the local Maxwell time vary as a function of radius. As an example, for $\mu/K=0.1$ and a viscosity value of 10^{15} – 10^{16} Pa.s, the Maxwell time typically varies between 0.9–9 hours at the center of the core to 0.2–2 hours at the core surface, while the tidal period varies between 6 and 8 h. As a consequence, for $\eta=10^{15}$ Pa.s, the slope is negative, while it is positive for $\eta=10^{16}$ Pa.s. In both cases, the weak frequency dependence is compatible with the tendencies inferred from astrometric observations for Enceladus, Tethys and Dione frequencies. Remarkably, for this viscosity range, we can reproduce the typical value of the observed k_2/Q .

Even though Q values as low as 200 can be obtained for large cores and appropriate viscoelastic parameters, it is not possible to explain with viscoelastic dissipation, Q values of the order of a few thousands at Enceladus' tidal frequency and of a few hundred at Rhea's tidal frequency. Additional dissipation processes in the deep gaseous envelope are thus required to explain the high dissipa-

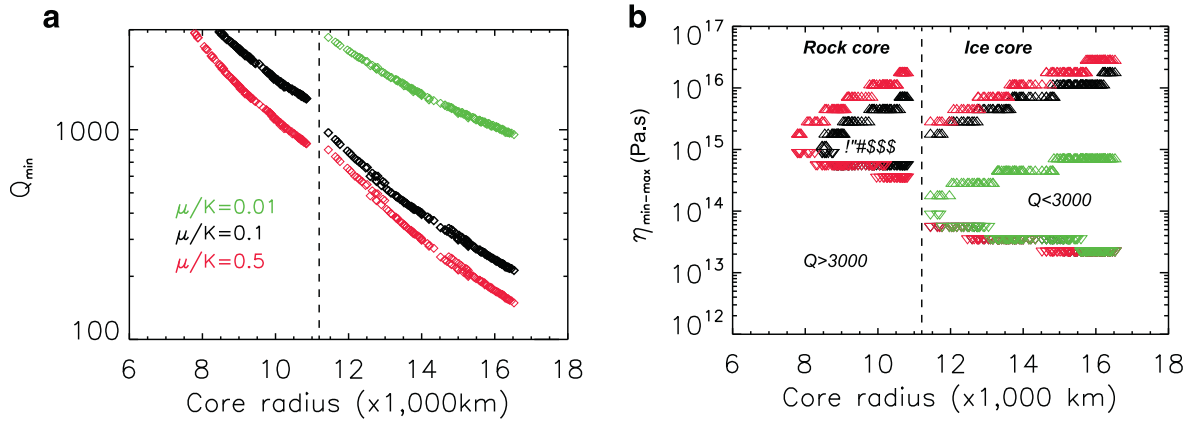


Fig. 3. (a) Minimum value of the quality factor, Q_{\min} , as a function of core radius for three different values of μ/K (0.01, 0.1, 0.5); (b) Range of viscosity values, $\eta_{\max}(\Delta)$ – $\eta_{\min}(\nabla)$, for which $Q < 3000$ for the three μ/K ratios displayed in (a). The dashed line indicates the transition between high density (rock-dominated) core and low density (ice-dominated) core. For this computation, the tidal frequency was fixed at $2.6 \times 10^{-4} \text{ rad.s}^{-1}$.

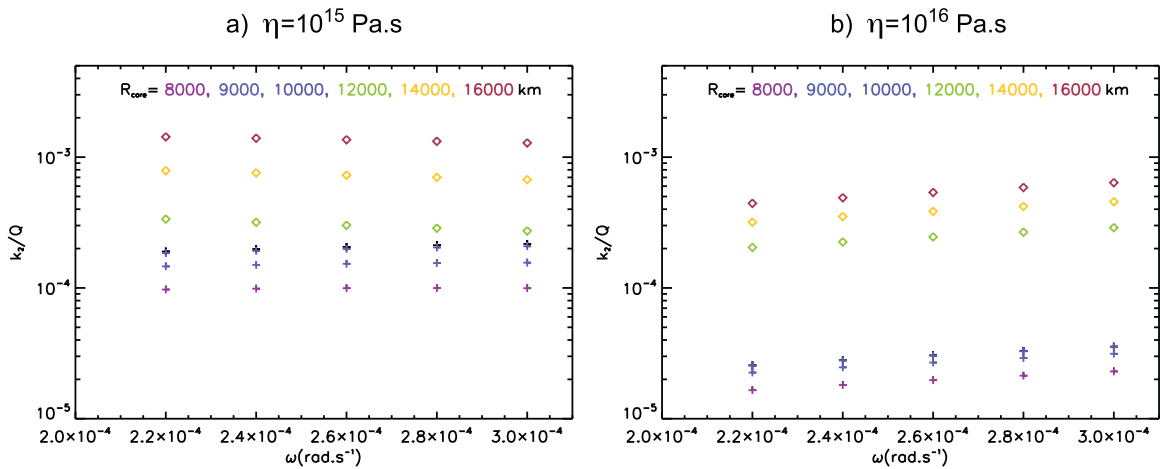


Fig. 4. k_2/Q values as a function of tidal frequency, ω , for two core viscosity values (10^{15} (a) and 10^{16} (b) Pa.s) for six different values of core radius. The μ/K ratio was fixed to 0.1 for these calculations.

tion inferred from observation at Rhea's tidal frequency. The best candidate is turbulent friction applied to tidal inertial waves (their restoring force is the Coriolis acceleration) in the deep, rapidly rotating, oblate convective envelope of Saturn that dissipates their kinetic energy (Ogilvie & Lin, 2004; Braviner & Ogilvie, 2015). This fluid dissipation is resonant and its amplitude can therefore vary by several orders of magnitude as a function of the tidal frequency (Ogilvie & Lin, 2004; Auclair-Desrotour, Mathis & Le Poncin-Lafitte, 2015), particularly in the case of weak effective turbulent viscosity expected in the case of rapidly rotating planets (Mathis, 2016). Hence, it can explain the increase by one order of magnitude of the dissipation over the small frequency range arising between Dione and Rhea. Fuller et al. (2016) also proposed an alternative scenario by studying gravito-inertial waves (their restoring forces are the Coriolis acceleration and the Archimedean buoyancy force) that propagate and are trapped in resonance in a potential stably-stratified layer surrounding the core (Fuller et al. 2014).

5. Discussion

In 1977, Gavrilov and Zharkov (1977) computed the value of Saturn's Love numbers and obtained for the lowest degree quadrupolar coefficient $k_2=0.341$. Even though this value is often used as the reference, it stands on physical assumptions and internal structure models that have since been improved (Guillot 1999, 2005; Hubbard et al., 2009; Kramm et al., 2011; Nettelmann et al., 2013; Helled & Guillot, 2013). Although all the models we consid-

ered following the approach of Helled and Guillot (2013) reproduced the gravitational coefficients J_2 , J_4 and J_6 with error bars, they lead to significant variations in k_2 . J_2 and k_2 are both sensitive to the density profile, but in a different manner. For slowly rotating bodies, J_2 and fluid Love number k_2^f (which is very close to the tidal Love number in the case of Saturn) can be related through the classical relationship $J_2=qk_2^f/3$ with q the rotational parameter: $q=\omega^2 a^3/GM$, with ω the rotation frequency, a the equatorial radius, M the mass of the planet and G the gravitational constant. For Saturn, the rotational ratio q ranges between 0.1544 and 0.1584 for rotation periods between 10h32' and 10h39'. Such a high q ratio, the fluid Love number predicted from the simple J_2 relationship is about 0.31, which is about 13–18% less than the fluid Love number computed from the density profile. This is due to the strong flattening of the planet and the gravitational signatures of the flattened internal interfaces. As already anticipated from the pioneer work of Gavrilov and Zharkov (1977) and further explored by Kramm et al. (2011), the Love number k_2 is very sensitive to the degree of mass concentration toward the center of the planet, but differently from J_2 . It evaluates the amplitude of the hydrostatic adjustment of the planet's structure to the tidal perturbations while J_2 gives the strength of the hydrostatic response to the centrifugal acceleration. Determinations of the tidal Love numbers (k_2 , k_3) and of the gravitational coefficients thus provide complementary information to constrain the density structure of Saturn. From the variety of internal models we explored in the present study, we notice that a large fraction of models compatible with

the J_n coefficients are compatible with the inferred k_2 because the uncertainties are still large. However, any further improvement in the estimation of k_2 and the spin rate will allow to restrict the number of acceptable models and provide crucial constraints on Saturn's interior.

Our estimation of Saturn's Q confirms the values previously derived by Lainey et al. (2012), which is one order of magnitude smaller than the value derived from the usually expected long term evolution of the Moons over the age of the Solar System (Sinclair, 1983). We recall that earlier studies constrained Saturn's Q using the current positions of the innermost main Moons. Considering the Moons' motions back in time, the averaged exchange of angular momentum between the planet and the Moons associated with tidal dissipation must have been limited in order to prevent the Moons from crossing their Roche limit 4.5 Byr ago (Goldreich & Soter 1966). Such a Q value was then re-evaluated by Gavrilov & Zharkov (1977) using a more realistic k_2 for Saturn and by Sinclair (1983) considering in detail the Mimas-Tethys 2:1 mean motion resonance. The low Q or high dissipation rate obtained in this work, implying rapid orbital expansion, suggests that either the dissipation has significantly changed over time, or that the Moons formed later after the formation of the Solar System (Charnoz et al. 2011; Ćuk 2014). Since tidal dissipation may arise both in the planet's fluid envelope and its presumably solid core (Guenel et al., 2014), we can look in more detail at the frequency dependency of the tidal ratio k_2/Q shown in Fig. 1. Despite large error bars, the tidal ratios associated with Enceladus, Tethys and Dione do not depart from their former constant estimates. On the other hand, we obtain a strong increase of dissipation at Rhea's frequency. Such a dissipation corresponds to an orbital shift in the longitude of about 75 km (see Appendix A.3). The fact that the strong orbital shift at Rhea is observed using both the IMCCE and JPL models, makes systematic errors unlikely. As Rhea has no orbital resonance with any other Moon, and no significant dynamical interaction with the rings, its strong orbital shift is more likely the consequence of strong tides.

The rather constant dissipation inferred at tidal frequencies associated with Enceladus, Tethys and Dione suggests dissipation processes dominated by anelastic tidal friction in a solid core (Remus et al., 2012, 2015). This is confirmed by the calculations performed here using more realistic density profiles. We further show that a Q factor lower than 3000 required a core viscosity lower than 10^{16} Pa.s. For large low-density ice-rich cores, Q values as low as 200–300, compatible with the k_2/Q estimate obtained at Rhea's frequency, can be obtained. However, due to the weak frequency dependence of dissipation in a viscoelastic core, a Q value of 1500–2500 at Enceladus, Tethys and Dione's frequency cannot be match simultaneously with a value as low as 300 at Rhea's. This suggests either that additional dissipation processes exist in Saturn at Rhea's frequency to reduce the apparent Q value, or that a value as low as 300 is representative of Saturn's dissipation that the orbital consequences of such a strong dissipation in Saturn is partially compensated by strong dissipation in the Moons. The best candidate for additional processes in Saturn to explain the reduced Q at Rhea's is friction applied to tidal inertial (or gravito-inertial) waves in the deep, rapidly rotating, gaseous envelope of Saturn that dissipates their kinetic energy (Ogilvie & Lin, 2004; Fuller et al., 2016). It can explain the increase by one order of magnitude of the dissipation over the small frequency range arising between Dione and Rhea.

6. Conclusion

Using a large set of astrometric observations including ground-based observations and thousands of Cassini-ISS data, we provide the first observationally-derived estimate of the Love number of

Saturn, k_2 . This determination could be done thanks to the presence of the lagrangian Moons of Tethys and Dione in the dynamical modeling. Moreover, we confirm the strong tidal dissipation found by Lainey et al. (2012), but associated with an intense frequency-dependent peak of tidal dissipation for Rhea's tidal frequency. Modeling the likely interior of Saturn, it appears two different tidal mechanisms may arise simultaneously within the planet. The first one is tidal friction within the dense core, while significant tidal dissipation may also occur inside the outer fluid envelope at Rhea's tidal frequency.

Note added in proof

Wahl et al. (2016) recently presented theoretical calculations for one symmetrically spherical Saturn model yielding a value of $k_2=0.367$, in agreement with the theoretical static values presented in Section 4. However, they show that accounting for dynamical flattening due to rotation increases the total theoretical k_2 value by +0.046. This is still compatible with our constraint $k_2=0.390 \pm 0.024$ but would imply that our analysis in Fig. 2 should be reconsidered.

Acknowledgments

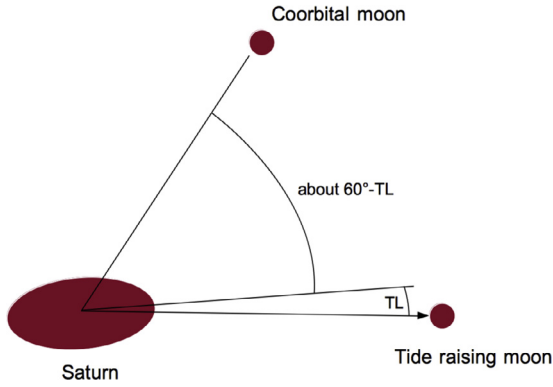
The authors are indebted to all participants of the Encelade WG. V.L. would like to thank Michael Efroimsky for fruitful discussions. This work has been supported by the European Community's Seventh Framework Program (FP7/2007–2013) under grant agreement 263466 for the FP7-ESPaCE project, the International Space Science Institute (ISSI), PNP (INSU/CNES) and AS GRAM (INSU/CNES/INP). The work of R. A. J. was carried out at the Jet Propulsion Laboratory, California Institute of Technology, under a contract with NASA. N.C. and C.M. were supported by the UK Science and Technology Facilities Council (Grant No. ST/M001202/1) and are grateful to them for financial assistance. C.M. is also grateful to the Leverhulme Trust for the award of a Research Fellowship. N.C. thanks the Scientific Council of the Paris Observatory for funding. S. Mathis acknowledges funding by the European Research Council through ERC grant SPIRE 647383. G. Tobie acknowledges funding from the European Research Council under the European Community's Seventh Framework Programme (FP7/2007–2013 Grant Agreement no. 259285, ERC EXOATER). The authors are indebted to the Cassini project and the Imaging Science Subsystem Team for making this collaboration possible.

Appendix

A.1. The tidal effects on coorbital satellites

The effects of tidal bulges on one Moon's motion are generally far below detection, unless those tides are raised by the same Moon. Indeed, such a configuration produces a secular effect on the orbit that may be detectable after a sufficient amount of time. On the other hand, tidal bulges associated with another Moon will introduce essentially quasi-periodic perturbations, with much lower associated signal on the orbits. There exists an exception, however, if one considers the special case of lagrangian Moons. Indeed, in such a case the tidal bulges are oriented on average with a constant angle close to 60° (see figure below).

As a consequence, tidal effects arising on one Moon and acting on a lagrangian Moon will provide a significant secular signature on the orbital longitude that is hopefully detectable. To quantify how large this effect can be, we rely here on numerical simulation. A simple look at the differences on the positions of the coorbital Moons after adding/removing the cross tidal effects over about 10 years (roughly the time span of Cassini data) will be meaningless.



Indeed, one needs to take into account the fitting procedure of the initial conditions to the observations. In particular, the difference in modeling may be partly masked by a slight change of the initial conditions. As a consequence, the true incompressible part of the cross tidal effects in the dynamics will be revealed only after having fitted one simulation onto the other. We provide below prefit and postfit residuals associated with these cross-tidal effects, for 14 Moons of Saturn. The postfit simulations are obtained after having fitted all initial state vectors, masses, Saturn’s J_2 , polar orientation and precession, Saturn’s tidal Q .

We can see that the largest effects indeed appear on the coorbital Moons, with the highest effects on the lagrangian satellites of Tethys and Dione. When not considering these cross-tidal effects, the astrometric residuals of these former Moons can easily reach a few tens of kilometers, much above the typical 5 km residuals we obtained in the present work (see Appendix A.4 and Fig. A.4).

A.2. Validation of Love number computation

A.3. Rhea’s orbital acceleration under strong Saturnian tides

To estimate the impact of the large k_2/Q value obtained at Rhea’s tidal frequency, we perform prefit and postfit simulations (fitting the state vectors of all Moons) over a century. Assuming $k_2/Q=122.28 \times 10^{-5}$ (see IMCCE solution in Table 1), the postfit residuals below show that Rhea’s longitude is affected by a signal of a bit more than 75 km. This corresponds to about 12.5 mas (0.0125 arc second) at opposition, which represents roughly 10% of the global astrometric residuals from the ground (Lainey et al. 2012), and a huge signal when comparing with Cassini data.

Table A.4.1

(One single Moon per image): Statistics of the ISS-NAC astrometric residuals computed from IMCCE model (no tidal dissipation within Enceladus scenario) in pixel. μ and σ denote respectively the mean and standard deviation of the residuals computed on sample and line. N_s and N_l are the number of observations considered for the respective coordinate.

Satellite	μ_s	σ_s	μ_l	σ_l	N_s	N_l
Epimetheus	-0.0094	4.3180	0.1805	4.5340	350	350
Janus	0.0096	0.9780	0.5378	1.1566	322	322
Mimas	0.4190	0.2813	-0.0460	0.6600	20	20
Enceladus	-0.0014	0.3547	-0.1116	0.2783	108	108
Tethys	-0.1232	0.5284	0.0814	0.2600	25	25
Dione	-0.0278	0.4808	0.0748	0.4730	84	84
Rhea	-0.2925	0.4644	-0.0035	0.2055	58	58
Titan	0.0000	0.0000	0.0000	0.0000	0	0
Hyperion	0.0000	0.0000	0.0000	0.0000	0	0
Iapetus	0.0000	0.0000	0.0000	0.0000	0	0
Calypso	-0.0348	0.2508	-0.1742	0.2546	230	230
Teleso	-0.0190	0.2220	-0.0366	0.2960	279	279
Helene	-0.0164	0.2731	-0.0456	0.2492	262	262
Polydeuces	-0.0554	0.2508	-0.0584	0.2422	139	139

Table A.4.2

(Multiple Moon per image): Statistics of the ISS-NAC astrometric residuals computed from IMCCE model (no tidal dissipation within Enceladus scenario) in pixel. μ and σ denote respectively the mean and standard deviation of the residuals computed on sample and line. N_s and N_l are the number of observations considered for the respective coordinate.

Satellite	μ_s	σ_s	μ_l	σ_l	N_s	N_l
Epimetheus	0.0203	0.2778	0.0449	0.2912	28	28
Janus	-0.0203	0.2778	-0.0449	0.2912	28	28
Mimas	0.0255	0.1784	-0.0064	0.2745	134	134
Enceladus	-0.0307	0.1784	0.0084	0.1248	327	327
Tethys	0.0211	0.1088	0.0186	0.1359	424	424
Dione	-0.0204	0.1061	0.0054	0.1070	592	592
Rhea	0.0175	0.1370	-0.0234	0.1208	556	556
Titan	0.0000	0.0000	0.0000	0.0000	0	0
Hyperion	0.0000	0.0000	0.0000	0.0000	0	0
Iapetus	0.0000	0.0000	0.0000	0.0000	0	0
Calypso	0.1470	0.0000	-0.5137	0.0000	1	1
Teleso	-0.0997	0.0702	0.2454	0.1691	3	3
Helene	-0.1308	0.0508	0.2090	0.0096	2	2
Polydeuces	0.1379	0.0731	-0.2135	0.1657	3	3

A.4. Astrometric residuals and linear correlations

To illustrate the various simulations that we performed, we provide astrometric residuals of the IMCCE solution that considered a

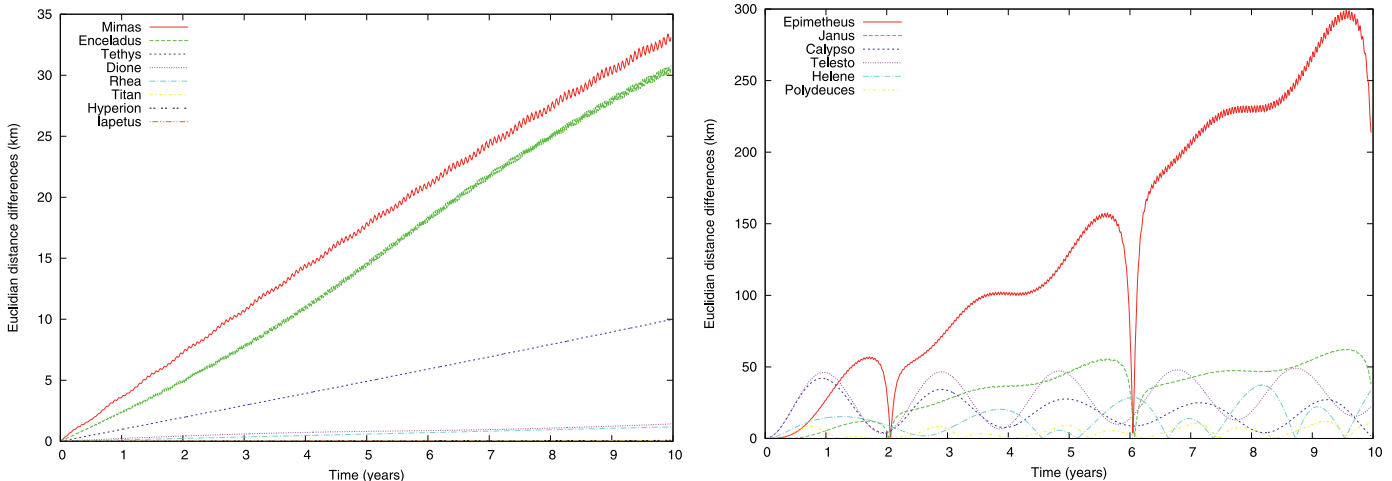


Fig. A.1.1. Prefit residuals associated with cross-tidal effects.

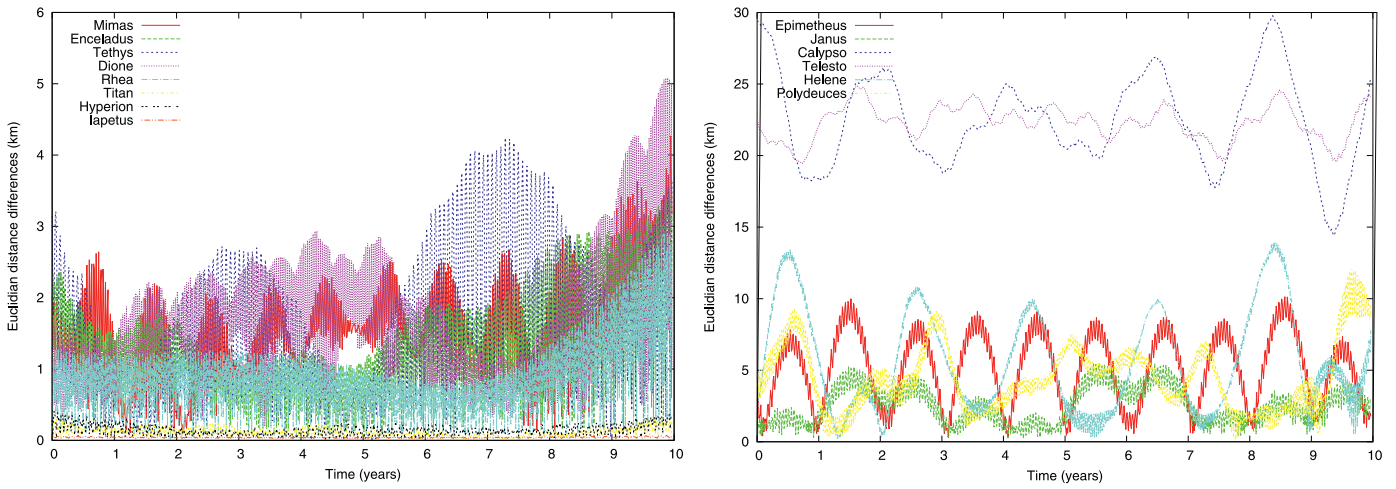


Fig. A.1.2. Postfit residuals associated with cross-tidal effects.

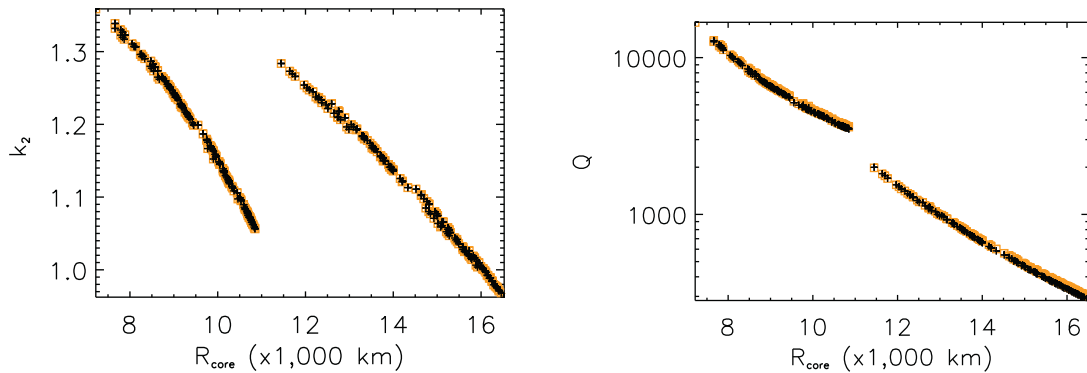


Fig. A.2. Comparison between numerical (black crosses) and analytical (orange squares) solutions of tidal Love number, k_2 (left) and dissipation factor, Q (right) as a function of core radius, R_{core} , computed for a solid viscoelastic core and a fluid envelope with constant density, assuming a core viscosity of 10^{15} Pa.s and a shear modulus of 1000 GPa.

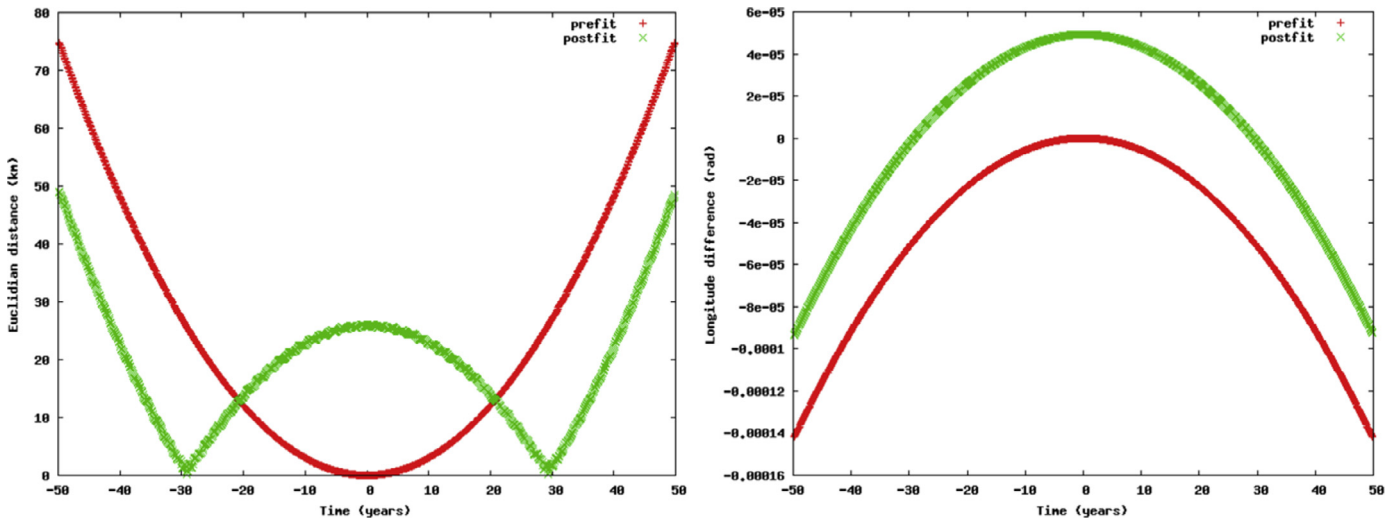


Fig. A.3.1. Left: residuals in distance (km); right: residuals in the orbital longitude (rad).

constant k_2/Q ratio and no tidal dissipation scenario within Enceladus. To save space, we do not provide here statistics of ground-based and HST data, since they are pretty similar to the ones published in Lainey et al. (2012). We provide below the plots of the O-Cs, only. Full statistics are available on request.

Fig. A.4 shows the astrometric residuals of the lagrangian satellites of Tethys and Dione. Tables A.4.1–A.4.3 provide the astrometric residuals of all observations for the 14 Moons considered. Table A.4.4 provides the correlations between all our fitted parameters and the tidal parameters k_2 and Q .

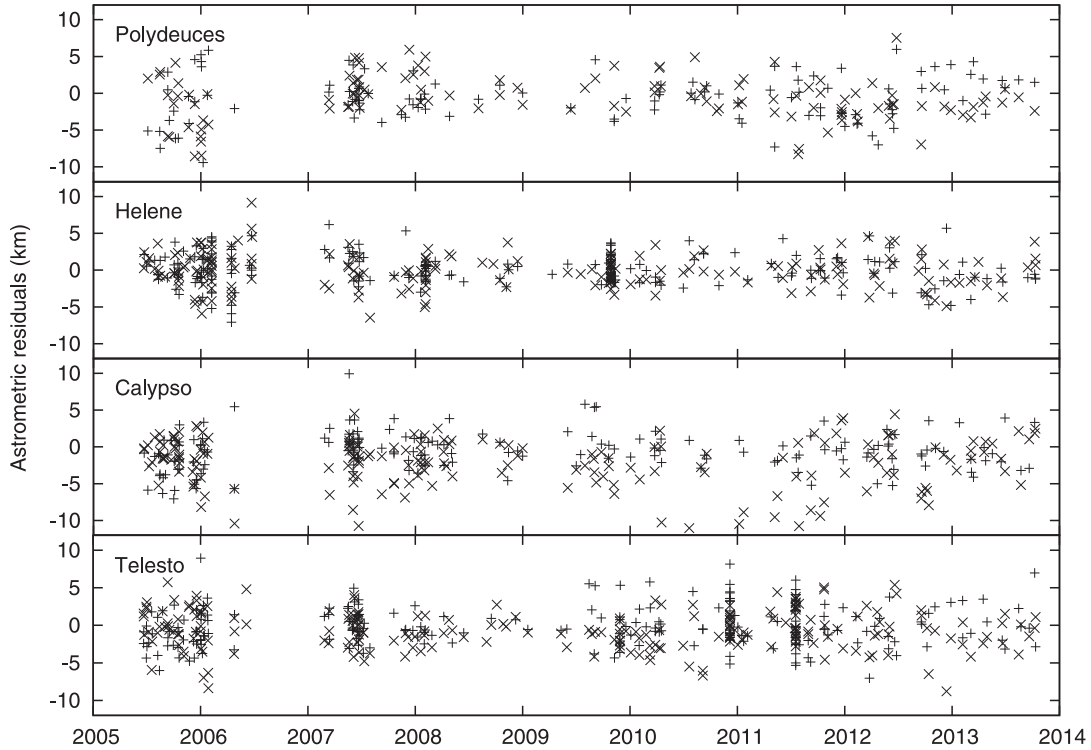


Fig. A.4.1. Astrometric residuals of the four lagrangian satellites from ISS-Cassini. Telesto and Calypso are the two coorbital Moons of Tethys. They move around the lagrangian stable points L4 and L5. Helene and Polydeuces are in equivalent orbital configurations but along the orbit of Dione. The associated ISS-NAC astrometric data are fitted in sample and line coordinates (pixel). Residuals are here converted to kilometres.

Table A.4.3

(One Moon per image): Statistics of the ISS-NAC astrometric residuals computed from IMCCE model (no tidal dissipation within Enceladus scenario) in km. μ and σ denote respectively the mean and standard deviation of the residuals computed on RA and DEC. N_{RA} and N_{DEC} are the number of observations considered for the respective coordinate.

Satellite	μ_{RA}	σ_{RA}	μ_{DEC}	σ_{DEC}	N_{RA}	N_{DEC}
Mimas	-1.1001	3.9151	-1.1401	2.8370	826	826
Enceladus	-0.1979	2.8234	0.2713	2.6588	732	732
Tethys	0.0532	4.5654	-0.0123	3.5007	924	924
Dione	-0.2068	4.1726	-0.5264	3.4948	948	949
Rhea	-0.3170	3.3581	-0.1138	2.4739	1021	1021
Titan	0.0000	0.0000	0.0000	0.0000	0	0
Hyperion	-0.1292	15.4526	-5.9373	12.7287	92	90
Iapetus	1.4754	5.1951	-1.1544	5.4322	1534	1534

Table A.4.4

Correlation between all our fitted parameters and the tidal parameters k_2 and Q . Here a is the semi-major axis, l is the mean longitude, e is the eccentricity, Ω is the longitude of the node, ω is the argument of the periaapsis, $k=e \cos(\Omega+\omega)$, $h=e \sin(\Omega+\omega)$, $q=\sin(i/2) \cos(\Omega)$ and $p=\sin(i/2) \sin(\Omega)$. Numbers 1,2,3,...,14 refer to Epimetheus, Janus, the eight main Moons (Mimas,...Iapetus), Calypso, Telesto, Helene, Polydeuces, respectively. Full table is available on request.

	k_2	Q
a_1	0.006	0.023
l_1	0.002	-0.014
k_1	-0.000	-0.001
h_1	0.002	0.002
q_1	-0.000	-0.002
p_1	0.000	0.003
a_2	0.008	0.025
l_2	-0.004	-0.029
k_2	-0.001	0.002
h_2	-0.002	0.001
q_2	0.000	-0.001
p_2	-0.000	0.002
a_3	0.009	0.025

Table A.4.4 (continued)

	k_2	Q
l_3	-0.013	0.232
k_3	-0.013	0.017
h_3	-0.003	0.002
q_3	0.017	-0.024
p_3	0.002	0.070
a_4	0.009	0.027
l_4	-0.012	0.182
k_4	0.017	0.084
h_4	-0.026	-0.026
q_4	0.004	-0.000
p_4	-0.006	0.127
a_5	0.009	0.024
l_5	0.009	-0.223
k_5	0.000	0.020
h_5	-0.003	-0.074
q_5	-0.027	0.012
p_5	0.011	0.069
a_6	0.009	0.026
l_6	0.002	-0.509
k_6	0.011	-0.005
h_6	-0.010	0.082
q_6	0.005	-0.012
p_6	-0.007	0.154
a_7	0.009	0.023
l_7	-0.003	-0.216
k_7	-0.006	-0.029
h_7	-0.003	-0.008
q_7	-0.006	0.203
p_7	-0.007	0.036
a_8	0.010	0.019
l_8	-0.002	-0.005
k_8	-0.002	-0.003
h_8	0.003	0.025
q_8	0.006	0.059
p_8	0.002	-0.013
a_9	0.007	0.016
l_9	-0.001	-0.005

Table A.4.4 (continued)

	k_2	Q
k_9	−0.001	0.001
h_9	0.002	0.014
q_9	−0.003	−0.000
p_9	0.000	−0.018
a_{10}	0.008	0.008
l_{10}	−0.004	−0.007
k_{10}	−0.008	−0.005
h_{10}	−0.007	−0.007
q_{10}	0.000	0.005
p_{10}	−0.002	−0.022
a_{11}	0.010	0.025
l_{11}	−0.024	−0.114
k_{11}	0.034	0.003
h_{11}	−0.012	−0.002
q_{11}	−0.028	0.029
p_{11}	0.018	0.051
a_{12}	0.008	0.025
l_{12}	0.142	−0.216
k_{12}	−0.002	−0.011
h_{12}	−0.012	−0.006
q_{12}	0.025	−0.018
p_{12}	0.011	0.026
a_{13}	0.005	0.025
l_{13}	−0.028	−0.254
k_{13}	0.010	0.033
h_{13}	−0.002	0.026
q_{13}	−0.000	−0.031
p_{13}	0.001	0.062
a_{14}	0.010	0.029
l_{14}	−0.073	−0.254
k_{14}	0.020	−0.055
h_{14}	0.007	−0.052
q_{14}	0.004	−0.021
p_{14}	−0.005	0.054
M	0.009	0.026
m_1	−0.004	0.003
m_2	−0.004	0.003
m_3	−0.001	−0.378
m_4	0.038	−0.064
m_5	0.118	−0.019
m_6	0.120	0.029
m_7	0.011	−0.062
m_8	0.000	0.004
m_9	0.000	−0.003
m_{10}	−0.005	−0.011
a_0	0.003	−0.591
d_0	−0.010	0.138
c_{20}	−0.005	0.014
da/dt	0.017	0.186
dd/dt	0.012	−0.129
k_2	1.000	−0.030
Q	−0.030	1.000

References

Alterman, Z., Jarosch, H., Pekeris, C.L. 1959, Proceedings of the Royal Society of London Series A, 252, 80.

Auclair-Desrotour, P., Mathis, S., Le Poncin-Lafitte, C., 2015. Scaling laws to understand tidal dissipation in fluid planetary regions and stars I. Rotation, stratification and thermal diffusivity. *A&A* 581, A118.

Braviner, H.J., Ogilvie, G.I., 2015. Tidal interactions of a Maclaurin spheroid. II: Resonant excitation of modes by a close, misaligned orbit. *Mon. Not. R. Astron. Soc.* 447, 1145–1157.

Charnoz, S., et al., 2011. Accretion of Saturn's mid-sized Moons during the viscous spreading of young massive rings: Solving the paradox of silicate-poor rings versus silicate-rich Moons. *Icarus* 216, 535.

Cooper, N.J., et al., 2014. Cassini ISS mutual event astrometry of the mid-sized Saturnian satellites 2005–2012. *Astron. Astrophys.* 572, 8.

Čuk, M. Recent Origin of Titan's Orbital Eccentricity. American Astronomical Society, DDA meeting #45, #301.01 (2014).

Dermott, S.F., 1979. Tidal dissipation in the solid core of major planets. *Icarus* 37, 310.

Desmars, J., Vienne, A., Arlot, J.E., 2009. A new catalogue of observations of the eight major satellites of Saturn (1874–2007). *Astron. Astrophys.* 493, 1183.

Dziewonski, A.M., Anderson, D.L. 1981, Physics of the Earth and Planetary Interiors, 25, 297.

Fuller, J., Luan, J., Quataert, E., 2016. Resonance locking as the source of rapid tidal migration in the Jupiter and Saturn systems. *MNRAS* 458, 3867.

Fuller, J., 2014. Saturn ring seismology: Evidence for stable stratification in the deep interior of Saturn. *Icarus* 242, 283–296.

Gavrilov, S.V., Zharkov, V.N., 1977. Love numbers of the giant planets. *Icarus* 32, 443–449.

Goldreich, P., Soter, S., 1966. Q in the Solar System. *Icarus* 5, 375–389.

Guenel, M., Mathis, S., Remus, F., 2014. Unravelling tidal dissipation in gaseous giant planets. *Astron. Astrophys.* 566, L9.

Guillot, T., 1999. Interior of giant planets inside and outside the Solar System. *Science* 286, 72–77.

Guillot, T., 2005. The interiors of giant planets: Models and outstanding questions. *Annual Rev. Earth Planet. Sci.* 33, 493–530.

Helled, R., Galanti, E., 2015. Kaspi, Yohai Saturn's fast spin determined from its gravitational field and oblateness. *Nature* 520, 202.

Helled, R., Guillot, T., 2013. Interior models of Saturn: including the uncertainties in shape and rotation. *Astrophys. J.* 767, 113.

Hubbard, W.B., Dougherty, M.K., Gautier, D., et al. The Interior of Saturn. In: Dougherty, M. K., Esposito, L. W., Krimigis, S. M., Saturn from Cassini-Huygens. ISBN 978-1-4020-9216-9. Springer Science+Business Media B.V., 2009, p. 75 (2009).

Jacobson, R.A., Antreasian, P.G., Bordi, J.J., et al., 2006. The gravity field of the saturnian system from satellite observations and spacecraft tracking data. *The Astron. J.* 132, 2520–2526.

Jacobson, R.A., et al., 2006. The gravity field of the Saturnian system from satellite observations and spacecraft tracking data. *Astron. J.* 132, 2520.

Kaula, W.M., 1964. Tidal dissipation by solid friction and the resulting orbital evolution. *Rev. Geophys. Space Phys.* 2, 661.

Karato, S.-i. 2008, Physics of the Earth and Planetary Interiors, 170, 152.

Kramm, U., Nettelmann, N., Redmer, R., et al., 2011. On the degeneracy of the tidal Love number k_2 in multi-layer planetary models: application to Saturn and GJ 436b. *Astron. Astrophys.* 528, A18.

Lainey, V., Dehant, V., Pätzold, M., 2007. First numerical ephemerides of the martian Moons. *Astron. Astrophys.* 465, 1075–1084.

Lainey, V., Arlot, J.E., Karatekin, Ö., et al., 2009. Strong tidal dissipation in Io and Jupiter from astrometric observations. *Nature* 459, 957–959.

Lainey, V., et al., 2012. Strong tidal dissipation in Saturn and Constraints on Enceladus' thermal state from astrometry. *Astrophys. J.* 752, 14.

Lainey, V., 2008. A new dynamical model for the uranian satellites. *Planet. Space Sci.* 56, 1766–1772.

Mathis, S., Auclair-Desrotour, P., Guenel, M., et al., 2016. The impact of rotation on turbulent tidal friction in stellar and planetary convective regions. *A&A* 592, A33.

Meyer, J., Wisdom, J., 2007. Tidal heating in Enceladus. *Icarus* 188, 535–539.

Morales, M.A., et al., 2009. Phase separation in hydrogen-helium mixtures at Mbar pressures. *Proc. Nat. Acad. Sci.* 106, 1324–1329.

Moyer, T.D., 2000. Formulation for observed and computed values of Deep Space Network data types for navigation. In: Deep Space Communications and Navigation Series: Monograph 2. Jet Propulsion Laboratory, Pasadena, CA.

Nettelmann, N., Püstow, R., Redmer, R., 2013. Saturn layered structure and homogeneous evolution models with different EOSs. *Icarus* 225, 548.

Newhall, X.X., Standish, E.M., Williams, J.G., 1983. DE 102 - A numerically integrated ephemeris of the Moon and planets spanning forty-four centuries. *Astron. Astrophys.* 125, 150–167.

Ogilvie, G.I., Lin, D.N.C., 2004. Tidal dissipation in rotating giant planets. *Astrophys. J.* 610, 477–509.

Peters, C.F., 1981. Numerical integration of the satellites of the outer planets. *Astron. Astrophys.* 104, 37.

Remus, F., Mathis, S., Zahn, J.-P., et al., 2012. Anelastic tidal dissipation in multi-layer planets. *Astron. Astrophys.* 541, 165.

Remus, F., Mathis, S., Zahn, J.-P., et al., 2015. The surface signature of the tidal dissipation of the core in a two-layer planet. *Astron. Astrophys.* 573, 23.

Robert, V., et al., 2011. A new astrometric reduction of photographic plates using the DAMIAN digitizer: Improving the dynamics of the jovian system. *Mon. Not. R. Astron. Soc.* 415, 701.

Robert, V. et al., A new astrometric measurement and reduction of USNO photographic observations of the main Saturnian satellites 1974–1998. *A&A* (2016) to be submitted.

Saito, M., 1974. Some problems of static deformation of the Earth. *J. Phys. Earth* 22, 123.

Sinclair, A.T., 1983. A re-consideration of the evolution hypothesis of the origin of the resonances among Saturn's satellites. In: Dynamical trapping and evolution in the Solar System; Proceedings of the Seventy-fourth Colloquium, Gerakini, Greece, August 30–September 2, 1982 (A84-34976 16–89). D. Reidel Publishing Co., Dordrecht, pp. 19–25.

Tajeddine, R., Cooper, N.J., Lainey, V., et al., 2013. Astrometric reduction of Cassini ISS images of the Saturnian satellites Mimas and Enceladus. *Astron. Astrophys.* 551, 129.

Tajeddine, R., Lainey, V., Cooper, N.J., et al., 2015. Cassini ISS astrometry of the Saturnian satellites: Tethys, Dione, Rhea, Iapetus, and Phoebe 2004–2012. *Astron. Astrophys.* 575, A73.

Takeuchi, H., Saito, M., 1972. Seismic surface waves. *Meth. Comput. Phys.* 11, 217–295.

Tobie, G., Mocquet, A., Sotin, C., 2005. Tidal dissipation within large icy satellites: Applications to Europa and Titan. *Icarus* 177, 534.

A new dynamical model for the Uranian satellites

V. Lainey

IMCCE, UMR 8028 du CNRS, 77 Avenue Denfert-Rochereau, 75014 Paris, France

Accepted 5 February 2008
Available online 20 July 2008

Abstract

We have developed a new dynamical model of the main Uranian satellites, based on numerical integration and fitted to astrometric observations. Old observations, as well as modern and Voyager observations have been included. This model has provided ephemerides that have already been used for predicting the mutual events during the PHE-URA campaign. It is updated here to improve the prediction of these events. We also tried to assess the real accuracy of our ephemerides by checking the distance differences of the Uranian satellites, using simultaneously our former and new model. It appears that both solutions are very close to each other (within few tens of kilometers), and most probably accurate at the level of few hundred of kilometers. Using new available meridian observations of the Uranian satellites, we have checked the Uranian ephemeris accuracy using DE406. An error of more than 0.1 arcsec on the Uranian position is observed.

© 2008 Elsevier Ltd. All rights reserved.

Keywords: Uranian satellite; Orbital dynamics; Ephemerides

1. Introduction

The Uranian mutual events (occurring mainly between May 2007 and February 2008) are an opportunity to observe Uranus and its satellites with a high accuracy. Observations of these events will provide photometric lightcurve drops, and after proper reduction some highly accurate astrometric positions of these satellites. The feasibility to observe these events is dependent on our capacity to predict them. In particular, accurate ephemerides of the Uranian satellites are required.

In the middle of the 1980s, analytical ephemerides of the Uranian satellites were developed for the need of the Voyager 2 mission (Laskar, 1986; Laskar and Jacobson, 1987). These ephemerides, called GUST86, were completely analytical and fitted to an important set of observations covering the years 1911–1986. The computational precision over 12 years of the model was estimated, by comparison with numerical integration, to be between few tens of kilometers (Miranda, Ariel and Umbriel), to one hundred kilometers (Titania and Oberon). More difficult is estimating the real accuracy of a theory. In particular, the

time elapsed since the development of GUST86 leads one to expect a decrease of the accuracy. Hence, these ephemerides may have more important residuals when compared to nowadays observations. Stone (2001) found discrepancies between GUST86 and FASTT astrometric observations suggesting the necessity to perform a new fit. In the other hand, further analytical developments should be done to increase GUST theory, like increasing the number of analytical terms in the series and adding the Solar perturbation (Laskar and Jacobson, 1987).

More recently, Taylor (1998) has developed ephemerides of the Uranian satellites by means of numerical integration. He used a smaller set of observations spanning from 1977 to 1995. Despite the probably higher accuracy of this model for the present day computations, mutual events of the Uranian satellites have essentially been predicted by GUST86 theory (Christou, 2005; Arlot et al., 2006).

Arlot et al. (2006) predicted the Uranian mutual events using two different ephemerides. As mentioned above, the first ones were the GUST86 ephemerides, while the second ones, called LA06, have been developed by a new numerical model, and fitted to observations from 1948 to 2003. Differences of few tens of seconds on the prediction of the midtime events were commonly found, and most of

E-mail address: lainey@imcce.fr

the events were predicted within 5 min (one minute of time corresponding roughly to a position shift of 180 and 400 km for respectively Oberon and Miranda, which are the slowest and the fastest among the main Uranian satellites). Very few were the number of events that have been predicted by one model only. However, the flux drop differences reached frequently up to 50%. It is a critical parameter when one wants to observe mutual events of such faint objects. The second model, however, is expected to be a better predictor of the satellite positions, as it is based on numerical integration and considers more recent observations. Nevertheless, it is difficult to deduce the real accuracy of a model, and so of the mutual event predictions. It is clear that the use of new observations can help to solve this problem. By computing the residuals for a new set of observations, one can estimate the accuracy of the ephemerides. Another way is to perform a new fit, and then, check the differences on the satellite positions delivered from the model before/after the new fit. Both approaches are explored in this paper.

Observations of Titania and Oberon, done between 2001 and 2006 at Flagstaff with the FASTT instrument, have recently been released on the internet via the United States Naval Observatory (USNO) FTP server¹ (thanks to the effort of A.Monet), as well as observations done at Bordeaux observatory between 1997 and 2003 (courtesy of G. Dourneau). We have tried to quantify the accuracy of LA06 ephemerides by using these new sets of observations. New ephemerides, called LA07, that take into account some of these observations and the former sets introduced in LA06 have been developed. By looking at the differences between LA06 and LA07, as well as the residuals with the Bordeaux observations we tried to estimate the real accuracy of the Uranian satellite ephemerides. In the same time, we had an opportunity to check the accuracy of the Uranian ephemeris by looking for systematic errors on the Uranian satellite residuals.

Section 2 presents the astrometric observations used in this paper. In Section 3, we summarize the equations and perturbations introduced in the numerical model that were only briefly mentioned in Arlot et al. (2006). Section 4 presents the fitting method and the residuals of LA07 ephemerides. Section 5 discusses the real accuracy of these ephemerides.

2. The observations used

The observations used in this work are almost the same as those mentioned in Arlot et al. (2006). Just two sets of observations are new. The first one consists of the recently available observations of the FASTT meridian telescope done between 2001 and 2006. These observations done each year can be found on the FTP server of the USNO, doubling the number of observations previously available with this instrument. The second set of observations is a

courtesy of G. Dourneau. All these observations were done at the meridian telescope of Bordeaux (Flourac).

During our fitting procedure we have used the inter-satellite method to get rid of the inaccuracy of the Uranian position. Meridian observations usually do not allow for having the astrometric positions of a complete satellite system at exactly the same time. However, FASTT observations are reduced with a specific treatment that provides astrometric observations of Titania and Oberon at the same time (Stone et al., 1996). The only exception is the year 2006 for which no observations of Titania are available. Hence, we have benefited from all the FASTT observations during the fit process, except for the year 2006. For the same reason, we have not used Bordeaux observations in the fit. However, we could still use these observations as two independent observational sets to test the accuracy of the Uranian ephemeris and the present Uranian satellite ones.

3. The numerical model

The software used for numerical integration is called Numerical Orbit and Ephemerides (NOE). It was developed for computing the ephemerides of the natural satellites, and has been applied successfully to the Martian system (Lainey et al., 2007). It is an N-body code that incorporates highly sensitive modeling and can generate partial derivatives, which are needed to fit the initial positions, velocities, and other parameters (masses, oblateness coefficients, precession frequency, etc) to the observational data.

The model presented in this work takes into account: (i) the Uranian gravity field up to degree 4 adopting the numerical values from French et al. (1988), (ii) the perturbations of the Sun using DE406 ephemerides (Standish, 1998), (iii) the mass of each Uranian satellite with numerical values from Jacobson (1992), and (iv) the IAU2000 Uranian northern pole orientation (Seidemann et al., 2002).

The dynamical system is numerically integrated in a planetocentric frame with inertial axes (conveniently the Earth mean equator J2000). Hence, denoting \mathbf{r}_i the position vector of a satellite, the related equation of motion has the usual form of

$$\ddot{\mathbf{r}}_i = -\frac{G(m_0 + m_i)\mathbf{r}_i}{r_i^3} + \sum_{j=1, j \neq i}^{\mathcal{A}} Gm_j \left(\frac{\mathbf{r}_j - \mathbf{r}_i}{r_{ij}^3} - \frac{\mathbf{r}_j}{r_j^3} \right) + G(m_0 + m_i)\nabla_i U_{\hat{\mathbf{r}}_i} + \sum_{j=1, j \neq i}^{\mathcal{A}} Gm_j \nabla_j U_{\hat{\mathbf{r}}_j} \quad (1)$$

where $U_{\hat{\mathbf{r}}_i}$ denotes the oblateness gravity potential of the planet. The associated force is computed using a rotation matrix of angles² ($\alpha_0 + \pi/2, \pi/2 - \delta_0, W$) and its associated inverse.

¹ftp://ftp.nofs.navy.mil/pub/outgoing/plansats/

²The angles (α_0, δ_0, W) are defined in (Seidemann et al., 2002).

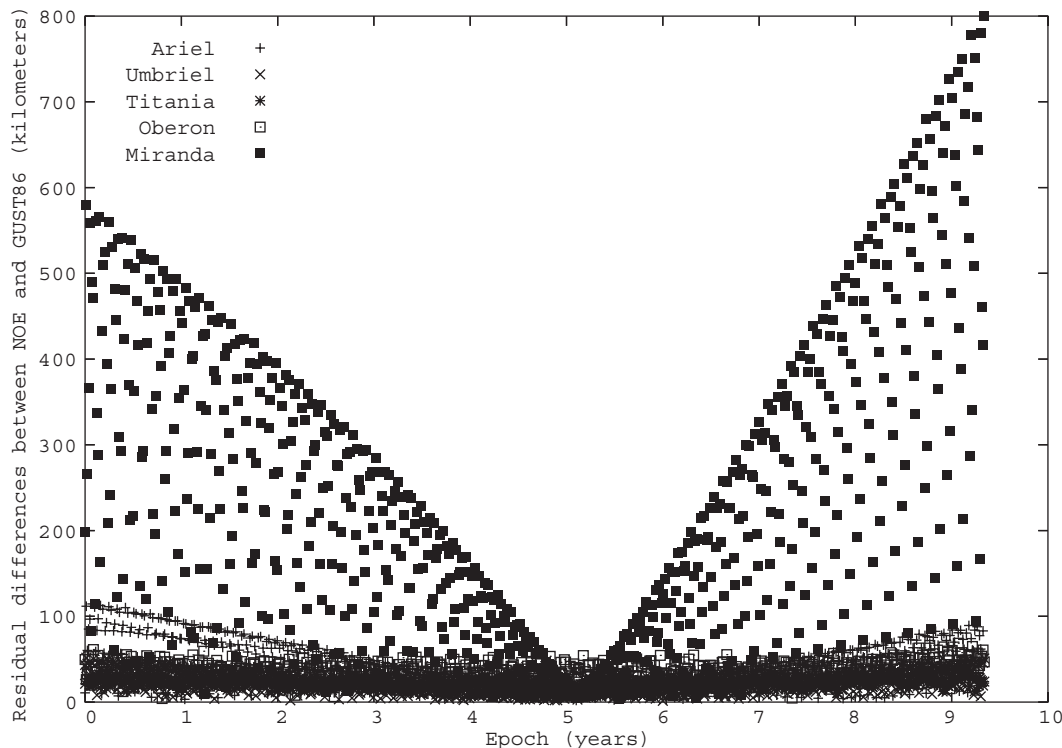


Fig. 1. Differences in distance after fitting the numerical model to the GUST86 ephemerides. The satellite initial positions and velocities have only been fitted here. The horizontal axes are in years relative to Julian day 2446299.5 (22/08/1985).

Denoting c_l as an unspecified parameter of the model that shall be fit (e.g. $\mathbf{r}(t_0), \dot{\mathbf{r}}(t_0), m_0, \dots$) a useful relation is

$$\frac{\partial}{\partial c_l} \left(\frac{d^2 \mathbf{r}_i}{dt^2} \right) = \frac{1}{m_i} \left[\sum_j \left(\frac{\partial \mathbf{F}_i}{\partial \mathbf{r}_j} \frac{\partial \mathbf{r}_j}{\partial c_l} + \frac{\partial \mathbf{F}_i}{\partial \dot{\mathbf{r}}_j} \frac{\partial \dot{\mathbf{r}}_j}{\partial c_l} \right) + \frac{\partial \mathbf{F}_i}{\partial c_l} \right] \quad (2)$$

Hence, partial derivatives of the solutions with respect to initial positions and velocities of the satellites and dynamical parameters are computed from numerical integration of Eq. (1) and simultaneously with Eq. (2). For an explicit formulation of the dynamical equations and the variational equations used, we refer to Peters (1981) and Lainey et al. (2004).

The integrator subroutine is from Everhart (1985) and called RA15. It was chosen for its computational speed and accuracy. During the different integrations, a constant step size of $\Delta t = 0.025$ day was used. To increase the numerical accuracy during the fitting procedure, we performed forward and backward integrations starting at an initial Julian epoch of 2446299.5 (22/08/1985 TDB). This epoch was chosen to keep high precision during the time span of the Voyager observations. The numerical accuracy of our simulation in computing the satellite positions is at the level of a hundred meters over one century.

Before fitting the numerical model to the astrometric observations, we used the GUST86 theory to start with proper initial conditions. A sample of 759 Cartesian coordinates in a J2000 Earth mean equatorial frame centered on Uranus was used with a step size of 4.5 days.

Post-fit residuals after few least square iterations are shown in Fig. 1.

The residuals are found to be of the same order of the ones presented in Laskar (1986). Only the residuals on Miranda are found to be much larger. This is easily understandable as we did not use the same physical modeling for the Uranian system. In particular, our values of the masses and gravity coefficients are not the same. Being the closest satellite to Uranus, Miranda is affected the most by errors in the Uranian GM and zonal harmonics.³ Nevertheless, such agreement was sufficient to fit the numerical model and provide LA06 ephemerides of the Uranian satellites. In the present work, we used LA06 initial conditions to perform the fit of LA07.

4. Post-fit residuals

Despite the possibility to fit the masses and Uranian precession of the system, we only fitted the initial positions and velocities of each satellite. A global solution involving the fit of a complete set of physical parameters and the use of older observations is still an ongoing work and shall benefit from the coming PHE-URA observations. Such

³This can be easily checked by computing different simulations with slightly modified values of the Uranian gravity field and check the position differences (simulations not shown here). In addition, a former fit to GUST using the same gravity field introduced in GUST provided similar differences for all satellites to the ones presented in Laskar (1986).

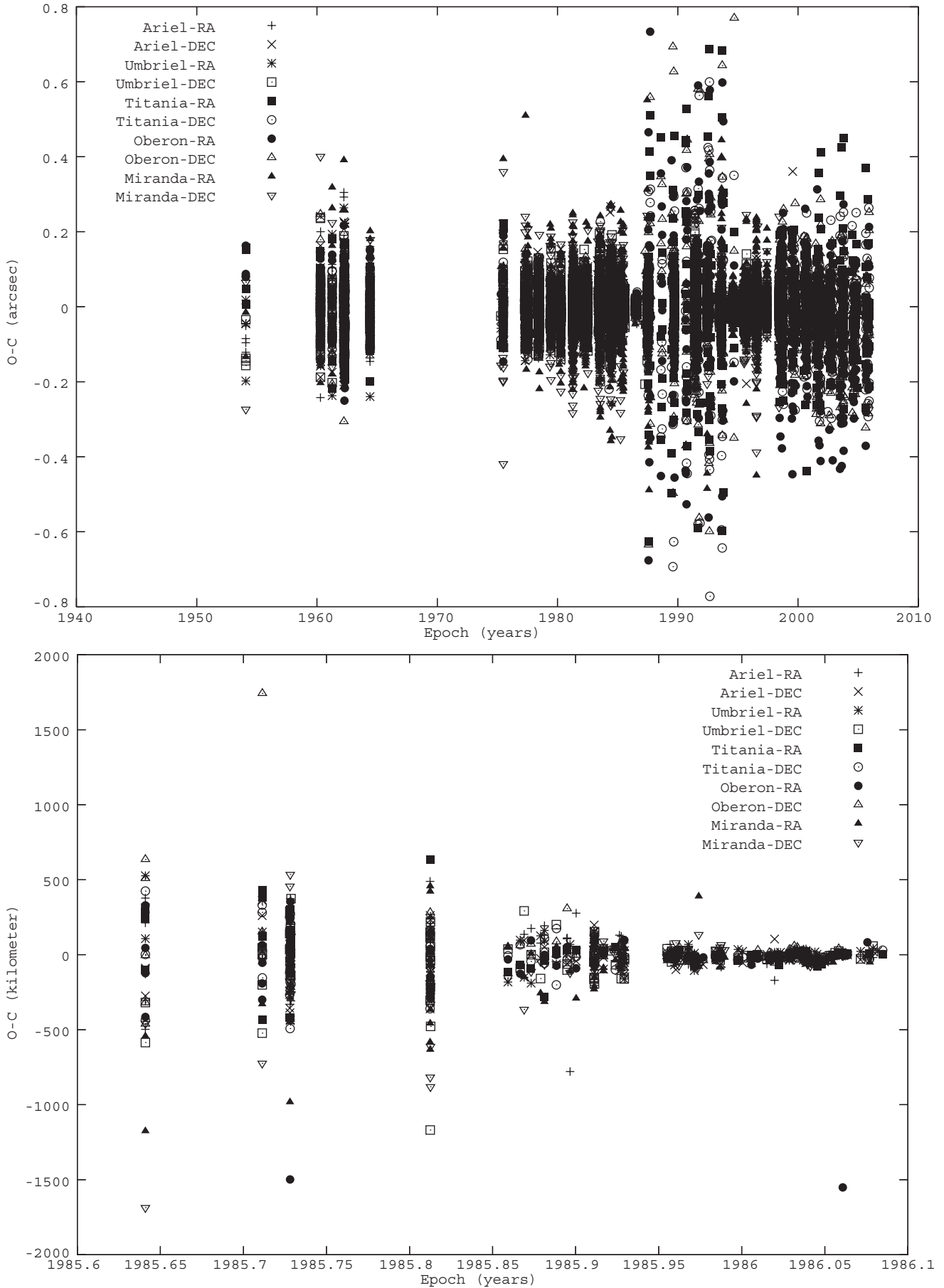


Fig. 2. Post-fit residuals on right ascension (RA) and declination (DEC) of our numerical model to the ground astrometric observations (top) and Voyager 2 observations (bottom).

work will be presented in a future paper. Residuals between observed and computed position (O–C)s were fitted using the least squares method. Convergence problem of the least-squares method had been noticed in Taylor (1998), and resolved by fitting the initial elliptical elements of each satellite, instead of the usual initial state vectors in Cartesian coordinates. This problem had also been encountered by Lainey et al. (2007) in the case of the Martian system. The present ephemerides have been done by fitting the initial elliptical elements.

Each observational set has been arranged by satellite and coordinate (right ascension and declination), and assigned

Table 1

Table showing the values of the mean $\langle v \rangle$ and standard deviations σ on right ascension and declination in arcseconds for each satellite

Observations	$\langle v_\alpha \rangle$	σ_α	$\langle v_\delta \rangle$	σ_δ	N	Satellite
1983–1998	0.0040	0.0668	0.0094	0.1084	1536	Ariel
Veiga et al. (2003)	0.0005	0.0665	0.0135	0.1081	1526	Umbriel
	0.0018	0.0680	0.0146	0.1087	1541	Titania
	0.0049	0.0744	0.0049	0.1113	1541	Oberon
	-0.0130	0.2317	-0.0493	0.4350	1320	Miranda
1987–1994	0.0137	0.3019	-0.0189	0.3339	106	Titania
Chanturiya et al. (2002)	0.0439	0.3270	0.0117	0.3220	103	Oberon
1998–2005	-0.0159	0.1868	-0.0171	0.1293	360	Titania
Stone (2001), Monet (priv. com.)	-0.0393	0.1827	-0.0275	0.1310	398	Oberon
1999	-0.0100	0.0150	0.3380	0.1454	3	Ariel
Owen (1999)	-0.0105	0.0229	-0.2028	0.1025	3	Umbriel
	0.0925	0.0731	-0.0719	0.0122	3	Titania
	-0.0720	0.0590	-0.0633	0.0386	3	Oberon
2001	-0.0531	0.0320	0.2141	0.0213	3	Umbriel
Owen (2001)	0.0208	0.0154	-0.1495	0.0189	3	Titania
	0.0323	0.0229	-0.0647	0.0085	3	Oberon
2003	-0.0163	0.0332	0.0528	0.0152	6	Titania
McNaught et al. (2003)	0.0163	0.0332	-0.0528	0.0152	6	Oberon
1984–1986	0.0025	0.0240	-0.0021	0.0175	34	Ariel
Walker et al. (1988)	-0.0014	0.0236	-0.0009	0.0284	33	Umbriel
	-0.0038	0.0238	0.0032	0.0250	34	Titania
	-0.0052	0.0210	-0.0014	0.0288	34	Oberon
	0.0668	0.0771	0.0096	0.1348	4	Miranda
1981–1985						
Pascu et al. (1987)	-0.0050	0.1149	0.0523	0.0779	76	Miranda
1979–1983	-0.0024	0.0384	0.0051	0.0424	88	Ariel
Harrington et al. (1984)	-0.0014	0.0525	-0.0005	0.0528	85	Umbriel
	0.0069	0.0417	0.0043	0.0368	86	Titania
	0.0010	0.0447	0.0025	0.0477	88	Oberon
	-0.0118	0.1032	-0.0330	0.0907	30	Miranda
1977–1982	-0.0042	0.0583	0.0047	0.0622	343	Ariel
Veillet (1983)	0.0020	0.0627	0.0003	0.0635	340	Umbriel
	-0.0049	0.0506	0.0045	0.0575	343	Titania
	-0.0123	0.0459	-0.0003	0.0556	345	Oberon
	0.0290	0.0997	-0.0138	0.0926	230	Miranda

N being the number of observations used by satellite. Note that some sets of data include too few observations to provide confident statistical data.

Table 2

Table showing the values of the mean $\langle v \rangle$ and standard deviations σ on right ascension and declination in arcseconds for each satellite

Observations	$\langle v_\alpha \rangle$	σ_α	$\langle v_\delta \rangle$	σ_δ	N	Satellite
1981						
Veillet (1983)	-0.0070	0.1136	-0.0436	0.1144	78	Miranda
1975–1977	0.0231	0.0813	-0.0093	0.0761	28	Ariel
Walker et al. (1978)	0.0111	0.0707	0.0195	0.0711	28	Umbriel
	-0.0082	0.1028	-0.0051	0.0732	28	Titania
	0.0022	0.0990	0.0092	0.1066	28	Oberon
	-0.0146	0.2754	-0.0294	0.1923	26	Miranda
1948–1964	-0.0145	0.1429	-0.0036	0.2242	91	Ariel
Van Biesbroek (1970)	-0.0005	0.1084	-0.0054	0.1531	108	Umbriel
	-0.0196	0.0918	0.0168	0.1072	111	Titania
	0.0199	0.1174	0.0132	0.1712	107	Oberon
	0.0254	0.1714	-0.0421	0.2348	56	Miranda

N being the number of observations used by satellite.

Table 3

Table showing the values of the mean $\langle v \rangle$ and standard deviations σ on right ascension and declination in kilometers for each satellite

Observations	$\langle v_\alpha \rangle$	σ_α	$\langle v_\delta \rangle$	σ_δ	N	Satellite
1985–1986	5.7216	167.9484	-17.8270	126.0694	104	Ariel
Jacobson (1992)	-6.9481	123.4069	-36.6868	176.7214	103	Umbriel
	7.6498	169.6340	-18.2472	144.8569	66	Titania
	-42.9281	298.7524	67.0665	257.9650	64	Oberon
	-76.9120	222.9311	-73.5027	248.1120	102	Miranda

N being the number of observations used by satellite.

a specific weight corresponding to the standard deviation of a former iteration. Observations with residuals higher than 2.5 sigmas were rejected in the corresponding iteration.

Intersatellite positions were used to cancel out the uncertainty of the Uranian ephemeris. However, Miranda is much fainter and difficult to observe than the other main Uranian satellites. To avoid the diffusion of the higher observational errors of Miranda on the other satellite fits, we fitted Miranda's initial elements with Uranocentric positions, only. Hence, we may expect a much better fit for Ariel, Umbriel, Titania and Oberon, but a worse one for Miranda.

Fig. 2 and Tables 1–3 present the post-fit residuals of our numerical model to the ground and Voyager 2 astrometric observations. The tables can be directly compared to the ones in Arlot et al. (2006). No important differences between the post-fit residuals of LA06 and LA07 can be found. This was expected as, firstly, the new observations concern the modern period only, and secondly, are not very numerous compared to the global amount of observations used in LA06. However, we may compare the residuals of FASTT observations in the present paper with those of Arlot et al. (2006). It appears that the new residuals in LA07 with the addition of roughly 200 new observations

for both Titania and Oberon are worse. This happens because some bad observations usually deleted in the FASTT reduction treatment were kept in the present sample (A.Monet priv. com.). Anyway, residuals between LA06 and LA07 are generally in good agreement.

5. Discussion

The problem of quantifying the accuracy of an ephemeris is recurrent in celestial mechanics. At least we can quantify the differences between LA06 and LA07, and estimate the influence of adding new astrometric observations. Fig. 3 presents the distance differences between the two ephemerides for the five Uranian satellites.

Titania and Oberon have the highest residuals as they are the only ones observable with FASTT. The residuals present linear trends but do not exceed 45 km. We may conclude that at least over a short time scale (few years) the ephemerides are drifting linearly. In particular, we expect the lack of observations available in 2006 and 2007 to decrease the accuracy of LA07 ephemerides of roughly 10–20 km.

Table 4 gives the residuals with LA07 of the FASTT observations of Oberon in 2006 and Bordeaux observations. As already explained, these observations can be used as an independent way to estimate the accuracy of LA07, but also of the ephemeris of Uranus. Neglecting the only 20 observations of Umbriel (that is also a satellite more difficult to observe than Titania and Oberon), one finds a shift in Bordeaux’s observations of -0.15 arcsec in the

mean of the residuals on the declinations. A less agreement is found when considering the mean on right ascensions. Anyway, a clear discrepancy of at least -0.1 arcsec appears. The observations of Oberon done in 2006 at Flagstaff present also some significant bias. The low number of observations, however, prevent us to be very confident in an accurate estimation of such bias. To test the

Table 4
Table showing the values of the mean $\langle v \rangle$ and standard deviations σ on right ascension and declination in arcseconds for each satellite

Observations	$\langle v_\alpha \rangle$	σ_α	$\langle v_\delta \rangle$	σ_δ	N	Satellite
1997–2003	-0.1154	0.2165	-0.0402	0.2421	20	Umbriel
G. Dourneau (priv. com.)	-0.1146	0.1488	-0.1508	0.1929	96	Titania
	-0.1431	0.2052	-0.1523	0.2486	117	Oberon
2006						
A. Monet (priv. com.)	-0.1634	0.2104	-0.0870	0.2616	39	Oberon
1997–2003						
Odd observations	-0.0427	0.2330	-0.1531	0.2065	10	Umbriel
	-0.1418	0.1411	-0.1585	0.1866	48	Titania
	-0.1568	0.2594	-0.1332	0.2473	59	Oberon
Even observations	-0.1883	0.1696	0.0726	0.2217	10	Umbriel
	-0.0878	0.1513	-0.1432	0.1988	48	Titania
	-0.1294	0.1268	-0.1718	0.2485	58	Oberon
2006						
Odd observations	-0.1668	0.2217	-0.1039	0.2763	20	Oberon
Even observations	-0.1598	0.1978	-0.0692	0.2440	19	Oberon

N being the number of observations used by satellite.

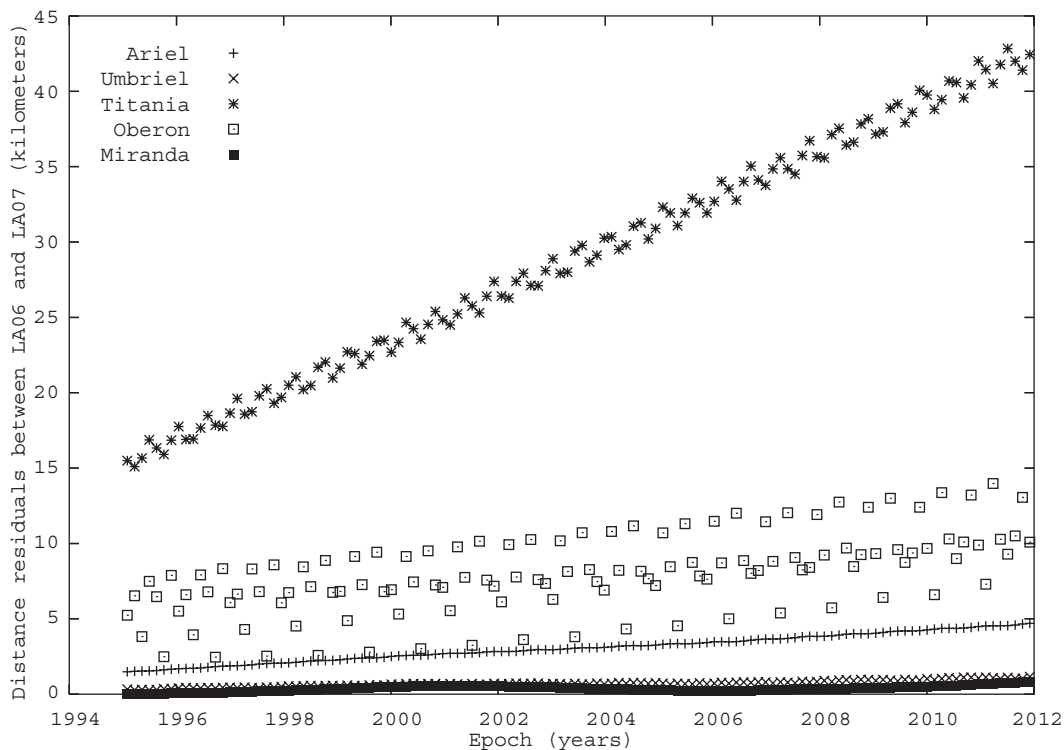


Fig. 3. Distance differences between LA06 and the present ephemerides LA07.

steadiness of our results, we divided both observational sets in two subsets, each one containing respectively the even and odd observations. Residuals are also shown in Table 4. Again, a clear bias of at least 0.1 arcsec on right ascension and declination is present.

The quantification of the accuracy of LA06 and LA07 is, however, difficult to deduce from Table 4. Standard deviation for all sets reach frequently roughly 0.2 arcsec. It is difficult to explain such residuals by the error of LA07, as residuals for such ephemerides with, for example, the observations of Veiga et al. (2003) and Stone (2001) are much smaller. In the other hand, the accuracy can be somewhat deduced from all the observational residuals already presented in Section 4. The high differences on the residuals from one set of observations to another one reflect essentially the differences of the observational errors. Hence one can expect the error of the ephemerides to be much lower. We remind that 0.1 arcsec is at opposition roughly equal to 1300 km at the distance of Uranus. Under such considerations, one can expect the accuracy of LA07 to be of the order of few hundreds of kilometers, only.

6. Conclusion

We have developed a new numerical model of the five main Uranian satellites. Observations done between 1948 and 2005 have been introduced in the model fitting procedure. The produced ephemerides can be used to predict the mutual events occurring in 2007 and 2008. These ephemerides can also be used for the reduction treatment of the related photometric lightcurves. A consequent error of at least 0.1 arcsec has been confirmed on the ephemeris of Uranus (DE406). LA06 and LA07 ephemerides have an expected accuracy of few hundreds of kilometers. They are available as FORTRAN subroutines on request to the author.

Acknowledgments

The author is greatly indebted to A. Monet for having provided all FASTT observations done these last few years, and to G. Dourneau for sharing the observations done at Bordeaux observatory. The author would also like to thank M. Standish and an other anonymous referee for useful suggestions and significant improvements in the present paper.

References

Arlot, J.E., Lainey, V., Thuillot, W., 2006. Predictions of the mutual events of the uranian satellites occurring in 2006–2009. *Astron. Astrophys.* 456, 1173–1179.

- Chanturiya, Kisseleva, Emelianov, 2002. *Izvestia Pulkovo*, 216, 349.
- Christou, Apostolos, A., 2005. Mutual events of the uranian satellites 2006–2010. *Icarus* 178, 171–178.
- Everhart, E., An efficient integrator that uses Gauss-Radau spacings, 1985, *ASSL Vol. 115: IAU Colloq. 83: Dynamics of Comets: Their Origin and Evolution*, 185.
- French, R.G., Elliot, J.L., French, L.M., Kangas, J.A., Meech, K.J., Ressler, M.E., Buie, M.W., Frogel, J.A., Holberg, J.B., Fuensalida, J.J., Joy, M., 1988. Uranian ring orbits from earth-based and Voyager occultation observations. *Icarus* 73, 349–378.
- Harrington, R.S., Walker, R.L., 1984. Positions of planets and natural satellites. II. *Astron. J.* 89, 889–898.
- Jacobson, R.A., 1992. Astrographic observations of the major Uranian satellites from Voyager 2. *Acta Astronautica* 96, 549–563.
- Lainey, V., Duriez, V., Vienne, A., 2004. New accurate ephemerides for the Galilean satellites of Jupiter. I. Numerical integration of elaborated equations of motion. *Astron. Astrophys.* 420, 1171–1183.
- Lainey, V., Dehant, V., Pätzold, M., 2007. First numerical ephemerides of the Martian moons. *Astron. Astrophys.* 465, 1075–1084.
- Laskar, J., 1986. A general theory for the Uranian satellites. *Astron. Astrophys.* 166, 349–358.
- Laskar, J., Jacobson, R.A., 1987. GUST86—an analytical ephemeris of the Uranian satellites. *Astron. Astrophys.* 188, 212–224.
- McNaught, R.H., Garradd, G.J. 2003. NSDC Comm. UM008.
- Owen, W.M., 1999. NSDC Comm. UM004.
- Owen, W.M., 2001. NSDC Comm. UM005.
- Pascu, D., Seidelmann, P.K., Schmidt, R.E., Santoro, E.J., Hershey, J.L., 1987. Astrometric CCD observations of Miranda-1981-1985. *Astron. J.* 93, 963–967.
- Peters, C.F., 1981. Numerical integration of the satellites of the outer planets. *Astron. Astrophys.* 104, 37–41.
- Seidelmann, P.K., Abalakin, V.K., Bursa, M., Davies, M.E., Bergh, C.d., Lieske, J.H., Oberst, J., Simon, J.L., Standish, E.M., Stooke, P., Thomas, P.C., 2002. Report of the IAU/IAG Working Group on Cartographic Coordinates and Rotational Elements of the Planets and Satellites: 2000, *Celestial Mechanics and Dynamical Astronomy*, 82, 83–111.
- Standish, E.M., 1998. JPL Planetary and Lunar Ephemerides, JPL IOM, 312.F-98-048.
- Stone, R.C., 2001. Positions for the Outer Planets and Many of Their Satellites. V. FASTT Observations Taken in 2000–2001. *Astron. J.* 122, 2723–2733.
- Stone, R.C., Monet, D.G., Monet, A.K.B., Walker, R.L., Ables, H.D., 1996. The Flagstaff Astrometric Scanning Transit Telescope (FASTT) and Star Positions Determined in the Extragalactic Reference Frame. *Astron. J.* 111, 1721–1742.
- Taylor, D.B., 1998. Ephemerides of the five major Uranian satellites by numerical integration. *Astron. Astrophys.* 330, 362–374.
- Van Biesbroek, G. 1970. Comm. to Lunar and Planetary laboratory, 8, 179.
- Veiga, C.H., Vieira Martins, R., Andrei, A.H., 2003. Positions of Uranus and Its Main Satellites. *Astron. J.* 125, 2714–2720.
- Veillet, C. 1983. Ph.D. University of Paris VI.
- Walker, R.L., Harrington, R.S., 1988. Positions of planets and natural satellites. III. *Astron. J.* 95, 1562–1566.
- Walker, R.L., Christy, J.W., Harrington, R.S., 1978. Positions of planets and natural satellites. *Astron. J.* 83, 838–844.